A STUDY OF THE METHODS OF MESON MASS DETERMINATION

A THESIS

Presented to

the Faculty of the Division of Graduate Studies

Georgia Institute of Technology

In Partial Fulfillment

of the Requirements for the Degree

Master of Science in Physics

by

Gilbert Carl Knollman

June 1950

A STUDY OF THE METHODS OF MESON MASS DETERMINATION

Approved:

Date Approved by Chairman May 29, 1950

ACKNOWLEDGMENTS

I wish to express my sincerest thanks to Doctor L. D. Wyly for his valuable assistance in preparing this work.

I would also like to thank my wife, Hilda, for her aid in proofreading the material.

TABLE OF CONTENTS

TABLE OF CONTENTS (continued)

LIST OF TABLES

LIST OF FIGURES

LIST OF FIGURES (continued)

LIST OF FIGURES (continued)

A STUDY OF THE METHODS OF MESON MASS DETERMINATION

CHAPTER I

INTRODUCTION

Statement of the problem. The term "cosmic rays" is somewhat over twenty years old, and the branch of physics with which it deals first began to open up about 1910. Prior to that year not a trace of evidence had appeared that any rays of a penetrating power greater than that of the γ-rays of radium existed, much less that rays entered the earth from outside its atmosphere.

In studying radioactivity by electroscopes it was noticed that with no emitting source present, any charged electroscope would always exhibit a residual rate of discharge. The conclusion was drawn that some very penetrating radiation was arriving continuously from outside. Balloon flights into the atmosphere established the fact that a radiation, called cosmic rays, was constantly bombarding the earth, the primary radiation consisting of high energy protons. In the uppermost layers of the atmosphere, some of the protons interact with the air nuclei to give mesons in groups of five to ten generated in a single act.

Each meson observed near the surface of the earth was

found to be short-lived (the half-life later approximated as about 2.3 millionths of a second), probably decaying into either a positive or negative electron and a neutrino. Since cosmic-ray particles are moving with velocities approaching that of light, the relativistic time contraction extends the lifetime in the observer's frame of reference to several hundred microseconds, thereby enabling the mesons to be detected at sea level.

The discovery of these particles at once initiated research as to their nature, that is, their charge and mass. A variety of results for the meson mass has been presented to date. It is the purpose of this thesis therefore (1) to examine the existing methods of meson mass measurement; (2) to investigate the experimental errors and inaccuracies of each method; and (3) to determine the possibility of unique meson masses from the many values obtained utilizing the several methods.

It is hoped that the present study will lead to more advantageous methods for future determination of the meson mass and its uniqueness, thereby indicating not only more about cosmic rays but also the answers to some interesting problems in high energy nuclear physics raised by the meson-producing process. Although the actual mechanism of meson production is unknown, the meson is involved in nuclear reactions and particularly in the disintegrations of nuclei. Hence, an accurate knowledge of the meson mass is essential in understandi

nuclear processes.

Discussion of the problem. In the thirteen years that have elapsed since the discovery of the meson, many attempts have been made to determine its mass. Although the fact that its mass appeared different from that of any known particle led to its discovery, the meson's mass is still not known accurately, nor is it known definitely whether it actually has a unique value or a distribution of values.

A description of the methods thus far developed for the determination of the mass of the meson is presented in the following pages. Three main types of determination are distinguished, namely, direct, indirect, and photographic plate methods.

The direct methods are based either on the measurement of a meson's deflection in combined electric and magnetic fields or on close elastic collisions between mesons and electrons. Although the first type involves severe experimental difficulties and has not yet been applied, the way in which this method possibly may be used in the future is discussed in Chapter VIII. The second type, the one with the soundest theoretical basis, involves measuring the kinetic energy or momentum of an electron in a cloud chamber (after a meson has collided with it) by determining its range or curvature in a magnetic field. This measurement, together with two others—momentum of the meson before collision and angle of ejection of the electron after collision—enables a determination of

the meson mass M. Also, by assuming both meson and electron to have the charge e, the mass M may be found by measuring the radii of curvature of a meson before collision and the electron after collision, the magnetic field intensity, and a measurement on the recoil electron track.

Assuming the meson to have unit charge, the measurable quantities in the indirect methods all depend on the mass and velocity of the meson. These quantities are cloud-chamber measurements such as range, curvature in a magnetic field, rate of change of curvature in a magnetic field when traversing matter, and specific ionization. A combination of any two, then, would indicate the velocity which, in turn, could be used to give the mass. The combinations which have been employed until the present to enable meson mass measurements are discussed separately in accordance with procedures found in the literature.

Since range, curvature, and specific ionization are the fundamental cloud-chamber observations involved in the mass determination methods, they are discussed in Chapter IV with the intention of presenting something of their general nature to enable a better understanding of the various methods.

Probably the simplest way to picture the dependence of mass on range, curvature, rate of change of curvature, and ionization is by a nomograph of the type published by Corson and Brode (1) and shown in Fig. 1. Any straight line crossing all the scales connects consistent values of $H\rho$ (magnetic

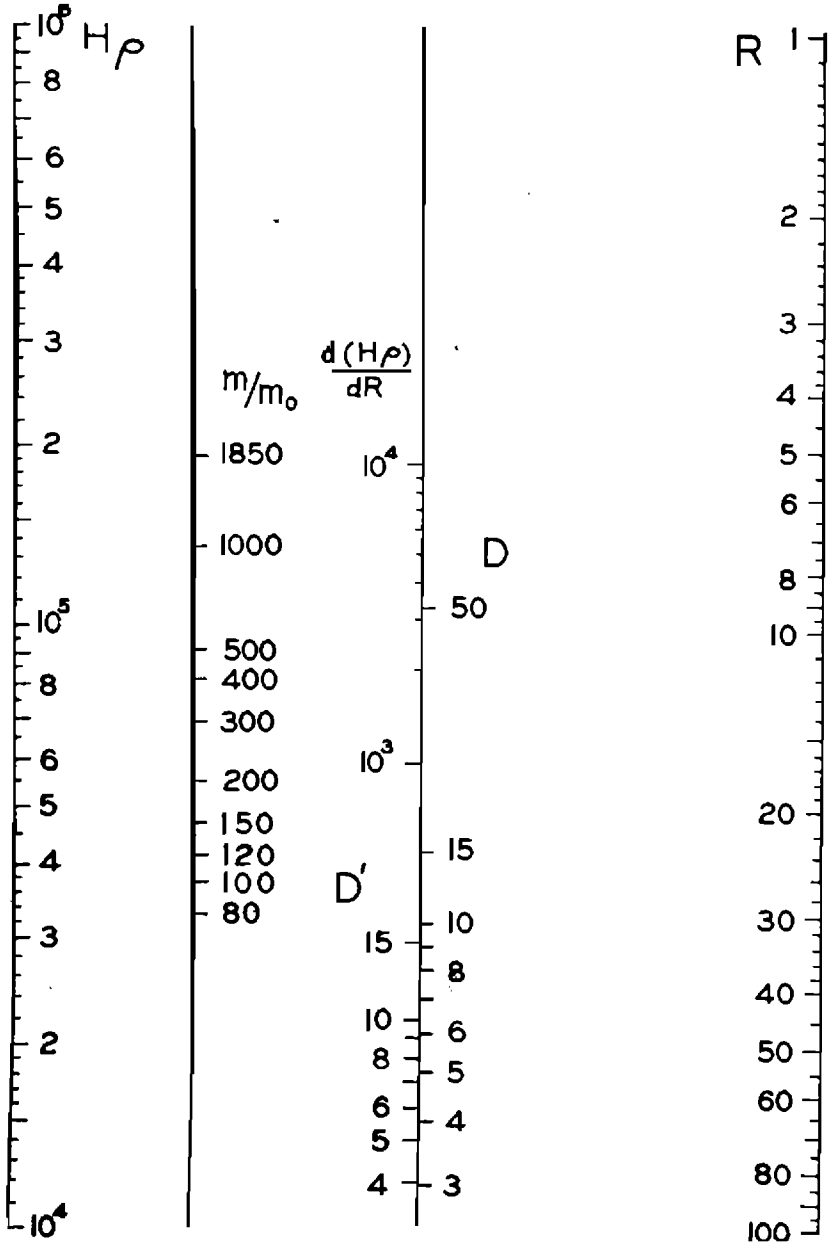

Figure 1. Nomograph giving the ratio of mass of a particle to that of the electron (m/m_0) in terms of variables such as D (ratio of specific ionization to specific ionization at the minimum), D' (same ratio for the classical $1/v^2$ variation of ionization with velocity), R (range in cm. of air at 15° C. and 750 mm. pressure), $H\rho$ (magnetic field strength x radius of curvature), and $d(H\rho)/dR$ (the rate of change of $H\rho$ with distance), all determinable from cloud chamber data. Any straight line drawn across the nomograph gives consistent values for all variables plotted.

field strength X radius of curvature), density of ionization D, range R, and rate of change of $H\rho$ with distance. The ratio m/m_o is the symbol used on the chart for the ratio of the mass M of a meson to that of the electron.

Although the errors of the chart are not small, they are smaller in general than the experimental uncertainty of the mass determinations to be discussed. The nomograph is found to be sufficiently accurate for calculations involving meson mass determinations from typical cloud-chamber photographs and its use is justified by simplicity.

From an inspection of the nomograph it is seen that $H\rho$ and range afford the most accurate method of determining the mass, provided all the data has the same accuracy, $H\rho$ and D is a good method since a relatively large change in D produces a relatively small change in the mass ratio, and D and range is a poor way because D must be accurately given in order to determine the mass ratio within relatively small limits. This last method, however, does not involve curvature measurements making it free of distortions leading to spurious curvatures. An upper limit on the mass can be set by a value of $H\rho$ and a minimum range value.

In the discussion on mesons which follows, comparison with proton tracks is frequently introduced. It should be pointed out that the formula for the specific ionization, as a function of the velocity of a particle as given in Appendix II, and therefore the range of the particle, is theoretical,

but protons, as well as deuterons and alpha particles, of known energy as produced by the various types of heavy particle accelerators such as cyclotrons have been used to check the accuracy of the theoretical formula. Such experiments have shown the formula to be correct for particles of different mass and initial energy. The stopping power, etc. of cloud chamber gases and even photographic plates can therefore be calibrated with say protons of known energy and a comparison made with mesons of known energy to determine the unknown meson mass from the known proton mass.

A knowledge of the behavior of mesons in emulsions is required by the photographic plate methods. In the first of these methods, Coulomb scattering, the track of a meson in an emulsion is compared with that of a proton which has the same mean spacing of the silver grains along its path in a similar emulsion. The assumption is made that the mean grain spacing deposited per unit length of track along the paths of particles in a photographic emulsion is proportional to their kinetic energies. The kinetic energy of the meson is found from the curvature of its tracks in the plate due to scattering and that of the necessary proton from a plot of mean grain spacing versus kinetic energy for protons. The mass of the meson is obtained from the known mass of protons and the kinetic energies of the two particles.

The grain counting method postulates that the total number of grains in the paths of a meson and another particle of the same charge and the same initial kinetic energy and

of unequal mass is in the ratio of the two masses. The third of the photographic methods, known as magnetic deflection, requires a determination of the curvature of a meson in traversing an air gap as it travels from one photographic plate to another. By observing its range in the second emulsion, its change in curvature, and the places of exit from and entry into the two emulsions (the latter two enabling the meson curvature to be calculated), the meson mass can be found using the range and curvature combination as in the cloud chamber technique.

In Chapter III the apparatus employed in detecting mesons is discussed since it necessarily determines the methods of mass measurement which may be employed. From the discussion the reader will be able to obtain a general picture of the nature and operation of the instruments used in making meson mass determinations before their application to a specific type of measurement.

Meson mass values presented in the tables are those obtained by various experimenters over a period of more than ten years. Therefore, a large spread in the mass appears. Although the meson masses obtained years ago must be regarded as very doubtful due to the lack of equipment and cloud-chamber knowledge for proper interpretation of meson photographs, they nevertheless indicate a mean mass value consistent with later values for the ordinary meson of about 200 times the mass of an electron. Also, many of the values deviating largely from

this mass are due to large experimental errors some of which are pointed out in the discussion in Chapter IX and may be corrected to give approximately 200 times the electron mass as is indicated in Chapter X.

The equations which follow are numbered consecutively; those from Eq. 24 on, which are referred to repeatedly, are to be found in the Appendix. The mesons discussed from the beginning up until Chapter VII are commonly referred to as μ-mesons and have a mass in the neighborhood of 200 electronic masses. Mass values which digress radically from this perhaps are measures of the masses of other mesons to be taken up in detail under the photographic method in Chapter VII where they first come into prominence.

Definition of terms and symbols used. Before going into a detailed study of meson mass determination, an explanation of terms and symbols to be used is needed.

Meson, any particle with mass between that of a proton and an electron.

Turbulence, the irregular motion of a particle caused by impediments in the air, air friction, and changes in air pressure.

ev, electron volt. The energy of a particle is commonly expressed in electron volts, one electron volt being the energy which an electron acquires when accelerated by a potential difference of one volt. It is equivalent to 1.591×10^{-12} ergs.

Mev, million electron volts.

M, rest mass of the meson or an unknown particle.

m_e, rest mass of the electron. It is 9.02×10^{-28} gram.

k, mass number of an unknown particle in terms of the electron mass. It is equivalent to M/m_e.

M_p, rest mass of the proton. It is 1.67248×10^{-24} gram.

e, electric charge of the electron. It is 4.803×10^{-10} e.s.u.

v, velocity of a particle.

c, velocity of light. It is 2.99775×10^{10} cm./sec.

β, v/c.

$1/\sqrt{1-\beta^2}$, factor by which a particle's rest mass must be multiplied to obtain its mass when traveling with velocity v. It is needed only in considering large values of the velocity v.

H, magnetic field strength. It is usually expressed in gauss.

ρ, radius of curvature of the track of a particle measured in centimeters.

ρ_s, spurious radius of curvature.

R, range of a particle. It is usually expressed in terms of centimeters of air.

Residual range, range remaining beyond a certain point in a particle's track.

Z, charge number of a particle.

Ze, charge of a particle.

Z', atomic number of an element.

p, momentum of a particle.

I_o, specific ionization. It is the number of ions produced per unit length of track of a charged particle during its passage through a medium.

E, energy of a moving charged particle.

$-dE/dx$, rate of energy loss of a particle per centimeter of path in any material.

θ, the angle through which a particle is deviated from its path due to scattering.

CHAPTER II

MESON HISTORY

Early researches which indicated the presence of penetrating parts as well as less penetrating parts in cosmic radiation led, however, to difficulties in the identification of the penetrating component since it appeared to be different from any particles or radiations then known to physics.

Skobelzyn (2) first observed cloud tracks of cosmic-ray particles in 1929. Millikan and Anderson, in 1931, made a much more extensive study of the particles and, a year later, Rossi (3) (4) was able to show, by an arrangement of three counters in a vertical plane with various thicknesses of lead between them, that the particles are singly charged. This conclusion was later verified by the experiments of Street, Woodward, and Stevenson (5), Ehrenfest and Auger (6), and Leprince-Ringuet (7).

These and other observations established several main facts:

(1) The particles presumably had a charge of one electron (8) (9) since they produced about the same density of ionization as found along electron tracks and the density should be proportional to the square of the charge;

(2) That there are approximately equal numbers of positive and negative particles (8) (9) (10) (11);

(3) That it is unlikely that any appreciable number of the particles whose curvature corresponds to that of an electron of less than 500 Mev energy could have a mass of the proton due to the ionization exhibited by the particles (11) (12).

The foregoing facts, up until 1933, seemed to be reasonably consistent with the assumptions that the cosmic-ray particles arriving on the earth consisted mainly of positive and negative electrons. In 1934, however, additional experiments of energy loss of cosmic-ray particles below 250 Mev while traversing thicknesses of lead clearly established the particles as being not only more penetrating than electrons should be if the recent radiation theory of Heitler and Sauter (13) were valid at these energies but also as having too low a specific ionization to permit their being definitely associated with particles as massive as protons (14). Also, if all of the penetrating particles had a protonic mass, an abundance of heavily ionizing particles corresponding to protons near the ends of their ranges where their velocity is appreciably less than the velocity of light should be observed. These were not. Statistical data showed the particles not to be as massive as protons by determining the number and distribution in energy of the secondary electrons formed in elastic collisions between the cosmic-ray particles and atomic electrons in absorbing plates of lead and carbon.

As early as 1933, experiments such as those of Blackett

and Occhialini (12) measuring the curvature of the track of a cosmic-ray particle and estimating the ionization density along this track led to the conclusion that the particles were not of a mass comparable with that of a proton. Hence, a new type of particle was indicated, one with a mass intermediate between that of an electron and that of a proton.

Direct energy loss measurements in lead and platinum of those cosmic ray particles which occur exclusively in showers showed the values of energy loss to be proportional to the energy of the incident particle and thus to agree within observational uncertainty with the Bethe-Heitler theory (15) of absorption of electrons. The 10,000 cloud-chamber photographs made on Pikes Peak in 1935 by Anderson and Neddermeyer (16) made this possible. To establish the fact that this was not due to the breakdown of the radiation theory for electrons, Neddermeyer and Anderson (17) determined the change in curvature of 15 shower particles and 40 single ones which traversed a platinum plate. From previous measurements (18) of energy loss of shower particles in a thin lead plate, they found that the shower particles lost more than three-fourths of their initial momentum in nearly all cases. The single particles, however, were found to be generally less absorbable. From a plot of the above mentioned measurements of energy loss, and many more, versus incident energy, they determined the absorbable shower particles to be electrons since they behaved quite in accord with the general requirements of the Bethe-Heitler

theory. Therefore, the penetrating particles must distinguish themselves from electrons, yet could not be protons since their observed ionization was very much smaller than that to be expected from protons of the same momentum. An example of energy loss of a penetrating particle is shown in Fig. 2 (19). Yukawa,* on a purely theoretical basis, found a possible mass value of 200 m_e for a particle of intermediate mass between the free electron and the proton. He rejected his theory, however, since such a particle had until then not been established.

The name "mesotron" (intermediate particle) for this penetrating component of cosmic radiation was suggested by Anderson and Neddermeyer and agreed to by a small conference on cosmic-ray problems held in Copenhagen in 1938. Now the prefered name is "meson," although writings still show a wide scatter among "mesotron," "mesoton," "heavy electron," and "Yukawa particle."

The exact properties of the mesons or wherein they have their origin is as yet undetermined. Bowen, Millikan, and Neher (20) (21) postulate that they must arise as secondaries produced in the atmosphere or other absorbing material by the incoming primaries, which, in turn, presumably have their origin far removed from the solar system. At the present time a complete theory of the origin of the primaries does not exist,

*See collected papers from Faculty of Science, Osaka University, 2:52 (1935).

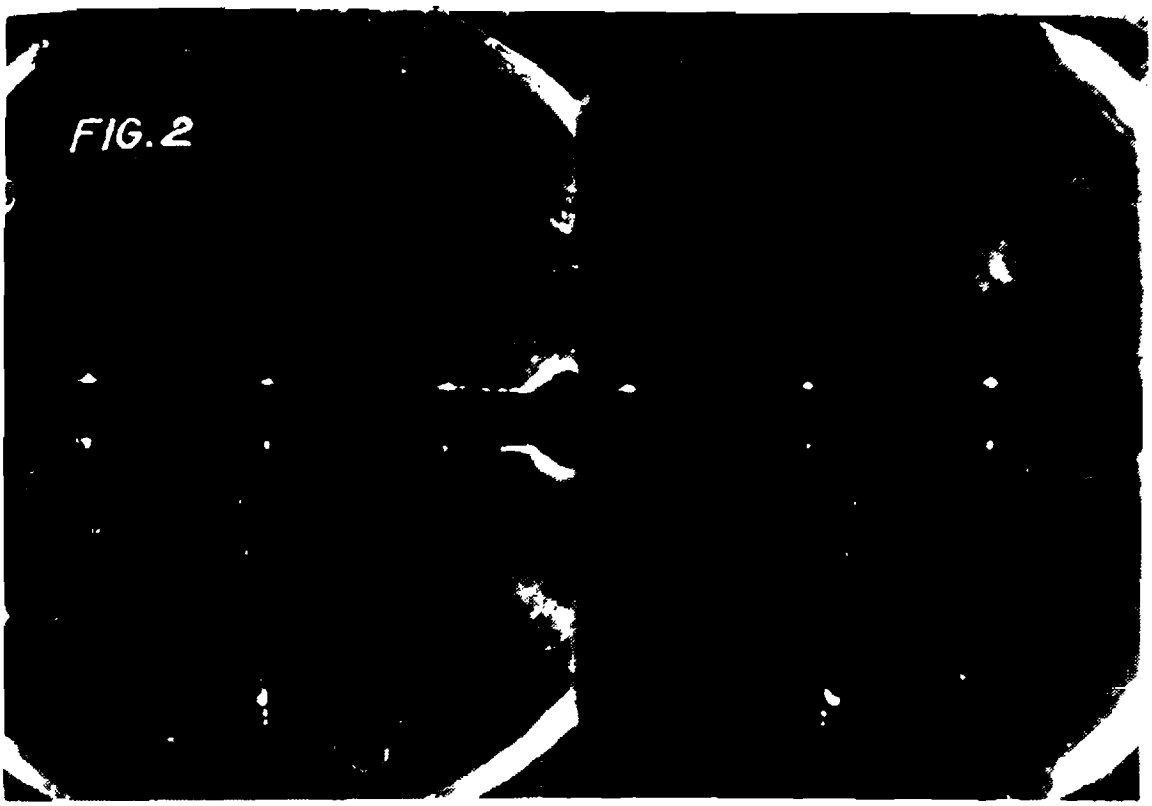

Figure 2. A negative particle of $H\rho = 7.1 \times 10^5$ gauss cm. passes through a 1-cm. platinum plate and emerges with an $H\rho = 6.3 \times 10^5$ gauss cm. A proton of momentum equal to that of the negative particle could not traverse the platinum plate. The probability, statistically, of an electron's losing less than three-fourths its incident momentum in 1 cm. of platinum as does the above particle is very small. Assuming a mass of the particle intermediate between that of an electron and a proton, say 200 m_e, the calculated energy loss would be 21 Mev/cm., agreeing closely with the experimental value. The field employed for this photograph was 7900 gauss. The left-hand view is the direct image of the chamber.

but it is apparent that a normal star like the sun is not a source of cosmic rays.

It has become customary to place the different kinds of particles in cosmic radiation into two groups, the hard and the soft components, the former consisting of about 55 per cent positive and 45 per cent negative mesons and the latter being primarily electronic in nature. Since, at sea level the hard component is about 77 per cent of the total intensity of the cosmic radiations, mesons, and a very small number of protons, neutrons, and perhaps other nuclear fragments which make up the remainder of the hard component, constitute the bulk of the radiation striking the earth. The soft component is stopped by a few centimeters of lead and, since the total atmosphere is equivalent in absorbing power to about 100 cm. of lead, is not found in the radiation striking the earth.

It is almost certain that mesons do not enter the atmosphere from the outside since they are radioactive and have a lifetime of but a few microseconds which is far too small for the time that would be required to reach the earth from interstellar space. Assuming, then, that the mesons are secondaries of a primary radiation, and since there is strong evidence that the majority of the hard component primaries are protons (22), it is plausible that protons upon entering the atmosphere produce the mesons in colliding with the nuclei of air atoms (23).

From the date, in the summer of 1936, of the final and unquestionable discovery of the existence of the meson of mass intermediate between that of the free electron and the proton, there have appeared many different determinations and estimates of this mass and several well defined methods of measurement. In 1938, Neddermeyer (24) brought forward the discussion of the possibility of the existence of multiply valued mesons, which stimulated suggestions as to the assignment of unique masses to mesons. Recently, various types of mesons with different masses have experimentally been produced in the Berkeley cyclotron; these will be discussed later.

CHAPTER III

GENERAL APPARATUS EMPLOYED IN MESON MASS MEASUREMENTS

Ionization chambers, counting tubes, cloud chambers, and, more recently, the photographic plate are the general research tools used in the determination of meson mass. They all are useful since each is capable of detecting ionizations produced by mesons. Since all are also used extensively in other fields of investigation, only those modifications used in cosmic-ray work will be reported here; a discussion of the specific variations used for mass determination will be included with each particular measurement.

Ionization chamber. In the ionization chamber the ions produced in an enclosed volume of gas are collected on a conductor and the resultant current is measured, the current increasing with the volume of the chamber and the pressure and temperature of the gas for a given radiation. The current is also a function of the kind of gas. Compton, Wollan, and Bennett (25) developed a typical large-volume ionization chamber which was filled with argon at a pressure of 50 atmospheres and was self-recording. Fig. 3 (26) is a photograph of an ionization chamber, its cross sectional view and a sketch of the apparatus.

The ionization chamber A consists of a hollow steel ball surrounded by one inch of bronze and two inches of lead. Lead minimizes the effects of local radiations as compared

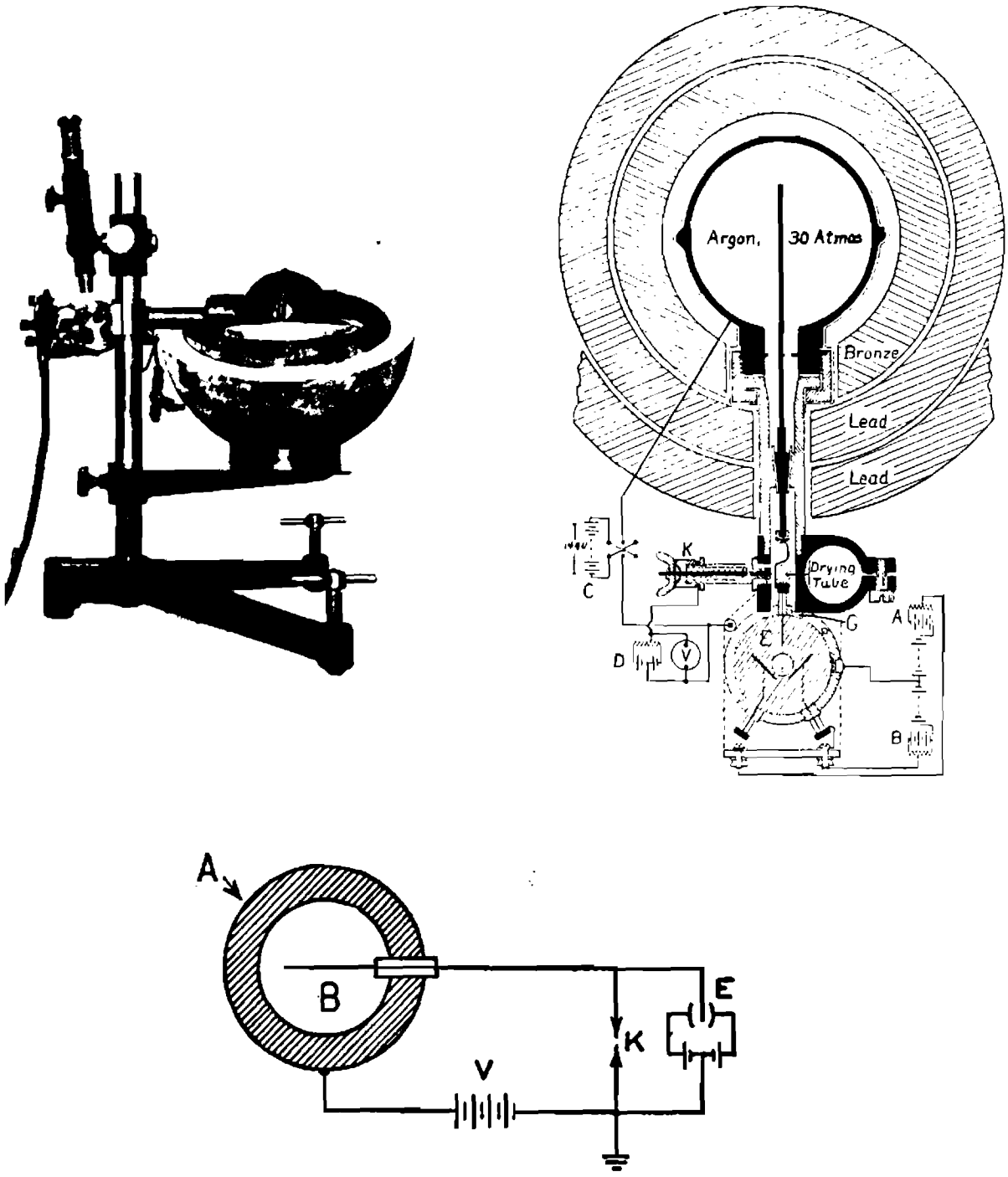

Figure 3. Apparatus to measure the ionization produced by mesons. The second view is a cross section of the chamber shown in the photograph, the third view being a schematic diagram. In the photograph, the top shields are removed and the microscope raised slightly to show the electrometer.

with that of the cosmic rays. The ions produced in the ball, which is filled with argon at a pressure of perhaps 30 atmospheres, are collected by a steel rod B. The rod is supported by means of an insulator and is connected to a sensitive electrometer E. The position of the electrometer is read through a window by a small microscope. When the key K is closed, electrode B is charged by the battery V. The key is then opened and the electrometer needle is deflected by a large amount, the deflection then decreasing regularly toward the undeflected position at a rate proportional to that at which the ions are formed in the chamber and collected on the rod B. The original potential is restored to the collecting rod by pressing key K for a brief time, thus reconnecting the battery. After calibrating the electrometer, it is possible to calculate the number of ions formed each second. An alternative form of the apparatus passes the ionization current through a high resistance and produces an e.m.f. between its ends, which is amplified and recorded on a meter.

Counting tubes. In the ionization counter, the ions produced by a fast particle such as a meson in a gas are used to produce a cascade of electrons and ions in a discharge tube. A schematic diagram of a counter, Fig. 4 (27), shows it as a coaxial condenser. When the gas under pressure between the electrodes is ionized, an electric pulse is initiated between the electrodes. The efficiency of the counter for detecting the passage of ionizing particles decreases as

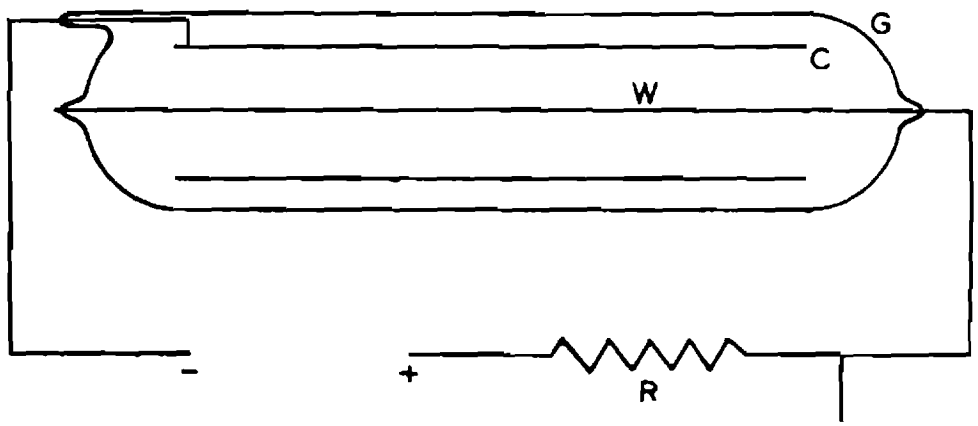

Figure 4. A Geiger-Müller counting tube. C is an outer thin-walled metal tube; W is the central electrode of fine wire with small diameter; G is a glass envelope enclosing the whole and containing a gas of 5 to 10 cm. of mercury; and R is an external resistance.

the number of pulses per second increases since the tube is insensitive for a small time interval after each pulse.

An inherent and valuable characteristic of counter tubes is the large internal amplification due to the cumulative ionization initiated by each ionizing particle. The currents in ionization chambers are usually of the order of magnitude of 10^{-10} to 10^{-15} ampere and require sensitive instruments or high gain amplifiers for their detection. With counter tubes, on the other hand, the currents are sometimes as great as 10^{-5} amperes. A two stage amplifier is often sufficient to operate a counter meter.

The best-known counter tube is the Geiger-Müller counter (28), which is an ionization counter consisting of a thin, fine wire, usually tungsten, extending along the axis of a conducting metal cylinder, enclosed in a concentric cylindrical sheath of glass. The tube performance is usually improved by having another conducting cylindrical sheath outside the glass and connected to the inner cylinder, so that the glass walls are free from an electric field. A gas such as hydrogen, generally at a pressure of several centimeters, is placed inside the inner metal cylinder and an electric potential of several thousand volts applied between this cylinder and the wire, the latter being made positive. The gas pressure and the potential are adjusted so that in the absence of ions in the gas no discharge occurs, but if one or more ion pairs are formed in the sensitive volume, a relatively large

flow of current takes place. The mechanics are roughly as follows. A single ion-pair formed between the electrodes will be followed by a drift of each ion, the negative ions or electrons toward the positive central wire and the heavy positive ion toward the cylindrical cathode. Close to the wire the electric field strength is strong and, since the electrons are very mobile, they soon acquire sufficient velocity to produce new pairs of ions by collisions with the gas molecules. Each of these ions can similarly produce additional ionization, so that a large number of electrons reach the wire for the original electron formed in the gas. If the potential is not too great, the discharge stops at this point. Such a counter is called a proportional counter (also called a Geiger-Klemperer counter) because the size of the discharge is roughly proportional to the number of ion pairs originally produced in the gas. Some electrons will recombine with positive ions, a process which may be accompanied by the emission of photons. In turn, if sufficiently energetic, the photons may eject photoelectrons from atoms in other remote regions of the tube. This causes the discharge to spread along the full length of the counter.

All this takes place in one-millionth of a second. The process then ceases because the positive ions, being very slow relative to electrons, accumulate around the wire in a sheath and by their space charge reduce the field strength to such a low value that electron multiplication can no longer occur. Every discharge thus builds up to a nearly constant size,

regardless of the original number of ions produced.

Geiger counters are employed in cosmic-ray studies to indicate and record the transit of a single particle such as a meson. When a meson passes through the gas in the tube, the ions which are created initiate an electrical discharge from a bettery through a resistance, the latter two being in an electrical circuit with the tube. The sudden potential drop which appears across the resistance for each meson is then amplified and may be used to operate a counting mechanism, cloud chamber, or other recording or measuring device. The number of such pulses per unit of time is found to agree with the number deduced from the variations in the ionization chamber currents.

Proportional counters are used to detect slow meson tracks giving rise to more than average ionization.

The most important advantage of the counter is that several of them can be arranged in such a manner that a pulse is only recorded when it occurs nearly simultaneously in all tubes. Hence, any pulses that may have been due to radioactivity in the area surrounding a single tube is completely eliminated by the coincidence arrangement just described. It is also possible for counters to be arranged in anti-coincidence. When one is interested in ascertaining events in which one counter is not set off when the others are, the anti-coincidence arrangement is used enabling one to pick out single events as, for example, when one wishes to study showers which are generated

in a lead plate by non-ionizing radiation. In this case, when an ionizing particle traverses an anti-coincidence counter placed above recording counters, the former counter suppresses coincidences in the latter counters.

Electron multiplier. An electron multiplier (29) is a device in which one or more electrons, having been ejected from a metal surface by a particle such as a meson, are multiplied to a readily measurable number by the ejection of secondary electrons at successive surfaces. Electron multipliers have two advantages over other counters: they operate in vacuum and they are fast. High speed is useful in almost any counting work.

Crystal counter. A crystal counter (30-36) is a crystal in which a pulse is produced by electrons moving in an electric field after having been raised in energy by the passage of an ionizing particle. The modern theory of the solid state predicts that when alpha-particles bombard an insulator, the electrons freed by ionization will be raised to the conduction band. Under the influence of an applied electric field, these electrons should move just as in the case of photo-conductivity. With a sufficiently high electric field across an insulator crystal which is relatively free of electron traps, it has been possible under favorable conditions to detect the movement of these charges and thus observe conductivity pulses. This phenomenon in certain crystals suggests the use of such a solid counter for cosmic-ray experiments, particularly since

it operates at room temperature. Its small size and possibility of rapid counting rate would give a crystal counter advantages over the conventional gas type counter.

Cloud chambers. The cloud chamber has enabled the direct observations of phenomena which otherwise would have remained purely conceptual. Almost all of the new particles uncovered in physics in the last half century have first been detected in cloud chambers.

The cloud or expansion chamber uses the tendency of over-saturated water vapor to condense on ions and thus makes it possible to see and photograph the "track" of an individual particle. This apparatus functions because of the fact that in a supersaturated vapor, condensing droplets will form, if possible, on any electrically charged particles that are present. A supersaturated condition is attained for water vapor and many of the alcoholic vapors which have a negative specific heat under the conditions of saturation by producing a sudden increase in the volume containing the saturated vapor. For saturated vapors with a positive specific heat, supersaturation can be produced by a sudden reduction in volume.

The most common expansion chamber in cosmic ray work today is the Wilson cloud chamber (37). A schematic diagram of a Wilson cloud chamber in current use is shown in Fig. 5 (38). An electric field of several volts per centimeter is applied to the chamber up until about one-fortieth of a second before the track is to be observed. This sweeping field effectively

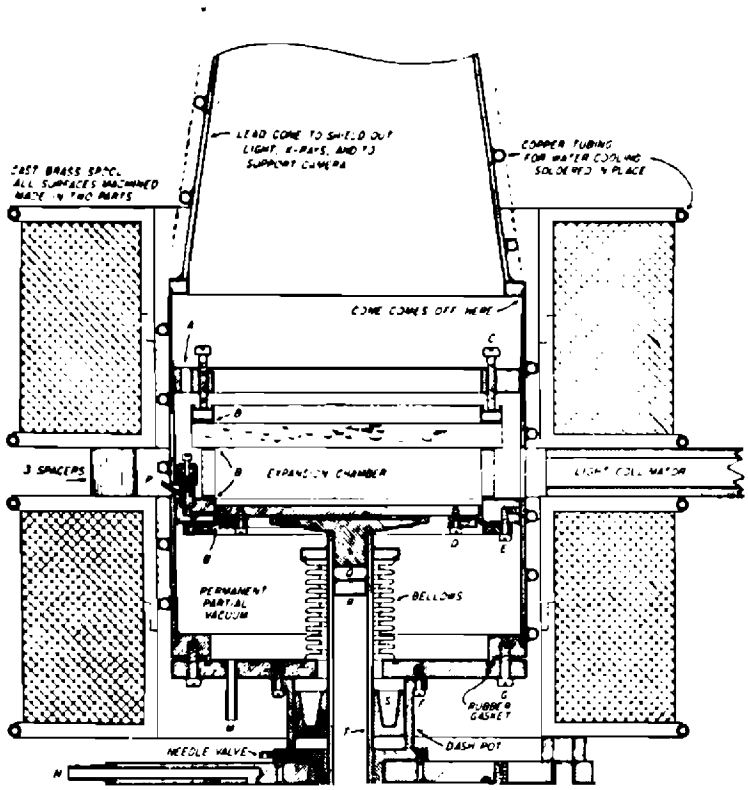

Figure 5. Detail of a Wilson cloud chamber.

removes the ions that would have diffused throughout the chamber. At the right moment after completion of the expansion, the chamber becomes momentarily illuminated. If a measurable magnetic field is applied perpendicular to the velocity of the particles to be photographed, their paths are circular and their moments and hence their energies can be determined by measuring the radii of curvature.

In order to secure fine, sharp tracks: (1) the gas must be saturated and at a constant, uniform temperature before the expansion, (2) the particles must pass through the chamber at approximately the time of the expansion, and (3) the expansion must occur quickly and be of a definite amount. For best curvature measurements, the particle should not be allowed to collide with anything and thus scatter during its path. To reduce the scattering, hydrogen is used instead of air in the chamber along with saturated water or alcohol vapor. Photographs may be taken with either a single camera or better with a stereoscopic camera. Typical photographs of meson tracks in a cloud chamber are shown in Fig. 6 (39). Usually, two cameras are used to take stereoscopic photographs in order that the tracks may be seen in three dimensions. For weak tracks, photographs are taken with the light scattered in the forward direction, since this is more intense than that at right angles to the beam.

Modifications of the expansion chamber were brought about by C. T. R. Wilson and J. G. Wilson (40), the first being

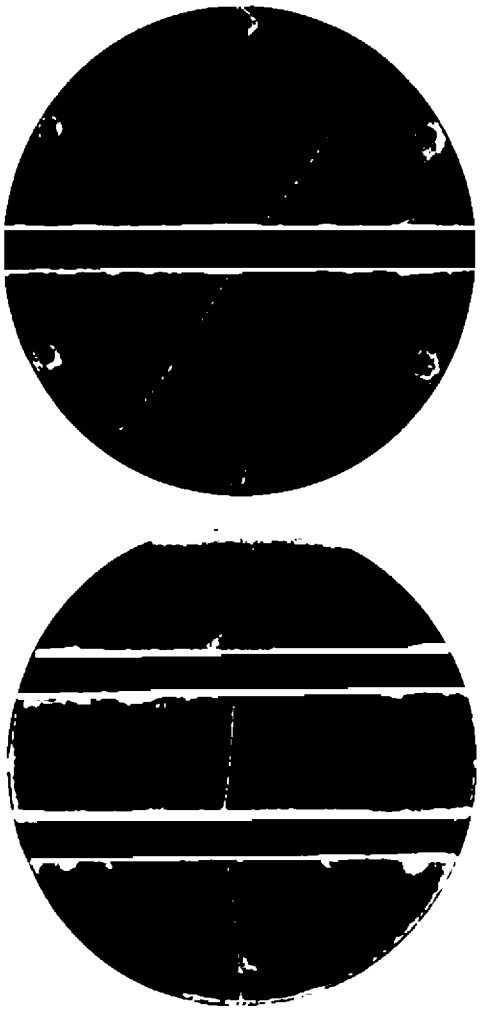

Figure 6. The tracks of two mesons in a cloud chamber which penetrate lead bars each a centimeter thick without changing largely their curvature.

a radially expanding chamber which greatly reduced the problem of proper illumination. The second modification was the development of a falling type chamber in which the chamber as well as the camera are allowed to fall freely under gravity. The falling type of chamber had the advantage that the disturbing effect of gravity is eliminated. As the droplets do not fall relatively with the gas in the chamber the convection effects are minimized. Without the risk of distortion because of the fall of the drops, the time interval between expansion and taking of photographs may be extended. With the falling camera, the time of exposure can be increased and a continuous source of illumination may possibly be used.

Blackett and Occhialini (12) and Anderson (11) almost simultaneously introduced the counter-controlled chamber, in which the time of expansion of a cloud chamber is controlled by a set of Geiger-Muller counters. Counters are placed on either side of, or in, the Wilson chamber. The chamber is normally inactive, but as a cosmic-ray particle passes through the counters a series of mechanisms is released automatically expanding the chamber and photographing the track of the particle. This system secures many more photographs that show significant events than do those obtained by the random exposure method. If a particle passes through the chamber appreciably before the expansion takes place, the tracks will be broad and dense. If the ions are formed in the chamber too late, the tracks are thin. Since the sensitive time, during

which reasonably sharp tracks can be formed, is usually only a fraction of a second, the counter-controlled chamber was designed mainly to study rarer and also some particular types of phenomena in cosmic rays, so that the expenditure to run the investigation might be minimized by an economic use of film and especially of time.

The shortcomings of the counter-controlled chamber are as follows: the chamber has some bias in favor or against some particular phenomenon; the magnet used must be a permanent one, in which case it will not be possible to produce a high field, or an electromagnet must be run continuously, expending a tremendous amount of electric power and making it difficult to control the temperature of the chamber. Thus, a chamber was devised which ran in a completely automatic way and yet recorded several tracks per random expansion. This chamber is known as the random operated slow chamber (41).

A slow rate of expansion is used in the above chamber to increase its sensitive time which, in turn, increases the yield of tracks per expansion above that obtained with a counter-controlled chamber. The field is switched on one or two seconds before the expansion and switched off after the expansion has been completed. A large diameter of the chamber also produces a larger yield. The average number of cosmic ray tracks recorded per photograph may be expressed as $2 j r d t_5$ where j is the number of cosmic-ray particles per $cm.^2$ per sec.; r is the radius of the region photographed; d is the depth of

focus of the camera used; and t_s is the sensitive time of the chamber.

The design of the extra high pressure Wilson chamber is one of the latest marked improvements in the technique of the Wilson chamber. It offers an increase in cosmic-ray track length which may be observed in a given time. At 200 atmospheres the effective track length across the one-foot diameter of the chamber is equivalent to 200 feet of normal argon in the conventional chamber. The efficiency, judged by good tracks, is almost 10 times greater because of the longer period over which the supersaturation is maintained inside the chamber. Since the sensitive time of a chamber has been found* to increase with the pressure, justification for the longer period is evident. The high-pressure chamber seems to be a satisfactory solution of the problem of recording the disintegration of the meson. High pressures or large volumes are required of a cloud chamber to increase the probability of occurrence, within the gas of the chamber, of this effect. Very large chambers make it very difficult to obtain proper photographs because of the large area that must be covered.

Many of the cosmic-ray measurements recently made have been brought about by using several counter-controlled cloud chambers in succession. Often the cloud chamber is separated

---

*See Das Gupta, N. N. and Ghosh, S. K., "A Report on the Wilson Cloud Chamber and Its Applications in Physics," Reviews of Modern Physics 18:254 (1946) for equations involved.

into two parts by horizontal lead plates, enabling the measurement of the change in momentum of a particle such as a meson in traversing a given thickness of lead.

Photographic plate. The photographic plate has been used very recently with considerable success for cosmic ray studies. Ions produced by the radiation form the center of a metallic silver crystal leaving a permanent record. One such technique has been developed by Wilkins (42) (43) to measure energy of incident particles. If the average number of electron volts per grain is determined, then it is necessary only to count the number of activated grains. The method is most successful under dark-field illumination. Since the tracks of heavily ionizing particles are much denser than those of electrons, the nature of the particle producing the track may be inferred from the density and length of the track.

Photographic plates have the advantage that they will detect very fast particles which are exceedingly difficult to identify in a cloud chamber; they afford a permanent record; they are continuously sensitive; and they have a light weight, making them particularly adaptable for use with pilot balloons. On the other hand, the photographic method is subject to severe limitations (44). Many grains appear due to background and there are usually various spurious appearances many of which may be easily mistaken for real tracks. These may be produced by scratches, by contractions of the gelatine during processing, and by the presence of foreign matter in the emulsion.

Inaccuracy in the measurement of tracks arises in the finite size of the grains. For fairly large grains the center of the grain may be appreciably displaced from the true path of the particle. To overcome some of these difficulties, the Ilford (45), Agfa, and Eastman Kodak laboratories have developed emulsions relatively free from background. An example of a track of a meson in an Eastman emulsion is shown in Fig. 7 (46).

Since the above photographic plate methods do not allow direct determination of the sign of particles investigated, emulsion surfaces separated by an air gap have recently been placed perpendicular to a magnetic field, the curvature of a particle's path in air being obtained from the tracks in the emulsions in either side (47).

Figure 7. Track of a negative meson (mass = 300 m_e) in an Eastman NTB emulsion. Range in the emulsion is 400 microns.

CHAPTER IV

GENERAL METHODS OF MEASURING RANGE, CURVATURE, AND SPECIFIC IONIZATION

Range. Range is usually given in terms of dry air at 15° C. and 76 cm. pressure measured under standard conditions (the equivalent height of a mercury column at 0° C., sea level, and 45° latitude is found). Hence, the range in a cloud chamber containing a gas is often converted to range in air.

If L_o is the image of a full length track of a particle of range R_o cm. in air at 15° C. and 760 mm. pressure as measured on a cloud-chamber picture, then, if L_a is the apparent length of any track, the reduced air range R_a is given by the following relation (48):

$$R_a = L_a \ (R_o/L_o).$$

It is assumed that the stopping power of the gas mixture in the cloud chamber is constant along the range of the particle, the stopping power being taken as independent of the particle's energy and velocity. Corrections due to temperature, pressure, latitude, and humidity must always be made; however, straggling of the particles makes exact determination of the range quite difficult. Range can be measured most accurately if the particle stops in the gas of the chamber.

Curvature. Since the track of a particle in a counter-controlled chamber lies in a plane at right angles to the

magnetic field and hence at right angles to the axis of symmetry of the photographic system, a rotation system is often employed to measure the curvature of a track when stereoscopic cameras are employed. The two films containing a track are replaced in the cameras, illuminated from behind, and the two images corresponding to a point O in the object space made to coincide on a screen whose plane is at right angles to the magnetic field. If the screen is then rotated about its vertical axis and/or a horizontal axis, the two images can be placed in exact coincidence. A microscope with a micrometer eyepiece is used to measure the coordinates of the point O. This is repeated for many points on the track, the values thus obtained plotted on a magnified scale, and ρ obtained. Blackett (49), Anderson (50), and others have used this method.

Curvature may actually be measured to a much higher precision by a method developed by Blackett (51). It is a null method in which the image of the track is reprojected through an achromatic prism, placed normal to the axis of the projection lens, on a magnesium-oxide coated screen which is viewed at grazing angle. The image of a straight line contains a curvature, r, introduced by the prism, which is given by

$$r = r_o \sin \phi ,$$

where ϕ is the angle between the line and the principal plane of the prism. In order to measure the curvature of the curved track the value of ϕ which produces a straight image must first

be determined. Straightness is judged by visual inspection of the projected image at a grazing angle. The value of r_o for the optical system used by Blackett was found by him to be 3.75 m.$^{-1}$ using lines of known curvature, and the accuracy of judgment of the straightness was found to increase as the angle of viewing the screen was decreased.

Blackett also found the probable error of curvature measurement (referring to the actual curvature on the photographic plate) to be 0.016 m.$^{-1}$ using the instrument just described. The actual length of the track images measured on the photographic plate was about 2.5 cm. It was found, however, that this device is limited to curvature measurements less than about 0.7 r_o and hence high accuracy cannot be obtained for low-momentum mesons. Wilson (52) used a model allowing curvature measurements up to 10 m.$^{-1}$ on the photographic plate to be made, corresponding with H = 10^4 gauss, and a photographic magnification of 0.1.

A microscope with a traveling stage was employed by Fretter (53) to determine the coordinates of the track on the film. The coordinates were plotted, and then a second plot made of the displacement from a straight line. This second plot, since it was on a large scale compared to the distance along the track, was found to conform to an ellipse. Any deviations indicated spurious effects such as scattering in the gas or turbulence making it necessary to reject the track as unreliable. The curvature was calculated by using the

sagitta formula on the curve or by fitting a curve to the observed points by the method of least squares. By comparing the plotted points with families of curves, calculating and comparing radii of curvature at various sections of the track, and observing other tracks on the same strip including many that were not deviated by the magnetic field enabled a means of checking turbulence. Tracks whose radii of curvature varied by more than 10 per cent along their length due to turbulence were rejected.

Fig. 8 shows a special arrangement devised by Jones and Hughes (54) for tracks of fairly great curvature. A reprojected track is made to intersect the ruled straight line DE, the intersection taking place at two points such as A and C. If the disk on the movable central platform is then set to coincide with the track, the displacement of the center of the track can be read to within 0.005 cm. from the micrometer screw which drives the platform. The smallest measurable deflection (0.005 cm.) corresponds to an energy of 5×10^{10} ev for a meson track of 20 cm. length and a field strength of 16,000 gauss.

Once the curvature is found, it is necessary to know the factor needed to convert this to curvature in the chamber. The magnification factor of the camera lens is determined by some method as photographing a piece of millimeter cross-section paper back of a glass plate corresponding to the front glass. The cross section paper is placed in the

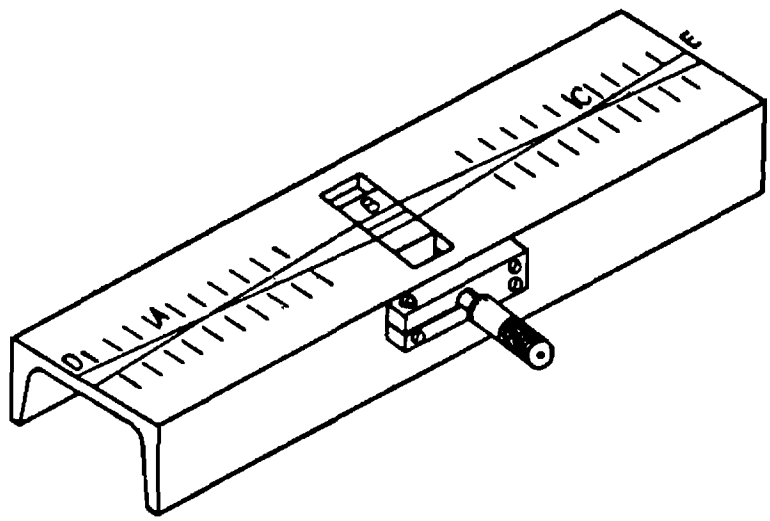

Figure 8. An apparatus for quick measurement of the radius of curvature of a particle.

center of the illuminated region of the experiment with the cloud chamber removed. The conversion factor often varies somewhat over the region, making it necessary to plot the factor as a function of position in the chamber.

Because of distortions of the tracks due to gas motions, there is always some curvature of the tracks even in the absence of magnetic fields. From a study of tracks without a magnetic field the probable error in the central displacement of a track length is often determined.

Specific ionization. Since specific ionization depends directly on the square of the charge of the moving particle, inversely on the square of the velocity of the incident particle as seen from Eq. 29 in Appendix II, and also directly on the number of electrons per cubic centimeter of the medium it traverses, high-velocity particles passing through the same medium will produce less ions per unit length of the track than particles with the same charge and lower velocities. Also, if the traversed medium contains light molecules, less ionization will be produced than if it contained heavier ones.

Secondary ionization is the ionizing of atoms and molecules in the medium by electrons liberated from atoms of the medium by an incident particle such as a meson. These primary electrons, which received their energy from the incident charged particle, must have, therefore, some energy above that which was required to liberate them. They liberate other electrons which, in turn, liberate still others, the process

continuing so long as the energy of the liberated electrons is greater then the ionization potential of the outermost electron in some of the atoms present.

The ionization chamber, Geiger-Müller counter, and the cloud chamber enable the determination of specific ionization, the latter, however, being the only device that makes possible separate determinations of the primary and the total ionization.

If a particle passes through the cloud chamber shortly before expansion, condensation takes place on ions, which then spread by diffusion. A primary ionization producing say 20 secondaries will appear as a cluster of ions. The resolution of the ions will depend on the interval (called delay time) between the passage of the particle and the expansion of the chamber. If the delay is very large, the ions produced will diffuse so much from their origin that they will not be distinguishable from other droplets which are always present in the chamber. If, on the other hand, the delay is too small, the primary ions will not be resolved into their secondary components. The delay has been found to depend on the gaseous medium of the chamber. Also, when a magnetic field is used simultaneously, the fact that gas motions may cause a distorted track leading to erroneous curvature measurements must be taken into account when deciding on the delay time.

When a particle passes through a cloud chamber just after expansion, condensation takes place on ions before they

have time to diffuse from their points of formation, the primary ionization now appearing as a blob. If a track is sharp and undiffused, the specific primary ionization may be determined by counting the number of blobs and clusters of ions along the main track. If a magnetic field is used to deflect the particles, the primary specific ionization may be obtained as a function of $H\rho$, or the momentum of the particle.

The total ionization can be measured using a delay method, but only counter-controlled chambers provide the means of obtaining the necessary delay. When the counters are tripped by an incident particle, a thyratron or cam mechanism is set into operation which controls a time delay circuit, the circuit eliminating the magnetic field for a desired interval. The expansion and illumination of the chamber then take place.

By reprojecting the photographic images of the tracks of a particle back into the object space, their lengths are measured. The total number of ions is found by counting the droplets on the developed film. Dividing the total number of ions by the length of the track gives the average specific ionization of the particle. By counting the number of other drops present in a region adjacent to the track and of the same size as the track, the error due to background density is determined.

The amount of illumination in the chamber must be carefully determined. If the chamber is expanded immediately after the passage of a particle, the illumination need not be strong

because the track can easily be photographed due to the scattering effect of the closely packed ions. For delayed expansions, however, the illumination must be stronger. Distortion caused by the lens system increases with the aperture size; hence, even though a large aperture will make the drops brighter, requiring less illumination, aperture size must be chosen with discretion.

CHAPTER V

DIRECT METHODS OF MESON MASS DETERMINATION

I. ELASTIC COLLISION

Discussion of the method and equations involved. One of the most direct methods of determining the mass of a particle is from its elastic collisions with an electron. It may be seen from Appendix II, that if T is the kinetic energy imparted to a free electron as a result of collision with a primary of mass M, momentum p, and if Θ be the angle between the direction of ejection of the secondary electron and that of M, we may obtain a relation between T, M, p, m_e, and Θ. The tracks of the incident particle, the secondary electron, and the direction of emission of this electron may be observed with the help of a cloud chamber placed in a strong magnetic field. A measurement of p and T from the range or curvature of the tracks of M and the electron, together with Θ, enables the determination of the mass M of the primary particle. The recoiling electron receives such a large amount of energy from the colliding primary particle that it can produce an ionization track of at least a centimeter length. In contrast to the ionization method, the elastic collision method can be used where the primary momentum is so high that no increased ionization is exhibited. However, in order to attain accuracy in mass determination the collision must be almost head-on and the primary momentum somewhat low.

The formula involved is given by Das Gupta and Ghosh (55) as

$$T = 2m_e c^2 \frac{p^2 c^2 \cos^2\theta}{\left\{m_e c^2 + [p^2 c^2 M^2 c^4]^{1/2}\right\}^2 - p^2 c^2 \cos^2\theta} . \qquad (1)$$

Fig. 9 (56) shows the variation of T with p for different M's and θ's. For $\theta = 0$ (head-on collision) mass discrimination is quite good for all values of p ; however, such collisions are very rare. For $\theta = 45^\circ$ the best p values correspond to an $H\rho$ of about 3×10^5 gauss cm. At higher momenta electrons and mesons are indistinguishable. For angles greater than 60°, the energy transferred to the electron becomes small and the accuracy of mass determination is lowered.

Fig. 10a (57) contains a picture for the case of a meson collision with an electron and Fig. 10b shows a diagram of a typical collision. In order to determine the data on the recoil electron, one tries to fit a circle to the track of the electron as closely as possible (see Appendix V for method). To make the radius of curvature as accurate as possible, the fitting should be done over as large an arc as possible. Parts of the track too far from the point of emission of the electron should not be used since multiple scattering will gradually make a track deviate from the circle so that the position of the center of the circle is shifted appreciably. The practical compromise is to make the fitting near the point at which the electron has been deflected through 90° by the magnetic field, and to use a track length of about a quarter circle. In Fig.

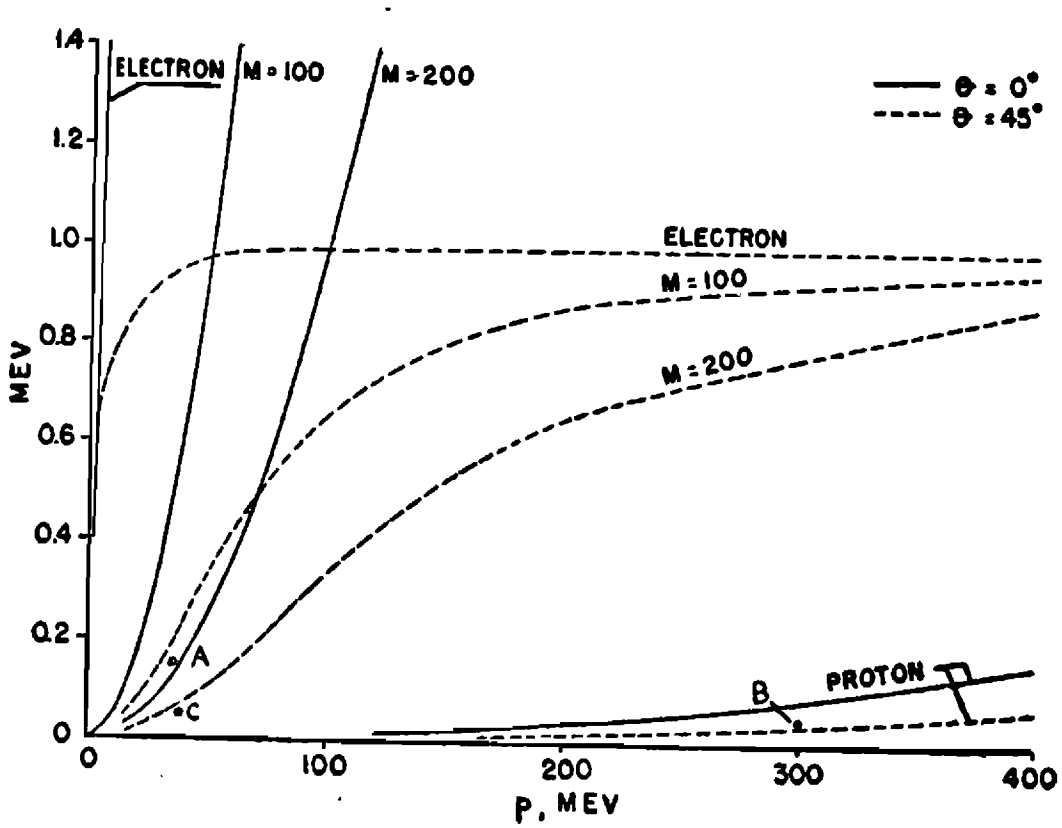

Figure 9. The energy (T) in Mev transferred to electrons as a function of primary momentum (p) for different primary masses (M) and angles of ejection (θ) of electrons.

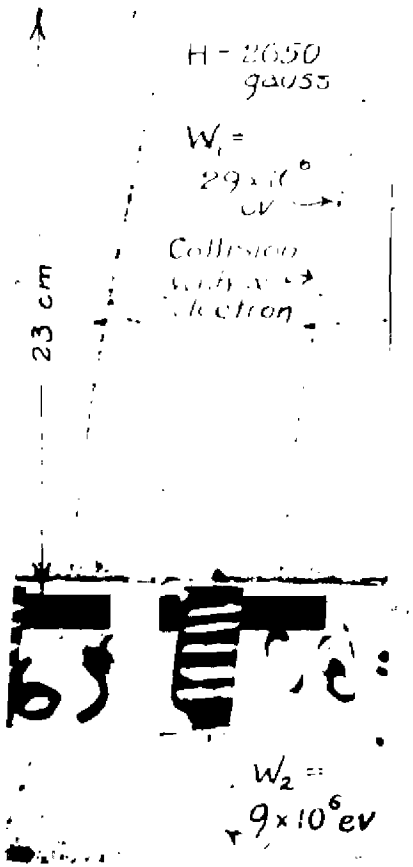

Figure 10a. Stereoscopic cloud-chamber photograph of a meson of mass M = (240+20) m_e, the mass value being obtained from the elastic collisions with an electron of the gas in the chamber.

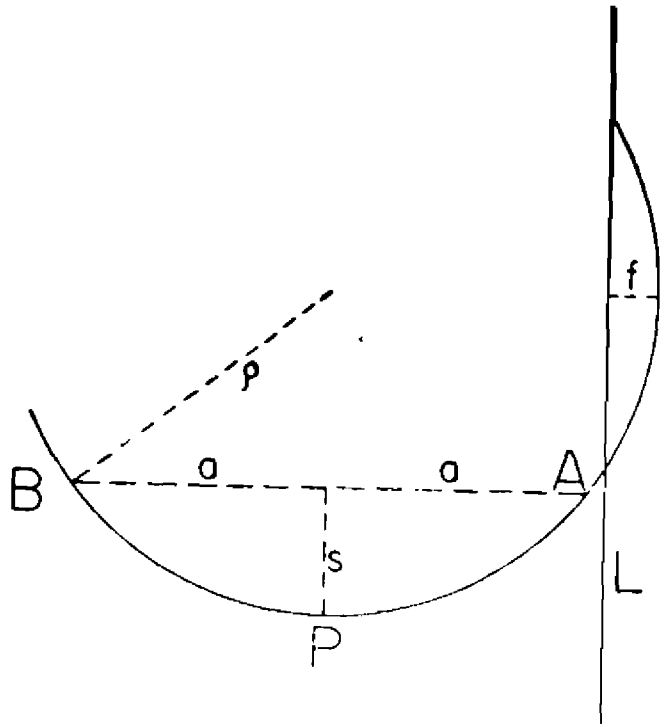

Figure 10b. Mass determination by the method of recoil electrons. APB is the measured section of the track of the electron while L represents the track of the primary.

10b, APB is the part of the electron track used for fitting (from $\theta' = 45^\circ$ to $\theta' = 135^\circ$).

Bethe (58) gives for the critical velocity β_0 of the electron in its path below which the major contribution to the curvature arises from scattering (making any calculation of the mass from the curvature meaningless) the following equation:

$$\beta_0 = 16.5 \frac{Z'}{HL^{1/2}} \left(\frac{BPL}{x}\right)^{1/2} \frac{\alpha^2}{2(1 - \cos \alpha)} . \qquad (2)$$

In Eq. 2, 2α is the angle subtended by the measured track length, in this case 90°; B is a constant close to unity; PL is the number of nuclei per $cm.^3$ of the gas in which the collision takes place ($P = 2$ for air at NTP, $P = 1$ for argon at NTP); L = Loschmidt's number $= 2.7 \times 10^{19}$; and x is the track length.

To find the angle of emission θ, it is necessary to extrapolate the electron track back to the meson track. If we designate the angle between electron and meson in the plane perpendicular to the magnetic field by ψ_1, and the angle between these particles in a plane parallel to the magnetic field by ψ_2, the sagitta f affords a convenient measure of ψ_1, assuming the meson track to be substantially straight. By defining a circular path as the closest approximation to the track between A and B in Fig. 10b, the relation between f and ψ_1 is given by

$$f = \rho(1 - \cos \psi_1) . \qquad (3)$$

Neglecting the electron mass in comparison with it, M is given by Bethe (59) as

$$Mc = p\left[\frac{E' + m_e c^2}{E' - m_e c^2} \cos^2 \psi - 1\right]^{1/2}, \qquad (4)$$

where p is the momentum of the primary, E' is the energy of the electron including rest mass, and

$$\cos \psi = \cos \psi_1 \cos \psi_2$$

provided the primary particle path lies in the plane perpendicular to the magnetic field as it normally does.

Assuming mesons that collide with electrons to have the charge e and that the paths of the two particles are normal to the direction of an applied magnetic field, Leprince-Ringuet et al. (60) derive formulas for the collision in which ρ_1 is the radius of curvature of a meson before collision, ρ_3 the radius of curvature of the recoil electron, ρ_o the value $m_e c/eH$ (which can be called the radius of curvature corresponding to the rest mass of the electron), ρ_4 the length $\rho_4 = \sqrt{\rho_3^2 + \rho_o^2}$, and f the sagitta of the electron's path (see Fig. 10b). The equations are

$$\frac{M}{m_e} = \frac{\rho_1}{\rho_o}\sqrt{\frac{2(\rho_o - f)}{\rho_3}}$$

for $\rho_1 >> \rho_3 >> \rho_o$; and

$$\frac{M}{m_e} = \frac{\rho_1}{\rho_o(\rho_4 - \rho_o)}\sqrt{(\rho_3 + \rho_4 - \rho_o - f)(\rho_3 - \rho_4 + \rho_o - f)}$$

for $\rho_1 >> \rho_3$ and ρ_3 not so large compared to ρ_0 (which is the case for a secondary electron of energy of the order of Mev's).

As was pointed out, the above relations are valid on the assumption for meson and electron tracks normal to the direction of the magnetic field. However, similar relations may be set up by introducing the angles made by the tracks of the particles with H if such is the case.

A consideration of the collision probability is given in Appendix VI, where the probability for a particle such as a meson to transfer a given amount of energy to a free electron is determined.

Specific experiments. The energy of a recoil electron may be obtained by measuring its range in a cloud chamber or its $H\rho$ value. Hughes (61) found a range of 30 cm. air equivalent and an $H\rho$ of 1.4×10^3 gauss cm. which are consistent as seen by the nomograph of Fig. 1, the electron energy being 150 kev. The primary meson's $H\rho$ was 1.3×10^5 gauss cm., θ was 18°, and hence the collision was nearly head-on ($\cos^2\theta = 0.9$). Point A in Fig. 9 corresponds to this "knock-on" electron. Eq. 1 gives the mass as $M = 180$ (+90, -50), the principal uncertainty arising in the measurement of $H\rho$ which, in this case, was difficult. The point B in the same figure is a plot of a proton of high momentum for which Eq. 1 gives only a lower mass limit. The point falls close to the $\theta = 45^\circ$ curve for protonic mass; the angle θ

was actually about 50°.

For an electron energy of 34 kev, an angle of 50°, and a primary $H\rho$ of 1.03×10^5, Hughes obtained a meson mass of 190 (+85, -50), plotted as C in Fig. 9, from Eq. 1.

Leprince-Ringuet, et al. (62) determined the mass (240 ±20 times that of an electron) of the particle shown in Fig. 10a by measuring the curvature of both the incident meson (115 - 120 cm.) and the recoil electron (1.05 - 1.10 cm.), the distance (f) the struck electron is deflected from the path of the primary (0 - .03 cm.), and θ ($\cos^{-1}.97$). The probability of obtaining a collision that enables the measurements described is very small. A strong magnetic field should be used to obtain the curvature of the primary meson accurately in view of the large energy of cosmic-ray particles, but then the displacement of the electron from the primary track will be very small and difficult to measure precisely on account of the nature of the incident ray. If a weak magnetic field is used, the conditions reverse.

Leprince-Ringuet found no possibility of error in regard to the nature of the ejected electron in his determination mentioned above. After collision, he allowed the meson to traverse a box containing 4.5 mm. of metal of specific gravity 8 and two Geiger-Müller coincidence counters. The kinetic energy of the meson changed from a value of 29×10^6 ev above the counters to a value of 9×10^6 ev below the counters. This energy loss of 20×10^6 ev was found to be

in good accord with the curves of ionization as a function of $H\rho$ (see Fig. 23) to be discussed later. For an assumed mass equal to 250 m_e and log $H\rho$ = 5.31 gauss cm., the expected mean ionization loss was found to be 160 ion pairs per cm. of air traversed, which corresponds to 19 x 10^6 ev. This is in good accord with the value of 20 x 10^6 ev obtained as shown in Fig. 10a checking the validity of the reported mass value of 240 m_e.

Meson mass values. Table I contains the values of meson mass obtained by several experimenters employing elastic collision methods. Leprince-Ringuet and Crussard (63) have observed a case of a secondary produced in the gas of a cloud chamber by a particle possibly a meson. By measurement of the angle and energy of the secondary, it was possible to conclude that the mass of the primary was less than that of a proton and apparently that of a meson. This measurement is not included in the table.

Variations in the method. If the angle of a recoil electron cannot be measured and only its energy is ascertainable, it is still possible to place an upper limit on the mass of a primary. With cos θ = 1 and taking $M \gg m_e$, Tmax is equal to $2m_e p^2/M^2$ from Eq. 32 which gives the maximum transferrable energy (Tmax) in the collision of a particle of mass M with an electron. This has been applied by Neddermeyer and Anderson (70) to place a limit on the mass of a particle which traverses 1 cm. of platinum with only a small

TABLE I

MESON MASSES FROM THE ELASTIC COLLISION METHOD

Mass ($\times 1/m_e$)	Reference
990 ± 120	Leprince-Ringuet and Lheritier (64)
189 ± 24	Hughes (65)
240 ± 20	Leprince-Ringuet, et al. (62)
120 ± 12	Steinmaurer (66)
~ 880 ~ 1170	Blau, Black, and Nafe (67)
180 (+90, -50) 190 (+85, -50) 280 (+250, -80) 340 (+300, -100)	Hughes (68)
240 ± 22	Leprince-Ringuet, et al. (69)

loss of energy and produces a secondary electron. The secondary has an energy of 16 Mev as it emerges from the lower face of the plate. An upper limit of 65 m_e is assigned to the mass of the incident positive particle. If the incident particle is a positron the probability that the same one should emerge below with so much of its original energy (as was observed here) should be of the order of a per cent. Perhaps this is an example of a meson of very low mass. As will be seen later, the possibility of the existence of mesons with such a small mass is admitted at present by some scientists.

A statistical argument based on the energy distribution of secondaries produced in a metal and the momentum distribution of the primaries as determined with an unobstructed chamber yields evidence as to the mass of the primary particles. Secondary data obtained by Wilson (71) from a 2-cm. plate of gold appear to be consistent with a mass of the order of 200 m_e when all the observed showers and single secondaries produced by particle traversals are interpreted as arising through ordinary electron secondaries. Except for this data, the available data on the production of secondaries tends to indicate a smaller mass than that obtainable from the other mass measurement methods.

To consider briefly* this statistical method, let us

---

*For details see Neddermeyer, S. H., and Anderson, C. D., "Nature of Cosmic-Ray Particles," Reviews of Modern Physics 11-12:203-207 (1939-1940).

assume that the primaries are all of mass 250 m_e. The distribution in energy of the emerging secondary electrons, to be expected theoretically if they result solely from elastic impacts, may then be calculated, as was done by Neddermeyer and Anderson (see reference in footnote) taking into account the energy lost by the secondaries before they emerge and a primary mass of 250 m_e. The average energy loss of the secondaries is assumed to be $-dE/dx = aE + b$, where a and b are constants depending on the material in which the secondaries are produced. The results of observation and theory may then be compared and an estimate of the mass of the primary particles made.

CHAPTER VI

INDIRECT METHODS OF MESON MASS DETERMINATION

I. RANGE AND CURVATURE

Discussion of the method and equations involved. This method is convenient since it does not involve measurement of specific ionization losses and is therefore independent of any special assumptions underlying the ionization loss formula given in Appendix II.

Neither $H\rho$ nor range R determines the velocity of a particle directly. From Eq. 27 giving M/m_e in terms of $H\rho$ and velocity we have

$$H\rho = 1704 \frac{M}{m_e} \frac{\beta}{(1-\beta^2)^{\frac{1}{2}}}, \tag{5}$$

and from Appendix III we find the range in air may in general be represented by an equation of the type:

$$R = \frac{M}{m_e} g\left(\frac{\beta}{(1-\beta^2)^{\frac{1}{2}}}\right) \tag{6}$$

where Z has been assumed to be 1 and g is a functional notation. It follows from Eq. 6 that $R/(M/m_e)$ is a function of only $\beta/(1-\beta^2)^{\frac{1}{2}}$.

Hence,

$$\rho \frac{H}{R} = 1704 \frac{\beta}{(1-\beta^2)^{\frac{1}{2}}} / g\left(\frac{\beta}{(1-\beta^2)^{\frac{1}{2}}}\right)$$

$$\rho \frac{H}{R} = h[\beta/(1-\beta^2)^{1/2}], \qquad (7)$$

where $H\rho$ is expressed in gauss cm. and R in cm. of air. The function $h[\beta/(1-\beta^2)^{1/2}]$ has been plotted from calculated values in Fig. 11 (72), curve 4. A measurement of $H\rho$ and R therefore indicates $\beta/(1-\beta^2)^{1/2}$. M/m_e may then be obtained from either Eq. 5 or Eq. 6.

As the range of a given particle is a function of velocity only, one can write $R = k\, M\, f(v)$, where $f(v)$ is some function of velocity and k is a constant to be determined. (This is true for relativistic as well as non-relativistic energies.) For all particles starting with the same initial velocity $R_1/R_2 = M_1/M_2$. When the velocities are the same, we also have $(H\rho)_1/(H\rho)_2 = M_1/M_2$. If we take the second particle a proton and use the empirical curves given by Livingston and Bethe (73) to find the range of a proton with a given velocity, we can find the mass M_1 of a particle of range R_1 and $H\rho = (H\rho)_1$ in terms of R_1, which will give M_1 by a measurement of its range, Similarly with the curvature. Hence, the mass of a particle may also be found by comparing its range or curvature to that of a proton of the same velocity.

Also, a reasonable value for M_1 may be assumed, M_2 be taken as the mass of a proton, and the range R_2 of the proton calculated from the previous relation using the measured value of R_1. Then the empirical curves mentioned will give the

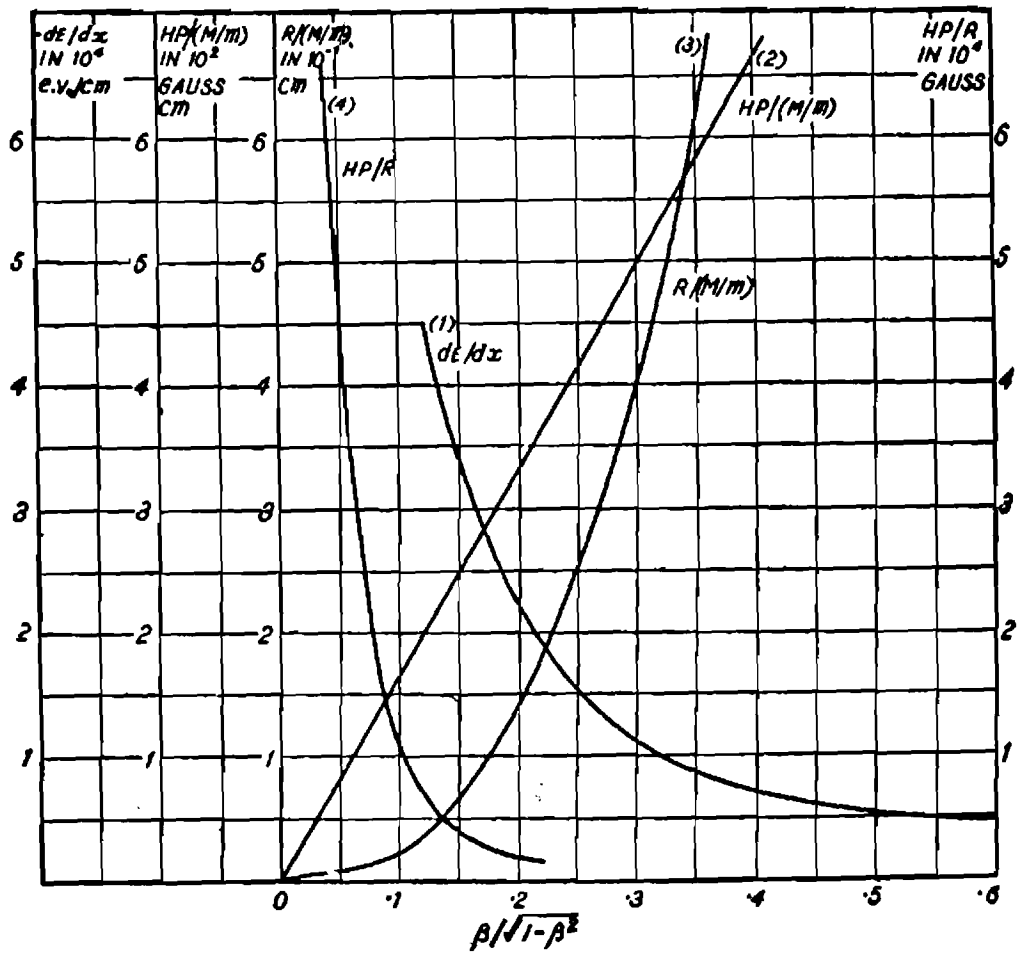

Figure 11. $-dE/dx$, $H\rho/(M/m_e)$, $R/(M/m_e)$, and $H\rho/R$ plotted as a function of $\beta/(1-\beta^2)^{\frac{1}{2}}$. The m_e is replaced by m on the graph.

velocity of the proton which, for the relation $R_1/R_2 = M_1/M_2$, must be the same as that of the particle of mass M_1. The correct value of M_1 will then be such as to satisfy Eq. 24 (relating a particle's curvature in a magnetic field with its mass and velocity) which, for $Z = 1$ and our purposes, may be written

$$\frac{M_1 \beta c^2}{(1 - \beta^2)^{\frac{1}{2}}} = (H\rho)_1 e ,$$

where $(H\rho)_1$ is obtained experimentally.

Corson and Brode (1) give the relation between range and velocity as closely approximating the equation $R = kv^n$ or $R = k\,(H\rho)^n/M^n - 1$, where n, as given by Corson and Brode, has a value varying from 3.45 to 3.70 for 10^4 gauss cm. $< H\rho < 10^5$ gauss cm. and $80 < M/m_e < 300$. From this is obtained

$$R = \rho / [\, n(d\rho/dR)] .$$

Thus it is seen that ρ and $d\rho/dR$, when determined from cloud chamber tracks of a particle, give sufficient information to determine the range of the particle and so the mass.

Types of apparatus used. The cloud chamber used to determine range and curvature for mesons is usually mounted in a permanent magnet supplying a field in the chamber sufficient to deflect the heavily ionizing mesons. This field is usually of several thousand gauss. The chamber is counter-controlled by a series of counter arrangements. If incoming

radiation is heterogeneous, horizontal metal plates are often placed in the cloud chamber to distinguish the mesons. Often, two cloud chambers are used. A typical arrangement of cloud-chambers and counters is shown in Fig. 12 (74). The four-counter telescope including the 10 cm. lead filter below the top counter was designed to eliminate the effects of other components of cosmic radiation. The upper cloud chamber was used to measure the curvature of the mesons selected by the counters, and the lower chamber to observe the corresponding penetration of the mesons, their ability to produce secondary radiations, and their ranges.

Brode (75) assembled cloud chambers above and below the gap in a permanent magnet. The curvature of the mesons could be determined from an accurate measurement of their change of direction above and below the magnet. Below the set of chambers was placed a large cloud chamber in which meson ranges could be measured. A detailed description of this apparatus as it was used to measure mass by momentum loss is given in Section II following. It has been pointed out here merely to illustrate a possible arrangement of cloud chambers to determine meson curvature and range.

Specific experiments. The lower track in Fig. 13 (76) is the trace of a positive meson (assuming it is moving downward) with an $H\rho$ of 1.05×10^5 gauss cm. It does not ionize very heavily and, since it does not stop in the chamber, its range can only be determined as being greater than that

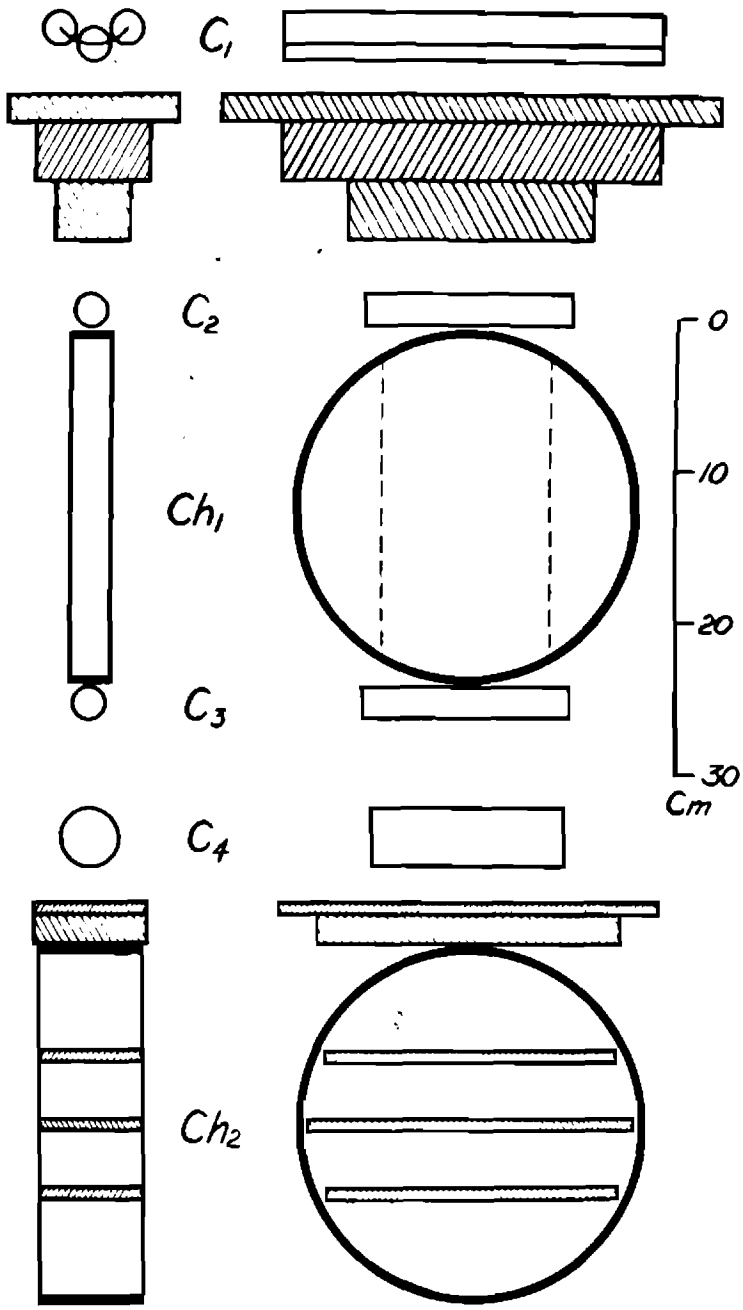

Figure 12. Apparatus for the study of the range, curvature, energy, and production of secondaries by mesons. The upper cloud chamber is in a magnetic field of approximately 7,000 gauss; the cross hatched material is lead; C_1, C_2, C_3, and C_4 are counters which control the simultaneous expansion of the two cloud chambers.

Figure 13. A positive meson of mass approximately 250 m_e as obtained by range and curvature data.

measurable (14 cm.). The nomograph in Fig. 1 shows the mass to be about 250 m_e using the above values of curvature and range.

Fig. 14 (77) shows a heavily ionizing track of unusually great curvature. A wire in the developing tank caused the heavy vertical white band to appear; the track in the right-hand view, however, was easily visible on the negative showing the trace to enter the illumination at the right and stop at its left end. The $H\rho$ at the center is 4.1×10^3 gauss cm. Here the residual or remaining range is 1.8 cm. of air equivalent. These values of range and curvature give a mass range of 10 m_e to 50 m_e from the nomograph in Fig. 1. This value is consistent with the ionization density. Bethe corrects this value by considering multiple scattering (see Chapter X) and shows it to be consistent with a mass of about 200 m_e.

Meson mass values. Table II shows the values of meson mass obtained by several workers from range and curvature measurements. The consistency of the results obtained is a proof of the accuracy of the method. Table III contains meson mass values obtained by Rüling and Steinmaurer (78) using the relationships of $H\rho$, R, and M of mesons to those of protons.

Ruhlig and Crane (87) utilized the rate of change of the radius of curvature (0.6 ± 0.2 cm./cm.) with the radius of curvature (9 cm.) to obtain a meson mass of (120 ± 15) m_e, assuming the particle to be singly charged, and (120 ± 30) m_e,

Figure 14. A negative meson whose curvature, range, and scattering show it to have an unusually low mass of 30 m_e.

TABLE II

MESON MASSES FROM THE RANGE AND CURVATURE METHOD

Mass ($\times 1/m_e$)	$H\rho$ (gauss cm.)	R (in cm. air)	Reference
<200	$>5 \times 10^5$		Brode and Starr (79)
<300	6×10^4		Neddermeyer and Anderson (17)
~ 350	5.5×10^4	>4	Anderson and Neddermeyer (16)
184-263	4.9×10^5	6.5	Nishina, Takeuchi, and Ichimiya (80)
<204	5.5×10^4	>18	Brode, MacPherson, and Starr (81)
220 ± 35	1.74×10^5		Neddermeyer and Anderson (17)
30 ± 20	4.1×10^3	1.8	Hughes (68)
140^{-}_{-} (+220, -60)	3.7×10^4	13	
175 (+55, -30)	1.03×10^5	10	
175 (+140, -60)	1×10^5	10	
250 (+190, -110)	1.05×10^5	20	
250 (+380, -100)	6.4×10^4	14	
270 (+330, -110)	2.8×10^5	30	
170 ± 9	3.88×10^4	7.3 - 8.1	Nishina, Takeuchi, and Ichimiya (82)
20	8×10^3	8.3	Maier-Leibnitz (41)
100 ± 30	3.4×10^4	16.5	
120 ± 30	3×10^4	6.5	
55 ± 30	5×10^4	3.6	
170 ± 100	3.8×10^4	6.0	

TABLE II (continued)

MESON MASSES FROM THE RANGE AND CURVATURE METHOD

Mass ($\times 1/m_e$)	$H\rho$ (gauss cm.)	R (in cm. air)	Reference
<1000	1.4×10^5	>5	Anderson and Neddermeyer (16)
192±5*			Retallack and Brode (83)
474			
538			
588			
717			
80 (+105, -55)		12	Johnson and Shutt (84)
70 (+150, -55)		6.4	
250±70	8.3×10^4	41	Williams and Roberts (85)
(160-200)±30			Fretter and Brode (86)

*This figure is the average of 37 of a set of 41 mass values.

TABLE III

MESON MASSES USING RANGE AND CURVATURE RELATIONSHIPS OF MESONS AND PROTONS

Mass (x $1/m_e$)	ρ (in cm.)	R (in cm. air)	H (in oersteds)
230±42	21.2	4.0	1512
200±35	19.3	5.0	1625
127±15	14.0	3.6	1535
125±30	13.6	3.8	1535
115±20	12.4	3.6	1695
100±30	11.7	4.0	1550
90±15	11.4	5.4	1580
87±13	11.1	5.4	1580

for a more liberal rate of change of radius of curvature (0.6 ± 0.4 cm./cm.).

Variations in the method. Gardner and Lattes (88) have recently measured negative meson masses* by $H\rho$ and range measurements, where the radius of curvature in the field was determined by measuring the point and angle of incidence of separate meson tracks on the edge of a photographic plate. The range in the emulsion was measured with an eyepiece micrometer and this value, together with the path length through a one mil aluminum foil covering the plates, taken as the meson range. Black paper may be taken to cover the plates, but then the meson ranges cannot be measured accurately due to the uncertain thickness of the paper. The photographic plates used were Ilford Nuclear Research plates, type C2, with an emulsion thickness of 50 μ ; the exposure times were about 10 minutes. A picture of a meson track on one of the photographic plates is shown in Fig. 15 (88). Each plate shows about 50 meson tracks along its edge, with about 10 times as many heavy-particle tracks in the same area.

The mean mass of a total of 49 mesons produced in the cyclotron at Berkeley, California, was found to be $(313 \pm 16)\ m_e$. Scattering of the mesons in the aluminum foil and in the first 80 μ of the emulsion contributed the most important error.

---

*The mesons were produced in a carbon target by bombarding it with 380 Mev alpha particles produced in the 184-inch Berkeley cyclotron.

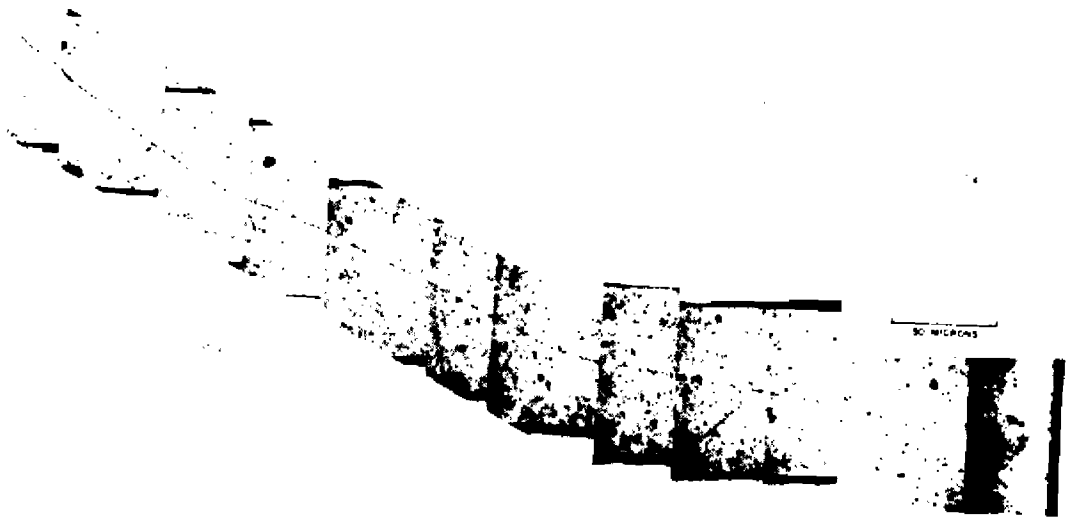

Figure 15. Track of a meson on photographic plates. The meson enters the edge of the photographic plate on the right and moves toward the left. Scattering in the track and an increase in grain density is noticeable toward the left.

The angle measurements could not be made closer to the edge because of the distortion of the emulsion on processing. Other errors were due to the lack of precision of location of the photographic plates.

Upon placing unwrapped plates in the cyclotron and inclining them to the meson trajectories in such a way that the mesons entered the emulsion through the top surface avoiding errors associated with the distortion at the edge of the plate, the following preliminary values (89) for meson masses were found:

heavy negative meson - 285 m_e,

heavy positive meson - 286 m_e,

light positive meson - 216 m_e.

The probable error in the measurements was hoped to be as low as two per cent.

By using Ilford C 2 and C 3 and Eastman NTB photographic plates, each of emulsion thickness of about 100 microns, Burfening, Gardner, and Lattes (90) found preliminary measurements indicating two groups of positive mesons (presumed to be π- and μ-mesons) having masses of about 300 and 200 m_e respectively. From $H\rho$ and range measurements of the light mesons on the plates due to decay of the heavy ones, the heavy meson masses measured greater than 260 m_e and the light meson masses between 150 and 230 times the electron mass.

Now that mesons can be produced at will under controlled conditions as was done at Berkeley, very definite mass values

of these particles will no doubt appear in the near future.

II. MOMENTUM LOSS

The change of momentum suffered by a fast particle after traversing a heavy metal plate of known thickness can be used for an accurate determination of mass in the non-relativistic region. It is to be noted that the momentum loss method (which is a combination of range and rate of change of curvature in passing through an absorber material placed in a cloud chamber) is in a sense a general method, the range and curvature method and the ionization and curvature method being special cases of this means. The three methods are dealt with separately in conformance with manners of presentation found in the literature.

Since the momentum loss method avoids difficult determinations of the density of ionization along the track and since the measurements of curvature of track in a magnetic field as described in the previous section and of thickness of material traversed are among the most direct in the whole field of cosmic-ray research, it has received much emphasis in recent years. Accuracy in this method is established only if the meson's velocity is not close to the speed of light. However, an abundance of data can be obtained since practically every meson whose curvature can be measured before and after penetration of the metal plate has a velocity in the acceptable range. Another noteworthy fact about this method is that the

law for the stopping power of matter for fast particles is, theoretically, exceedingly reliable. There are reasons why this method is poor for mesons of relativistic velocities.

If a meson has an energy large in comparison with its rest energy, its loss of energy, ΔE, in a given thickness of material will be, according to the theory of stopping power, practically independent of energy. Since, according to the relativistic relation between energy losses and momentum, $\Delta E \sim v\, dp$, the velocity v will be essentially a constant, the speed of light. Therefore, no matter of what mass a high-speed meson may be, it will lose the same amount of momentum in traversing a given thickness of a substance. For mesons of $H\rho \gg 4 \times 10^5$ gauss cm. and of relativistic velocity, the resolving power of the momentum loss method is found to be poor.

A meson's rate of energy loss per unit of distance for non-relativistic speeds may be approximated as

$$\frac{-dE}{dx} \sim \frac{K}{v^2} ,$$

where K is a constant. The mass M may then be expressed by

$$M \sim p(dp/Kdx)^{1/3} .$$

To obtain the percentage error in M, the percentage error in p or corresponding $H\rho$ must be considered, as well as the sum of one-third the percentage errors in the momentum loss measurements (if the loss is small compared to p), measurements of

stopping material thickness, and determination of the theoretical constant of the stopping power formula.

Discussion of the method and equations involved. Cloud chambers enable a physical measurement of the rate of change of momentum of a particle. A particle continuously loses energy and hence momentum along its path by ionization, radiation, etc., which causes the value of $H\rho$ for the particle to change from point to point along its path. Since for a medium of low density the various losses per cm. of track are very small, the change in ρ from point to point may be considered a constant over a fairly long path and an average curvature determined. The track inside a Wilson chamber placed in a magnetic field is assumed as constant.

However, for media of higher density such as lead or gold, the energy lost per cm. is comparatively high, depending on the particle. Therefore, the curvature of the track of a particle in a Wilson chamber will change if it were made to traverse say a lead plate several cm. thick. From a measurement of the separate curvatures above and below the lead plate, the rate of change of momentum could be obtained.

From Eq. 28 relating rate of change of momentum and curvature of a particle with distance,

$$\frac{d\,(H\rho)}{dx} = \frac{1}{300}\, c\, \frac{dp}{dx}$$

where x is the thickness of material traversed and Z is taken as unity, and from Eq. 35 giving E in terms of v and p,

$$\frac{d(H\rho)}{dx} = \frac{1}{300}\frac{1}{\beta}\frac{dE}{dx}.$$

Since Appendix II shows (-dE/dx) to be a function of $(\beta/(1-\beta^2)^{1/2}$, for Z = 1 we can in general write

$$\frac{d(H\rho)}{dx} = f[\beta/(1-\beta^2)^{1/2}], \qquad (8)$$

where f is the functional notation.

As the variation of (-dE/dx) with $\beta/(1-\beta^2)^{1/2}$ may be obtained from Eq. 34 (some values are given in Table XI in the Appendix and plotted in Fig. 11), the values of $d(H\rho)/dx$ corresponding to any value of $\beta/(1-\beta^2)^{1/2}$ can be calculated from Eq. 8. Table IV (91) gives calculated values of $d(H\rho)/dx$ in lead as functions of $\beta/(1-\beta^2)^{1/2}$. These values are shown graphically in Fig. 16 (56). From this curve and the measured value of $d(H\rho)/dx$, $\beta/(1-\beta^2)^{1/2}$ may be obtained. M/m_e is then obtained by means of Eq. 27 (M/m_e in terms of $H\rho$ and velocity).

The most common procedure for mesons, however, is to make measurements of the change in $H\rho$ and, with a consideration of the particular meson range in a given material other than air, determine the mass of the meson.

From Eq. 7, the range of a particle of mass M and charge number Z may be expressed by

$$R = \frac{H\rho}{f[\beta/(1-\beta^2)^{1/2}]}.$$

TABLE IV

VALUES OF $d(H\rho)/dx$ IN LEAD AS A FUNCTION OF $\beta/(1-\beta^2)^{\frac{1}{2}}$

$\beta/(1-\beta^2)^{\frac{1}{2}}$	β	$d(H\rho)/dx$ (in gauss-cm. per cm. lead) (x 1/105)
0.3	0.288	8.33
0.4	0.372	4.33
0.5	0.449	2.71
0.6	0.515	1.91
0.7	0.574	1.45
0.8	0.625	1.15
0.9	0.667	0.94
1.0	0.706	0.80
1.1	0.739	0.72
1.2	0.768	0.67
1.3	0.793	0.62
1.4	0.814	0.56
1.5	0.832	0.545
1.6	0.848	0.543
1.8	0.874	0.542

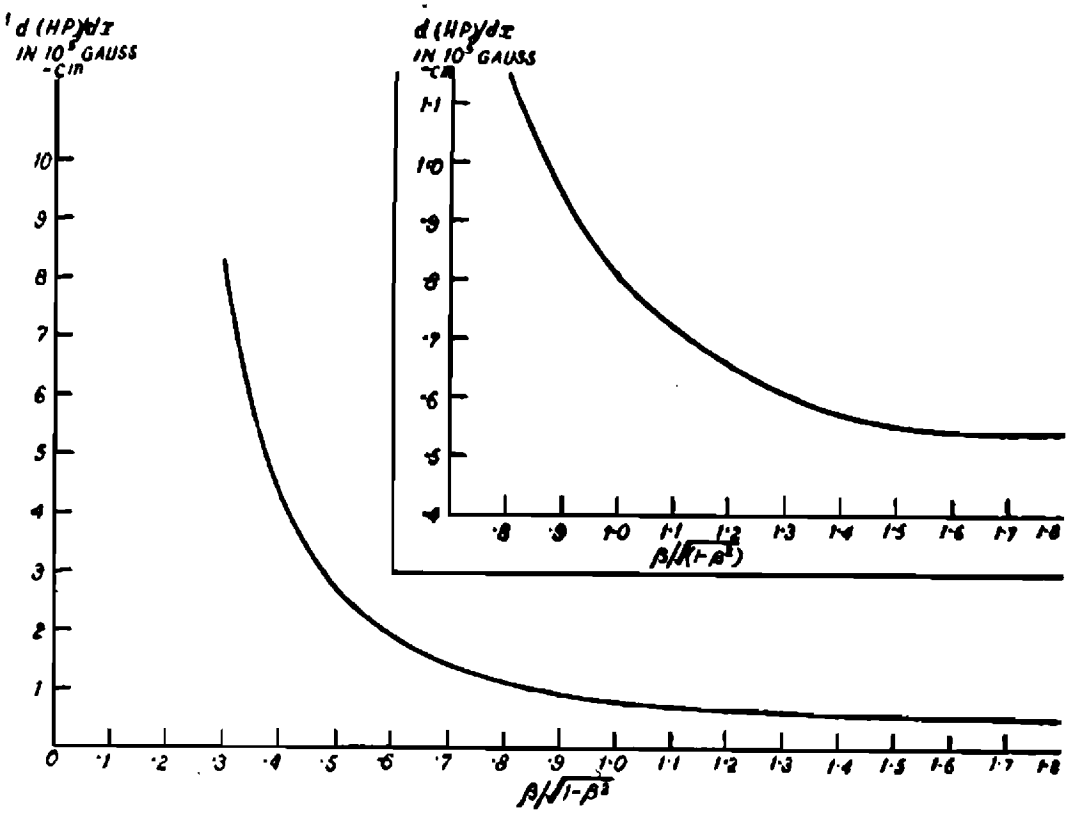

Figure 16. $d(H\rho)/dx$ plotted as a function of $\beta/(1-\beta^2)^{\frac{1}{2}}$.

The connection between range and energy or momentum in the form which is convenient for general use and at the same time suited for determining the mass of the meson by the momentum loss method will now be stated. The range of a particle of mass M and charge number Z may be considered to depend on any one of the following quantities (92):

kinetic energy	$E = Mc^2(\cosh \Theta - 1)$
momentum:	$p = Mc \sinh \Theta$
magnetic rigidity:	$H\rho = M(c^2/Ze) \sinh \Theta$
velocity:	$v = \tanh \Theta,$

where Θ is here a dimensionless number.

If the range is expressed in g./cm.^{2} it will fluctuate in an irregular way from element to element because of the lack of any precise relation between atomic number Z' and atomic weight, A. For this reason, the range is usually expressed in terms of a dimensionless range number defined as follows (92):

$$\text{Range Number} = 4\pi \cdot \text{Avogadro's number} \cdot \left(\frac{e^2}{m_e c^2}\right)^2 \cdot \left(\frac{Z'}{A}\right) \cdot (\text{range in g./cm.}^2)$$

$$= (0.601 \text{ cm.}^2/\text{g.}) \cdot (Z'/A) \cdot (\text{range in g./cm.}^2).$$

For lead of density 11.3 g./cm.^{3}, range number equals thickness multiplied by 2.68 cm.$^{-1}$

In terms of the range number, Eq. 29, the energy loss equation, takes the form (93)

$$\left(\frac{-dE}{dx}\right) = \left(\frac{Z^2 m_e}{M}\right) \text{(range number)}$$

$$= \int^{\theta} \frac{d\,(\cosh\theta + \cosh^{-1}\theta - 2)}{\ln\,(2\,m_e c^2/I) + 2\,\ln\sinh\theta - \tanh^2\theta} \qquad (9)$$

upon replacing Tm by its equivalent value. Numerical integration of Eq. 9 gives the curves shown in Fig. 17 (97) which illustrate how the meson mass is determined from $H\rho$ measurements before and after a meson traverses a plate of known thickness and its range in a given material.

If a meson ($Z = 1$) with an $H\rho$ of 528,000 gauss cm. passes through a 3.70-cm. lead plate, corresponding to a range number of 9.92, and emerges with an $H\rho$ of 238,000 gauss cm., the change in $H\rho$ is plotted as point A in the upper diagram of Fig. 17. The secant CD must be parallel to OA but the position of C and D individually remain to be found. By constructing a large transparent model of the template in the lower right hand corner of the Figure with lines SC and SD drawn such that D'B':C'B' = DE:CB = 528,000 gauss cm:238,000 gauss cm. = 2.22, the template, with its rulings parallel to OA and with corresponding points C'D' or CD, etc., kept on the curve for lead, may be moved until the prolongation B' of C'D' or B of CD, etc., lies on the line QR extended. From the location of D it is seen that $1.49 = (m_e/M)\,(H\ /1704) = 510\,(m_e/M)$, where the $H\rho$ is 528,000 gauss cm. This gives $M = 209\ m_e$.

Types of apparatus used. J. C. Street (94), who first experimentally investigated range-momentum relationships for

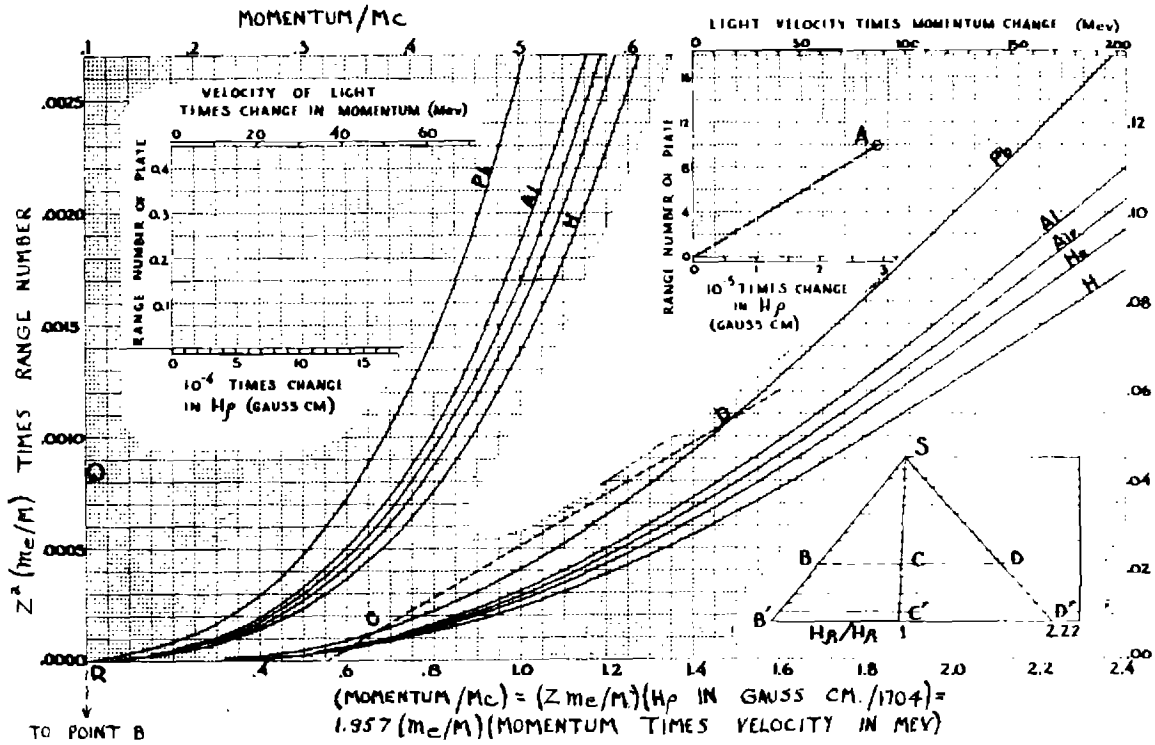

Figure 17. Calculated relation between range and momentum for hydrogen and helium nuclei and for mesons. For the stopping materials computations were based on the following values of the mean ionization energy: For atomic hydrogen (95), 1.103 ($m_e e^4/2\hbar^2$), for helium (96), 3.19 ($m_e e^4/2\hbar^2$), and for air ($Z^\dagger = 7.22$) (97), 5.92 ($m_e e^4/2\hbar^2$). For lead and aluminum the ionization energy was determined from Bloch's formula (98) with the constant of proportionality based on the data of R. R. Wilson (99).

mesons, used two cloud chambers, one in a magnetic field of 7000 gauss, the second containing three one-cm. thick lead plates and vertically in line beneath the first. The apparatus was counter-controlled and hence the meson curvature could be observed in the upper chamber and its range in lead in the simultaneously expanded lower chamber. There was an additional three cm. of lead between the two chambers.

Similar apparatus is still in use. Fretter (100) used an upper cloud chamber 12 inches in diameter, three inches deep, and filled with argon at 1.15 atmospheres containing an unsaturated mixture of water and ethyl alcohol. The chamber was placed in a 5300 gauss magnetic field produced by an electromagnet. In order to prevent turbulence of the tracks due to convection currents, the temperature of the upper cloud chamber had to be maintained uniform within 0.5° C.

The lower cloud chamber used by Fretter was 16 inches in diameter, nine inches deep, and contained eight 1/2-inch thick lead plates placed such that the track length between each pair of plates was about one inch. The chambers were controlled by triple-coincidence Geiger counters, the lead over the upper counters serving to select penetrating particles and to facilitate their being stopped in the lower chamber. Fig. 18 (101) illustrates the arrangement described.

To increase the accuracy with which the range was observed, Retallack and Brode (102) placed a cloud chamber below the electromagnet with fifteen 1/4-inch thick plates

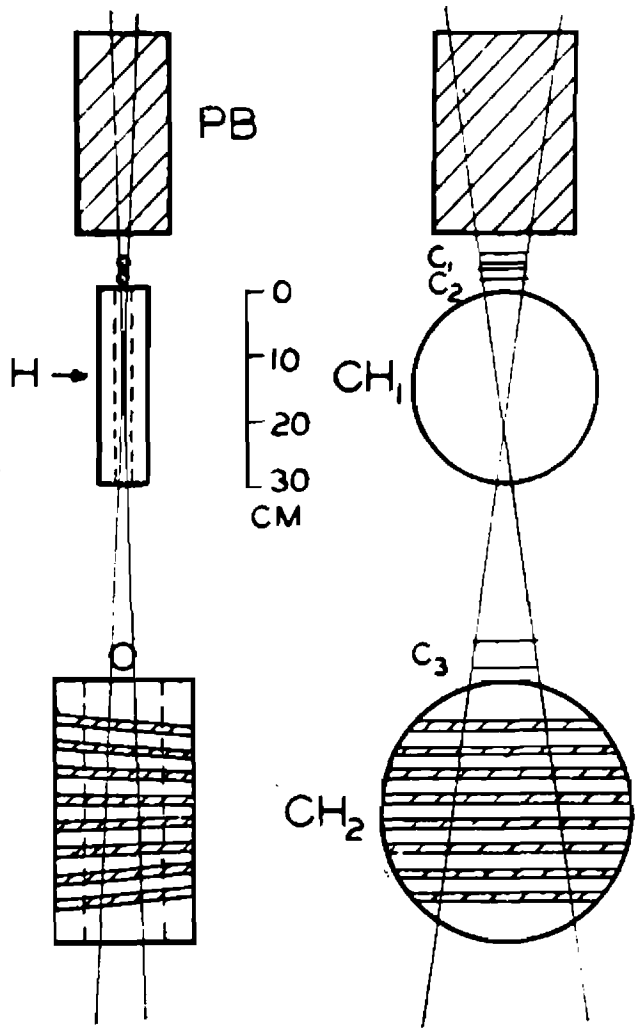

Figure 18. A schematic drawing of two cloud chambers CH_1 and CH_2. The chambers are expanded simultaneously upon the passage of a meson through the counters C_1, C_2, and C_3, the particle's momentum being determined in the upper chamber and its range in lead in the lower. The dotted lines indicate the extent of the illuminated region.

inside. The volume of this chamber (20" x 20" x 10") was large enough so that even particles with appreciable deflection in the lead plates could still be followed to the end of their range. The chamber was kept at constant temperature to avoid initial turbulence in the chamber. By measuring the curvature of 60 no-field tracks, they found that using air in the upper chamber instead of helium (as had been the original intention) decreased the error due to turbulence more than enough to offset the increase in the scattering area. The lower cloud chamber, in which the range in lead for mesons was measured, was a truncated pyramid 20 inches square at the middle of the illuminated regions and 17 inches deep. Triple-coincidence Geiger counters expanded the cloud chambers. At first 12 inches and later 16 inches of lead were placed above the apparatus to select penetrating particles and to increase the number of particles stopping in the lower chamber.

Fluctuations of the magnetic field in the electromagnet used by Fretter, and Retallack and Brode, has caused errors. The heat from the magnet caused turbulence which disturbed curvature measurements. New equipment has been constructed by Brode (103) in which a permanent magnet replaces the electromagnet. The apparatus is found to be cheaper. Fig. 19 (103) shows the general arrangement of the apparatus. The momentum of the mesons passing through the 5000-gauss gap of the permanent magnet is inversely proportional to the angle

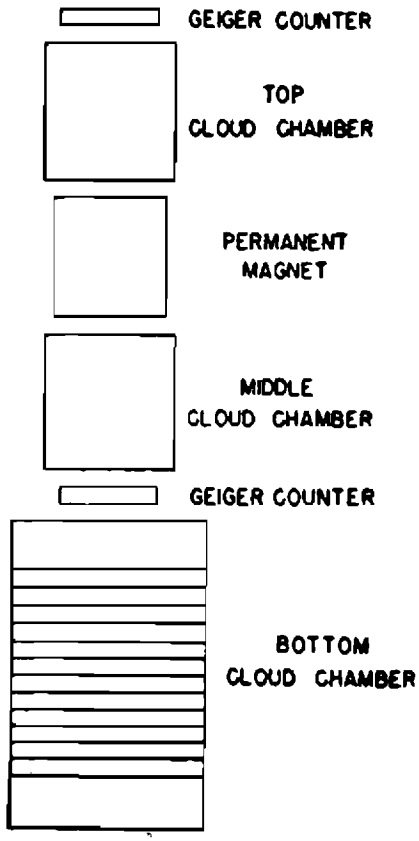

Figure 19. Arrangement of apparatus for meson mass measurement by the method of momentum loss.

of deflection in the magnetic field. A window of beryllium foil 10 mils thick in the bottom of the top chamber and in the top of the middle chamber reduced errors in angle due to scattering in the walls of the chamber. Helium in the space between the poles of the magnet further reduced possible scattering. There are 13 lead plates of 0.6 cm. thickness in the bottom cloud chamber. The top and middle chambers are photographed with one camera, the lower chamber being photographed by a stereoscopic camera so that the motion of the particle may be studied with a stereoscopic viewer. Forward or backward scattering is detected by mirror images at each side of the central picture taken of the upper two chambers.

Specific experiments. Fig. 20 (104) shows a meson stopped in one of the lead plates placed in a cloud chamber. The magnetic field was measured by a flip coil connected to a ballistic galvanometer. Fretter (105), in order to find the range of the particle in lead after it left the upper chamber, added to the amount of lead traversed in the lower chamber the thickness of lead to which the material between the chambers was equivalent calculated by means of energy loss equations given by Rossi and Greisen (106). This addition amounted to about .5 inches of lead. A fairly small correction for the additional material penetrated when the meson was scattered, or went through the lower chamber at an angle, was calculated by measuring the projected angles on the film between the track and the normal to the plate.

Figure 20. A meson, with $H\rho = 820 \times 10^3$ gauss cm. in the upper chamber, being stopped in the sixth of a series of lead plates with no increase in ionization above the plate. Its range is 7.90 to 9.62 cm. of lead equivalent and its mass is (244 ± 37) m_e.

When a meson is stopped in one of the plates of a cloud chamber, its range cannot be measured accurately since it is not known how deep the meson penetrated the plate. Observation of the ionization before penetration, however, helps to estimate this depth, for, if the meson had twice or more normal ionization, it may be assumed to have stopped in the first half of the plate. If its ionization was normal, the depth of penetration is assumed to be the full thickness of the plate since poor illumination may have been the only cause for the apparent lack of increase of ionization.

Since mesons of mass about 200 m_e are expected to have radii of curvature of 0.75 to 2.0 meters, the pictures of such tracks in the upper chamber are often picked out and the pictures of the lower chamber carefully examined to see if the meson had been stopped. Also, when the pictures from the lower chamber indicate a stopped meson, the corresponding upper-chamber picture is sought. Many of the particles in a given set of pictures are found to be scattered out of the illumination and are usually not considered for mass determinations. A very large scattering after entering the last plate, so that the meson travels a considerable distance before stopping, will lead to a greater computed mass value than the actual because the true range will be underestimated. Mesons which have not penetrated a sufficient number of plates must be rejected. They are not used because of the possibility of a meson stopping in the first or second plate and ejecting

an electron to go on to the next plate as if it were the original meson. The probability of this occurring after the meson has traversed several plates is negligible.

Fig. 21a (107) shows a plot by Fretter of the $H\rho$ versus range of mesons he observed to have stopped or appear to have stopped in his chamber. Fig. 21b (107) represents those particles for which $H\rho$ and range were accurately determined and shows a magnified section of the $H\rho$ range plot. The circles in Fig. 21a represent relatively accurate $H\rho$ and range values, the crosses known range and uncertain $H\rho$ (due to turbulence), and the vertical lines mesons that were leaving the illuminated region. It is seen that the mesons certain in both $H\rho$ and range group together giving the impression of no serious straggling.

The curves in Fig. 21b are the theoretical curves as given by Wheeler and Ladenburg (108) and discussed previously. The lines plotted on the diagram are the data for the various stopped particles, with the horizontal projection of each line representing the estimated uncertainty in $H\rho$ and the vertical projection representing the uncertainty in range.

Pictures of positive and negative mesons in Brode's apparatus described above are shown in Fig. 22 (109). Seventy eight determinations were made using the Wheeler-Ladenburg range-momentum curves giving the mean meson mass value as $(215\pm2)\ m_e$. Johnson and Shutt (110) have obtained a picture (Fig. 23) of a meson track ending in argon of 1.3 atmospheres

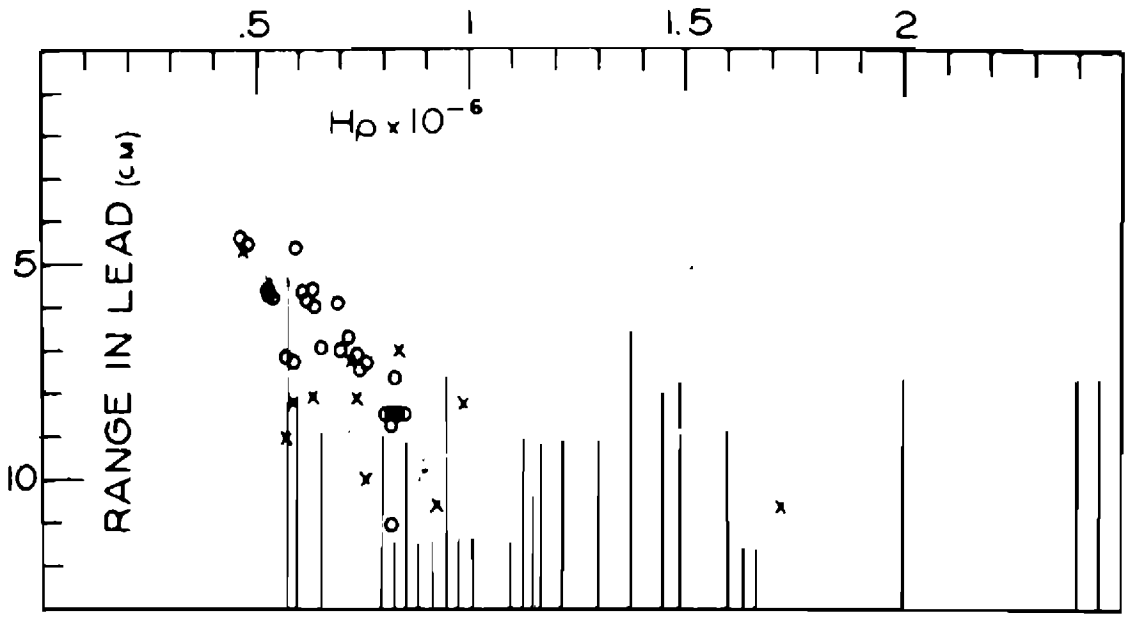

Figure 21a. Graph showing range and Hρ for mesons observed by Fretter. Circles represent particles for which both Hρ and range were accurately determined while crosses indicate that the Hρ was uncertain and vertical lines indicate that the range could only be given a minimum value.

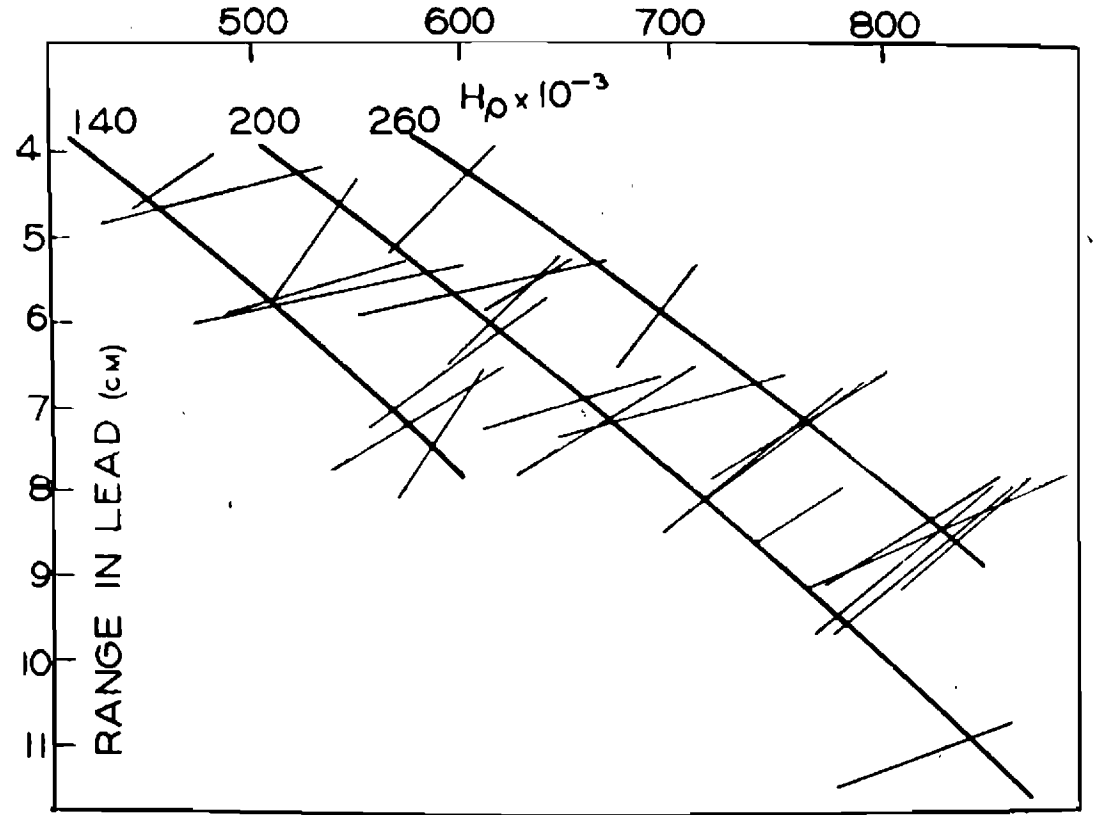

Fig. 21b. Graph showing data for particles of Fig. 21a for which Hρ and range were accurately determined. Each line represents the data for an individual particle, the horizontal projection giving the uncertainty in Hρ and the vertical projection giving the uncertainty in range. The curves are the calculated range-momentum relationships for mesons of mass 140, 200, and 260 electron masses.

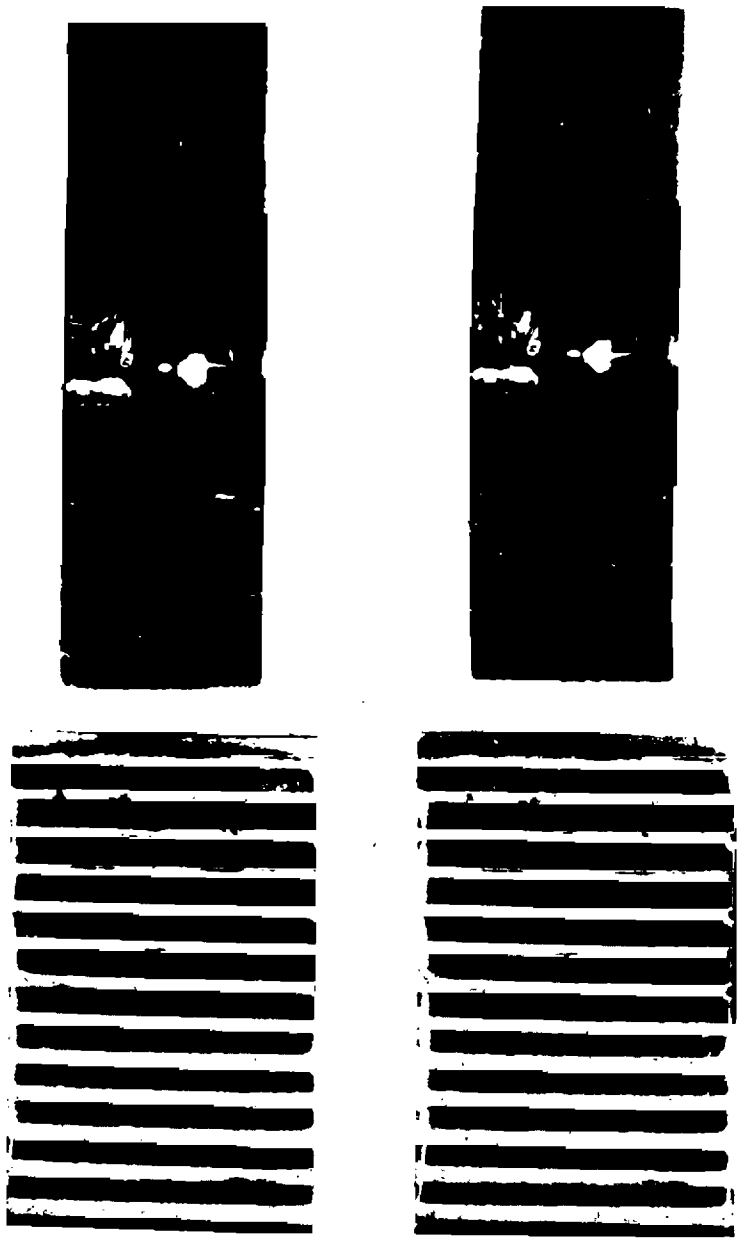

Figure 22. The left-hand view is a negative meson with a measured mass of $(225\pm20)m_e$; the right-hand view is a positive meson with a measured mass of $(215\pm20)m_e$.

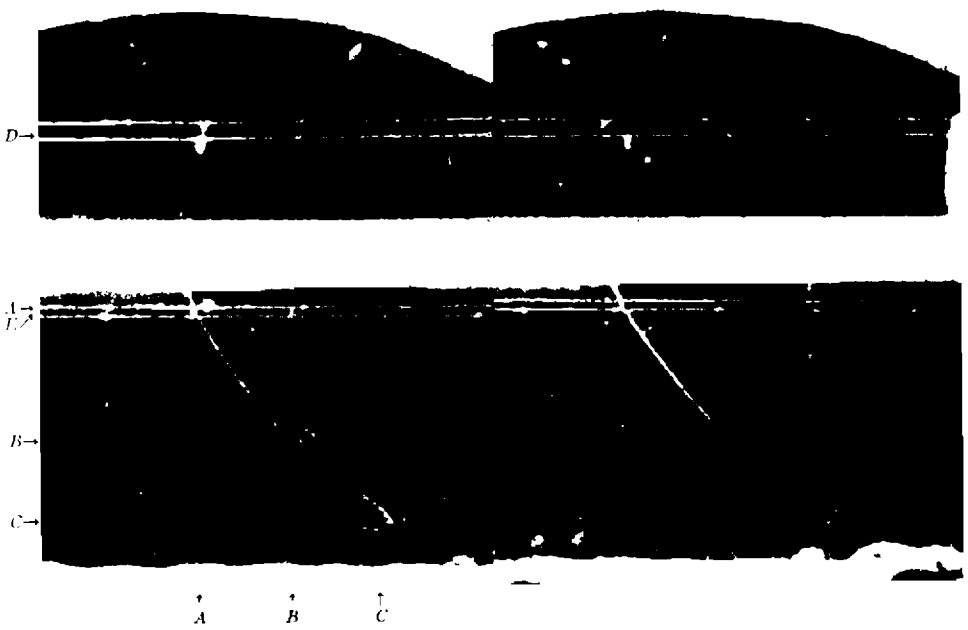

Figure 23. Stereoscopic photographs of a negatively charged meson stopping in the gas of a cloud chamber. There is a lead plate 1 cm. thick between the two compartments of the chamber. D and E indicate scales aiding in the exact determination of geometrical positions.

after having traversed a lead plate 1 cm. thick. The magnetic field is 1150 gauss, the curvature of the track above the plate about (150±50) cm., and its range approximately 1 cm. of lead. This gives a value of (100±50) m_e for the meson mass. For this computation the energy-momentum curves of Rossi and Greisen were used (111). The meson undergoes two single scatterings of about 3° each at A and B, and it ceases to ionize at C.

Neddermeyer and Anderson (112), by placing a Geiger counter inside a cloud chamber and coupling it by means of a coincidence circuit to a second counter placed above the chamber, measured a residual meson range after passing through a lead plate of 2.9 cm. From curvature change and range values a mass of 240 m_e was obtained.

Meson mass values. Fig. 24 gives the values of meson mass as computed by Retallack and Brode (113) using the method of momentum loss. The diagonal lines have their centers at the observed values of range and curvature. The extent of the probable errors ($\pm \Delta R$ and $\pm \Delta C$) are given by the projections on the R and C coordinates. Retallack and Brode (114) found a value of the mass which best fits the data shown in Fig. 24 by the least squares adjustment. Taking 37 observations, the mean value of the mass of the meson was found to be (215±4) m_e. This and other meson mass values obtained by the momentum-loss method is given in Table V.

A weighted mass spectrum of the values found by Fretter,

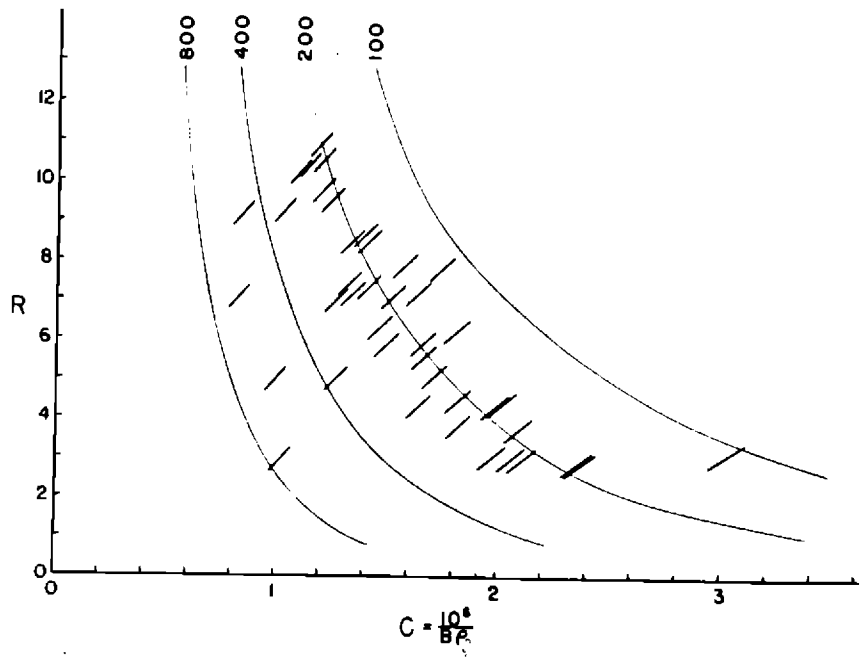

Figure 24. Meson mass measurements of Retallack and Brode using the momentum loss method. Each observation is plotted as a function of range, R, in centimeters of lead vs. curvature, C, in a unit magnetic field. The length of the lines representing individual observations is a measure of the probable error assigned to the measurement.

TABLE V

MESON MASSES FROM THE MOMENTUM LOSS METHOD

Mass ($\times 1/m_e$)	Reference
215 ± 4*	Retallack and Brode (116)
202 ± 5	Fretter (53)
~ 240	Neddermeyer and Anderson (117)
218 ± 5**	Brode (118)
161 250 226	Anderson and Neddermeyer (16)
170 ± 20	Wilson (52)
~ 200	Nishina, Takeuchi, and Ichimiya (80)
244 ± 37	Fretter (53)
> 188	Street (94)
~ 360	Neddermeyer and Anderson (17)
215 ± 2***	Brode (118)

*This value is a mean value of the meson mass deduced from a consistent set of 37 observations.

**This value is a mean value of the meson mass deduced from 18 mass determinations between 150 and 350 times the mass of the electron.

***This meson mass value is a mean value of 78 determinations of Fretter, Retallack, and Brode.

Retallack, and Brode, who have done most of the momentum loss measurements, is shown in Fig. 25 (103). The mean of the combined series of measurements leads to a value of (215±2) m_e for the meson mass. The probable error of ±2 is entirely that due to the statistical errors in range and curvature of the particles.

Variations in the method. Nishina, Takeuchi, and Ichimiya (115) assumed a meson mass, calculated its initial and final energies, and thus found the loss of energy due to collisions within lead. This energy loss was then theoretically calculated using Bloch's formula (119), the assumed mass, and the initial energy. The correct mass was found to be, by adjusting the mass value in such a way that both values of the energy loss agreed,

$$M = (180 \text{ to } 260)\ m_e.$$

Upon using a relativistic value of the maximum energy transferred from the meson to a free electron in a direct collision and the data:

$H\rho = (7.4 \pm 0.1) \times 10^5$ oersted cm. (before traversing plate)

Thickness of lead plate = 3.5 cm.,

Path length inside lead = 4.8 cm. (meson struck lead plate at an angle of 47°),

and $H\rho = (5.0 \pm 0.1) \times 10^5$ oersted cm. (after traversing plate), the meson mass was given as $M = (180 \pm 20)\ m_e$.

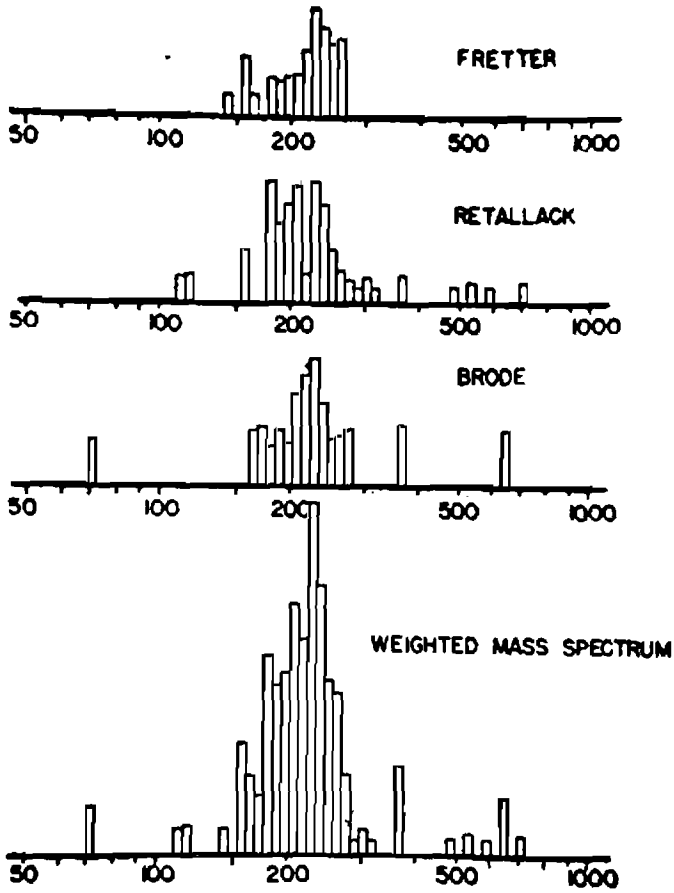

Figure 25. Weighted meson mass spectrum combining the values of Fretter, Retallack, and Brode using momentum loss method of mass determination.

III. IONIZATION AND CURVATURE

The largest number of meson mass determinations have been made from measurements of the curvature of particle tracks in a magnetic field together with a count of the average number of ions formed per cm. length of the track.

Two methods have been used. Method A requires the simultaneous measurement of primary ionization of slow electrons and curvature of the particle in a magnetic field. The former is determined by counting the number of distinct groups of droplets per cm. of path length in sharply defined Wilson chamber tracks giving the number of ion pairs formed. This is known as the "gap" method. In method B, the expansion of the cloud chamber is delayed to enable the oppositely charged ions produced along the track of the ionizing particle to separate under the influence of an applied electric field. The measurements then made do not give the primary ionization, but the probable ionization, that is, the primary ionization plus the ionization produced by secondaries of energy lower than a certain critical energy.

Method A

Discussion of the method and equations involved. From sharp delayed expansion tracks, the number of primary ions may be estimated in an indirect way attributed to Williams (120). If I_o be the true specific ionization, the mean free path between two ions is $1/I_o$. The number of mean free paths in a

total track length L as observed in a cloud chamber is $I_o L$. The probability p_o that a gap of length l will occur in the total length L of the track is given by

$$p_o = I_o L \, e^{-I_o l}. \qquad (10)$$

Large free paths appear as gaps in the track, the true gap being the observed gap plus a correction for the diffusion of the ions; this correction factor is approximately the width of the track.

If the number of gaps greater than 1 cm. occuring in a measured total meson track length L is observed, the value of I_o can be obtained from Eq. 10. If only the big gaps are counted, no large statistical error appears though the number of such gaps is small since the exponential term in Eq. 10 varies rapidly with I_o. The biggest error actually comes from the measurement of the gap length. From a knowledge of I_o, the average number of ions produced per cm. of path length, the average value of the energy loss -dE/dx can be determined, assuming that 32 electron volts are needed for the production of each ion pair.

From Eq. 34, giving (-dE/dx) in terms of the velocity, $\beta/(1-\beta^2)^{\frac{1}{2}}$ can be calculated having determined -dE/dx since (-dE/dx) is a function of $\beta/(1-\beta^2)^{\frac{1}{2}}$ only. Then, measuring the $H\rho$ of the same meson simultaneously with its specific energy loss, the mass can be obtained directly from Eq. 27

relating M/m_e, $H\rho$, and the velocity. A compromise has to be made, however, since accurate measurement of curvature requires a sharp track whereas determination of $-dE/dx$ by the method of droplet-counting implies a broadened track. In Fig. 11, $H\rho/(M/m_e)$ has been plotted against $\beta/(1-\beta^2)^{1/2}$ (curve 2). The mass of the meson can be read off directly from the curve by determining dE/dx and $H\rho$.

From the work of Williams and Terroux (121), the logarithm of direct counts of the number of primary ions per cm. of path produced by fast β-particles passing through a gas in a Wilson cloud chamber has been plotted versus the logarithm of the velocity, producing straight lines. A value for the variation of specific ionization with velocity for β-particles in gases is then given taking other observations into consideration. It is

$$I_o \sim \beta^{-1.4} \text{ for } 0.45 \leqq \beta \leqq 0.97,$$

the classical formula giving the variation with β as

$$I_o \sim 1/\beta^2 \text{ for } \beta < 0.9.$$

Williams (120) has counted the number of distinct groups of droplets per cm. length in sharply defined Wilson chamber tracks of electrons with velocities between 0.8 c and 0.97 c. Each group corresponds to one primary ion pair. The measurements on the electrons were made under the same conditions that existed when he obtained a meson track. Williams

then obtains the average ionization (I') of these electrons corresponding to a velocity 0.96 c, the velocity which gives a minimum value for the energy loss dE/dx as given in Eq. 29. Taking the ionization to vary as $\beta^{-1.4}$, the velocity of the meson is given as

$$v = 0.96\ c(I'/I_o)^{-1.4}.$$

The number of distinguishable spots along the meson track were counted. These, with one or two exceptions, represented primary ions. To obtain the true number of primary ions per cm. (I_o) using the number of spots counted (I), Williams used the formula

$$I_o = \sigma^{-1} \log_e (1 - I\sigma)^{-1},$$

where σ is a parameter representing the resolving power.

According to Corson and Brode (122) the expression can well be represented in the interval $0.20 < \beta < 0.90$ by

$$v = 0.96\ c(I'/I_o)^{-1.8}.$$

Since the ionization produced by fast electrons is similar to that produced by mesons, the foregoing equations for I_o have been assumed valid for mesons by various experimenters. Meson mass values derived from the former equation for v are larger than those obtained from the latter.

Types of apparatus used. A large randomly operated cloud chamber has been found by Williams (123) to be very

satisfactory for investigations as described above. His chamber is shown in Fig. 26. The tracks are formed in the cylindrical main compartment A of 30 cm. diameter and 30 cm. length. The rubber diaphragm B is close to the perforated brass plate C before expansion, the side of C facing A being covered with black velvet to prevent irregular motion of the gas in A during an expansion and providing a dark background for the tracks. The valve D is shut and the reservoir E partially evacuated before an expansion; for an expansion, the catch F, which is knocked in the direction of the arrow, opens the valve and allows the rubber diaphragm to fall on the perforated brass plate G. The camera is focused in the plane J between the magnetic field coils H.

The brass formers containing the field coils, which are within 2 cm. of the chamber walls, have the copper tubes K soldered to their sides. Water is passed through the tubes to keep the walls of the chamber at a uniform temperature and to avoid distortion of the tracks by convection currents. Hence, distortion is confined to less than 0.18 mm. in 10 cm. of track. Ethyl alcohol vapor is employed.

The sensitive time of the chamber is the interval of time after an expansion during which the supersaturation remains sufficient to cause condensation on ions. If a large chamber is used to give a long sensitive time, convection currents set up by the warming of the gas do not reach far from the walls of the chamber. A still larger sensitive time

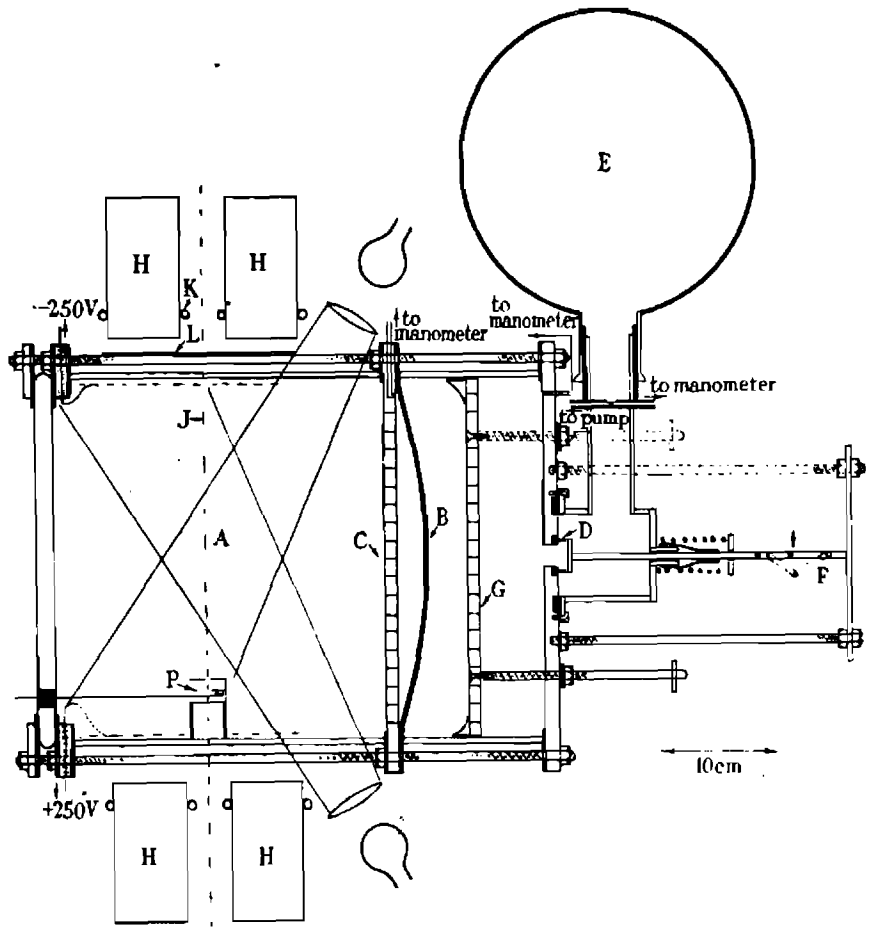

Figure 26. Diagram of a large randomly operated cloud chamber.

can be introduced in a chamber of the sort described by following the main expansion with another at such a rate to maintain the necessary supersaturation. The effective increase in sensitive time due to this second expansion is shown by Bearden (124) and Frisch (125). The sensitive time of the chamber in Fig. 26 is nearly half a second, and this, together with its large effective volume, makes it a very sensitive detector of weak radiations. Counter-control is usually not necessary with such a chamber since the efficiency of the chamber ensures on the average at least one cosmic-ray track per photograph.

Specific experiments. A large difference in ionization between a meson and a fast electron was found by Williams as is shown in the lower photograph of Fig. 27 (126), which reproduces a portion of the meson track shown in the upper portion of the figure alongside the track of a fast electron. The $H\rho$ of the meson deduced by Williams (123) from the curvature of the track (55 cm. in a magnetic field of 2300 gauss) is 1.26×10^6 gauss cm. and the ionization is about three times that of the fast electron. Taking the electron ionization to vary as $\beta^{-1.4}$, the velocity of the depicted meson is 0.41 c. Using the above data, the meson mass is given as 160 m_e with an estimated probable error of about 15 per cent.

Williams had previously found the meson mass to be 210 m_e using air instead of an air and hydrogen mixture in his chamber. Using the "gap" method, the specific primary

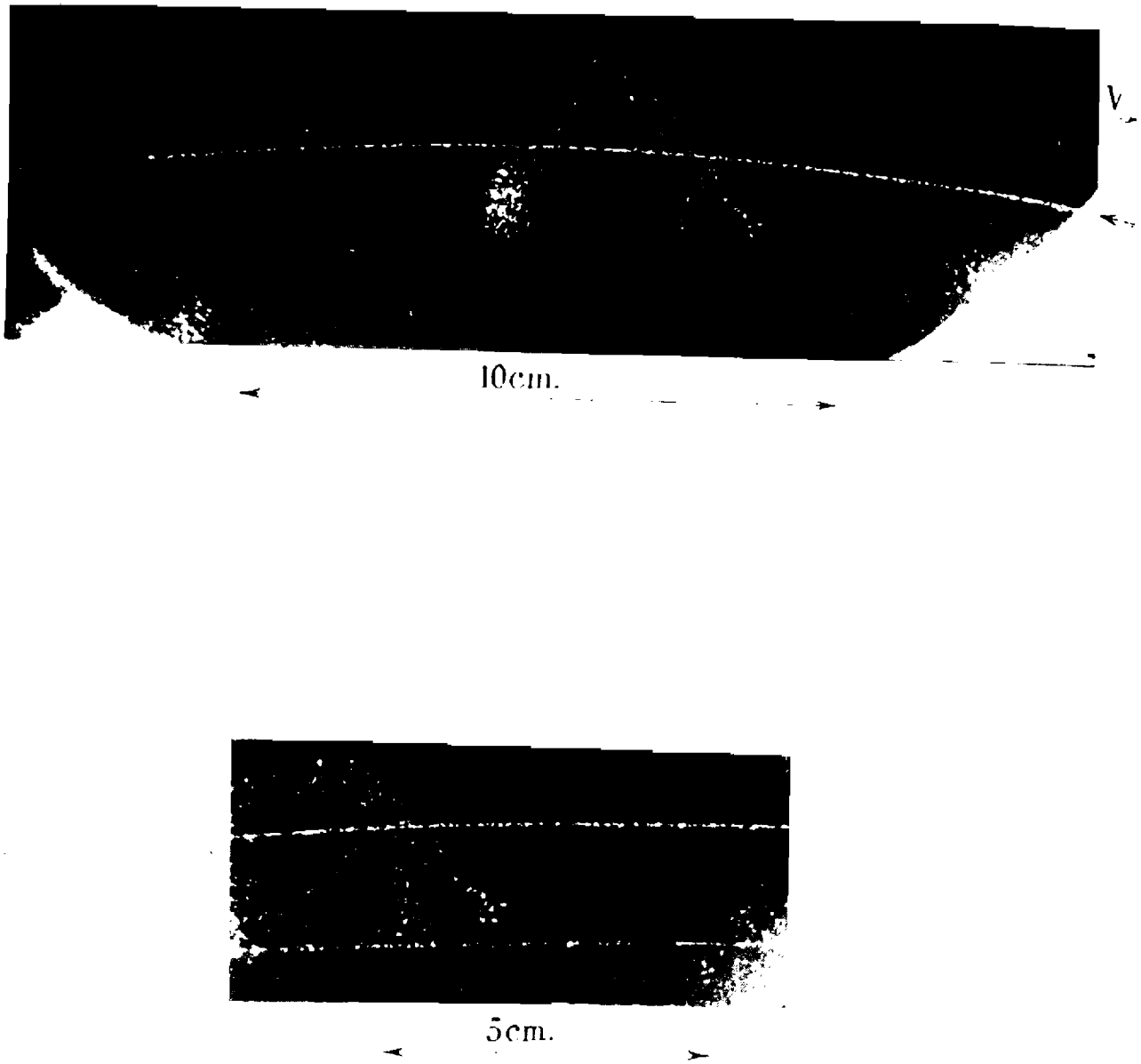

Figure 27. Tracks illustrating a difference in ionization between a meson and an electron. The lower photograph reproduces the meson track in the upper photograph above the track of an electron.

ionization was found to be 115 ions/cm. since 5 gaps greater than 0.5 mm. were found in a track length of 13 cm. The great density of ionization prevented a measure of the ionization by direct counting. The mass value was obtained by again taking the electron ionization to vary with $\beta^{-1.4}$, and calculating the velocity to be 0.30 c. This, together with the $H\rho$, gave 210 m_e with a probable error of about 20 per cent.

Sen Gupta (127), using the same methods, obtained an ionization of 113 ions/cm., which, after correction for temperature and pressure, became 106 ions/cm. In this case only one free path was measured on 5.2 cm. of track and was found to be 0.056 cm. in length. The curvature in the 1060-oersted magnetic field was found to be 76 cm., giving an $H\rho$ of 8.056 x 10^4 gauss cm. The mass of the meson was found to be 147 m_e. The track used for measurements ended in the cloud chamber.

Method B

Discussion of the method and equations involved. The generally accepted variation of the specific ionization of an electron of velocity $v = \beta c$ is given theoretically by the equation (128)

$$I_o = \frac{A}{\beta^2}\left[\log k + \log \frac{\beta^2}{1-\beta^2} - \beta^2\right], \qquad (11)$$

where $k = 1.6 \times 10^6$ for hydrogen and approximately 2×10^4 for nitrogen. A is a constant. The conclusion to which several researches has led is that the formula should remain valid for cosmic-ray energies. The formula is modified by

Oppenheimer (129) to give the probable ionization (130), which consists of the primary ionization plus that produced by secondaries of low energy, the secondaries of higher energy producing unresolvable clusters of ions in the chamber.

Eq. 11, with $k = 2 \times 10^4$, is plotted in Fig. 28 from the data of Corson and Brode (131) for mesons, the minimum ordinate being arbitrarily adjusted to make the curve fit their data. Thus it is a plot of probable ionization. The dotted curve is a plot of the classical inverse square law variation of ionization with velocity, while the solid curve shows the actual variation of ionization with $H\rho$.

Eq. 11 is seen to vary nearly as $1/\beta^2$ for $\beta < 0.9$, passes through a minimum at $\beta \sim 0.97$, and then increased with increasing β. Defining the relative specific ionization D as the ratio of the specific ionization (I_o) at a given β to the ionization at the minimum ($\beta \sim 0.97$), the value of D can be calculated by obtaining I_o from Eq. 11 as modified by Oppenheimer if the specific ionization at the minimum and the velocity are known.

Experimentally, D is found by dividing the number of droplets per cm. in the track by the observed minimum value of the ionization as shown on a graph as the one in Fig. 28. In this way the value of β for any track is found from the modified form of Eq. 11; by determining $H\rho$, the meson mass is then calculated by means of Eq. 27.

Types of apparatus used. The cloud chamber employed

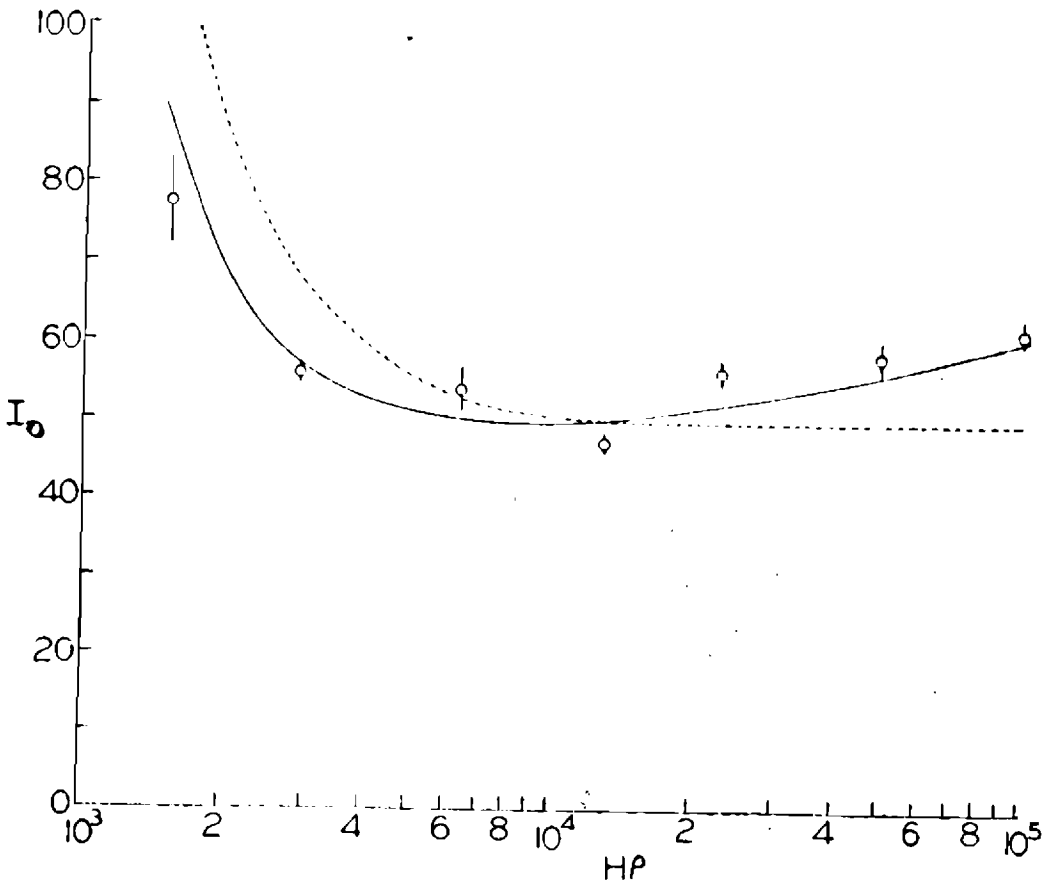

Figure 28. Specific ionization versus $H\rho$ for mesons. I_o is the number of droplets per cm. in nitrogen at 0° C. and 760 mm. pressure. The continuous curve is Eq. 11, the dotted curve is the inverse square law, and the vertical lines the probable errors of the measurements.

by Corson and Brode (132) was 18 cm. in diameter and filled with nitrogen at about 1.5 atmospheres pressure. An 800-gauss magnetic field passed through the chamber, which had a delayed expansion to make possible the counting of the individual droplets in the tracks. In the time between the passage of the meson and the expansion of the chamber, the tracks were broadened by diffusion of the ions. Quite accurate values for the curvature of paths were still obtained in spite of the breadth of the tracks by measuring the coordinates of the estimated center of the band of droplets when observed with a measuring microscope. Turbulent distortions were checked by examining no-field tracks.

Specific experiments. The track of a heavily ionizing meson is shown in Fig. 29 (1); it has an $H\rho$ of 1.5×10^5 gauss cm. and 265 droplets per cm., which is about 5.5 times the minimum density of normal tracks. Its mass is found to be 250 m_e. The mean number of droplets per cm. for this meson was found by weighting the mean number per cm. in each of a group of tracks proportional to the total number of droplets in the track.

A track reported by Street and Stevenson (133) has an $H\rho = 9.6 \times 10^4$ gauss cm. and an ion density six times that of minimum ionization. Using Corson and Brode's method, the meson mass is found to be 160 m_e, while the value is only 130 m_e by the classical $1/v^2$ law for ionization, the probable error being estimated as 25 per cent.

Figure 29. Photograph of a heavily ionizing meson track.

Meson mass values. Table VI contains the values of meson mass computed using both variations of the ionization and curvature method. Methods A or B are those referred to previously. The values containing braces are those of a single track employing the two methods. The upper limit on one of the values given by Williams and Pickup was set by a minimum range equal to the observed length of track in the chamber. Mass values below the heavy line are calculated by Das Gupta and Ghosh (73) from curves 1 and 2 in Fig. 7 using the values of dE/dx and $H\rho$ as found by the persons listed in the reference. I_o' is the minimum ionization as shown in Fig. 28.

Variations in the method. Nielsen and Powell (140) have realized the possibility of removing errors from inaccurate ionization measurements and eliminating uncertainties in interpretation of the data from cloud chamber photographs by observing, under identical conditions to those existing when a meson was seen, the curvature and ionization of slow electrons of the same speed as the mesons. Since two particles with equal charge ionize equally when moving at the same speed, the masses will be proportional to their $H\rho$ values. This, however, calls for accurate determinations of the ionization of slow electrons which are now being awaited.

IV. IONIZATION AND RANGE

Discussion of the method and equations involved. The ionization and range method is not very accurate as both the ionization and the range are likely to be underestimated, the

TABLE VI

MESON MASSES FROM THE IONIZATION AND CURVATURE METHOD

Mass ($\times 1/m_e$)	Method	Ionization ($\times 1/I_o'$)	$H\rho$ ($\times 10^{-5}$) (in gauss-cm.)	Reference
130	A			Street and Stevenson (133)
160*	B			
250	B	5.5	1.5	Corson and Brode (134)
230±20	A	2.5	2.26	Nielsen and Powell (135)
210±20	B			
225±20	A	6.0	1.08	
180±20	B			
240±15	A	6.2	1.11	
190±15	B			
155±30	A	2.4	1.6	
145±30	B			
160±30	A	3.3	1.26	Williams (136)
210±60	A	5	1.10	
220±50	A	5	1.10	Williams and Pickup (137)
>430 < 800	A	>7	1.83	
190±60	A	3.0	1.47	
160±30	A	3.3	1.15	
147	A		0.8056	Sen Gupta (127)

TABLE VI (continued)

MESON MASSES FROM THE IONIZATION AND CURVATURE METHOD

Mass ($\times 1/m_e$)	Method	Ionization ($\times 1/I_o'$)	$H\rho$ ($\times 10^{-5}$) (in gauss-cm.)	Reference
$\sim$ 200	B		1.6	Ehrenfest (138)
180±25	B		>5	Brode and Starr (79)
~170	A	4.5	1.03	Hughes (65)
~180	A			
230	A		1.1	Williams and Pickup (137)
210	A		1.47	
230	A		.96	Street and Stevenson (133)
214	A		1.00	Hughes (65)
184	A		.55	Brode, MacPherson, and Starr (81)
200	A		.60	Anderson and Neddermeyer (16)
370	A		2.5	

*This value is calculated by Corson and Brode (126) from the data of Street and Stevenson.

two errors acting in the same direction tending to give only a lower limit of the meson mass.

Discussion of the method and equations involved. Eq. 29 gives the average rate of energy loss through ionization and excitation by a fast particle. Plots of the equation as a function of v/c for air and lead are shown in Fig. 30a (139) and the corresponding range curves found by graphical integration in Fig. 30b (139).

If substances of large atomic numbers are being dealt with, radiation losses for particles of mass much greater than that of an electron are negligible even up to very high energies ($\beta = 0.9$). Das Gupta and Ghosh (72) have shown the radiative loss in 1 cm. of lead for a meson of 1.5×10^8 ev to be approximately 0.01 Mev. Comparing this with the ionization loss (10 Mev) in the same thickness of material, the radiative loss may be neglected and the total energy loss suffered by the meson taken as that of the ionization loss.

Under this condition, the energy loss is a function of velocity only and the range may generally be expressed as a function of the velocity as seen from Appendix III. If we write

$$R = k\, g(\beta),$$

where k is the mass of a particle in terms of the electron mass, then $g(\beta)$ is the function plotted in Fig. 30b. Curve 3 in Fig. 11, plotted from values of R/k for different values of $\beta/(1-\beta^2)^{1/2}$, is very general and applies to a particle of

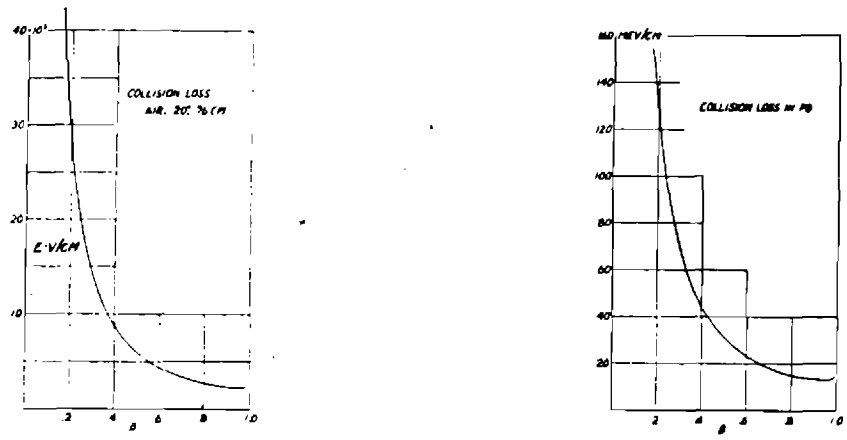

Figure 30a. Theoretical collision loss as a function of v/c for air and lead.

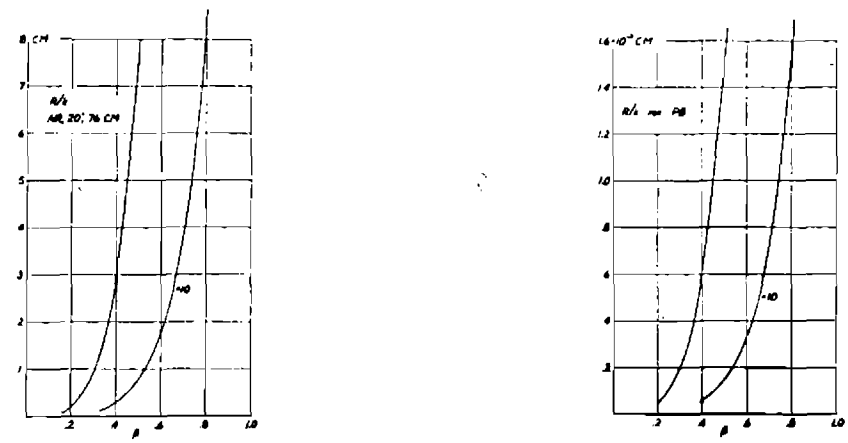

Figure 30b. Theoretical range divided by mass number for air and lead. These curves are valid for mass numbers much greater than one.

any mass.

As explained under the range and curvature method and under the previous method, the specific ionization -dE/dx determines $\beta/(1-\beta^2)^{\frac{1}{2}}$ uniquely. Hence, if the range of the meson and its specific ionization inside a cloud chamber are determined, the plotting of a curve of β, or $\beta/(1-\beta^2)^{\frac{1}{2}}$, versus R/k would enable the determination of its mass.

Types of apparatus used. Since the best estimates of range can be made from mesons ending in a cloud chamber, a Geiger counter is usually placed inside the cloud chamber and coupled by means of a coincidence circuit to a second counter placed above the chamber to increase the probability of observing mesons near the ends of their ranges. The apparatus is much the same as that employed in range and curvature measurements.

Neddermeyer and Anderson (140) used, as a counter, a flattened copper cylinder 85 mm. long, 18 mm. wide, and 7 mm. high enclosed in a glass tube whose upper and lower surfaces were flat and parallel to one another. The gas in the chamber consisted of 2/3 helium and 1/3 argon at a combined pressure of 1 atmosphere, which together with the alcohol vapor corresponded in stopping power to about 0.5 atmosphere of air.

Specific experiments. From a photograph of a meson in a field of 15,000 gauss, Neddermeyer and Anderson (140) assigned a mass value of 150 m_e to the particle corresponding to an ionization 10 times the minimum and a mass of 200 m_e

should the ionization be as much as 15.5 times the minimum. Since a magnetic field was also applied when this photograph was taken, the $H\rho$ measurement, together with the range determination, enabled an upper limit of 300 m_e to be set on this meson.

Meson mass values. Estimates of the mass of the meson made by Das Gupta and Ghosh (141) from specific ionization and range values of different experimenters appear in Table VII. $R/(M/m_e)$ is deduced from curves 1 and 3 of Fig. 11. The reference refers to the observers who reported the data used.

TABLE VII

MESON MASSES FROM THE IONIZATION AND RANGE METHOD

Mass (x $1/m_e$)	$-dE/dx$ (in 10^3 ev per cm. air)	$R/(M/m_e)$	R (in cm. air)	Reference
> 167	25.0	0.11	>18	Brode, MacPherson, and Starr (81)
> 50	13.7	0.29	>15	Corson and Brode (134)
> 28	15.0	0.25	> 7	Street and Stevenson (142)
< 73	25.0	0.11	< 8	Anderson and Neddermeyer (16)
150-200				Neddermeyer and Anderson (17)

CHAPTER VII

PHOTOGRAPHIC PLATE METHODS OF MESON MASS DETERMINATION

History. In 1912, Reinganum (143) discovered the effect that an alpha particle, striking a photographic plate at grazing incidence, alters the grains of silver bromide in its path. After development of the plate, each alpha-track appears as a minute trail of discrete silver grains when viewed under a microscope. W. Michl (144) confirmed and extended Reinganum's findings, measuring the track length and number of grains per track for alpha-particles of different range. He concluded that both were linear functions of the air range of the alphas. Reinganum had reported a number of deflections in his tracks which he attributed to scattering. However, Michl and some of the later workers pointed out that the apparent deflections, although possibly due to scattering, might also be "bends" due to two contiguous tracks.

Tracks in photographic emulsions produced by protons were reported by Blau (145) in 1925. He found the average spacing between adjacent silver grains to be greater in the proton tracks than in the alpha-tracks. Blau and Wambacher (146) measured the density of silver grains in proton tracks as a function of the ionizing power of the rays and discovered the grain density to be independent of the range for an air equivalent of 2 cm. or less. Upon discovering that the nature of the tracks produced depends on the grain size and on the

concentration of silver bromide in the emulsion, proton-sensitive plates were easily developed. A new tool for the investigation of cosmic rays was provided when the plates were developed into suitable detectors of these rays.

Advantages and disadvantages. One of the advantages of the photographic plate in cosmic ray studies is that it can record individual particles, acting thus as a continuously sensitive cloud chamber. The plates are light and therefore portable, afford permanent records of any investigations, and may be examined at will. Meson tracks can be clearly distinguished from those of heavier particles as a meson track shows frequent changes in direction due to Coulomb scattering while the track of a heavier particle is comparatively straight. Further, the rate of change of ionization near the end of a meson track is much greater than it is near the end of the track of a heavier particle.

The photographic plate, however, does not give the fine distinction between tracks of different particles nor the possibility of recording the bending of particles in a magnetic field as do cloud chambers. One of its severest limitations is "fog," or the appearance of a great number of silver grains as background after development of the plate, making it difficult to study particle tracks. The background is almost unavoidable regardless of how carefully a plate is developed. It can be ascribed to chemical action of the various reagents employed in the preparation and development of the plate, to

photons from radioactive materials in the surroundings, phosphorescent materials in the darkroom, weakly ionizing cosmic rays, temperature variations, and possibly mechanical shock. The existence of the background makes it difficult to find and to study particle tracks.

Discussion. Because of its high stopping power (about fourteen hundred times that of air), the photographic plate is suitable for development into a device which will record cosmic-ray particles over wide ranges of energy. Presently, only mesons of energy below 10 Mev become visible. The Ilford laboratories, the Agfa laboratories, and the Eastman Kodak laboratories have made possible cosmic ray research with their developments of photographic plates. The photographic method is making a distinctive contribution since it is relatively insensitive to electrons which would ordinarily cloud the tracks of heavy particles such as mesons due to the necessary long exposure.

In the microscopic examination of the plate, the tracks stand out much more clearly if a contrast is obtained by dark-field illumination. Eyestrain and fatigue may be reduced by using a binocular microscope. Grain spacing and small angle scattering make it possible to distinguish unmistakably the tracks of a meson and a proton. Hence, the density of developed grains in a track is of extreme importance. Particles of different charge but with the same velocity produce different grain spacing in photographic tracks, as do identical particles

having different velocities.

In analyzing the tracks of mesons in the photographic emulsion, the experimenter must rely on such features as the range of the particle in the emulsion, small angle scattering along the track, and the grain spacing along the track. The actual range of the meson and the small angle scattering will depend on the composition of the emulsion and hence may be expected to be constant from one emulsion to another. However, the sensitivity of the individual grains of the emulsion determine the range and the grain spacing at the beginning of the track. It is essential that the plates used in experiments based on range or grain spacing be given control exposures to particles of known characteristics. At any rate, a calibration of the plates of each new emulsion batch in the energy range in which the plates are to be used is highly desirable.

As representative values for the Ilford plates, a 1 Mev meson is expected to have a range of 56 μ and a 5 Mev meson a range of about 1000 μ. The trajectories of the particles must be in the plane of the emulsion in any type photographic plate and the length of the projection of the paths must be greater than 50 μ. If a meson track dips at a large angle to the plane of the emulsion or if its projection is less than 50 μ, it is likely either to excape observation or to provide insufficient evidence to justify its being identified as due to a meson.

The masses of mesons observed in the photographic plate have been determined by Coulomb scattering, grain counting, and magnetic deflection. Grain counting is especially favorable for the determination of the ratio of the masses of particles involved in contemporaneous events, such as the decay process in which a π-meson, or the meson found at high altitudes, decays into the μ-meson, which is the meson we have generally been considering thus far and which is the one commonly observed at the surface of the earth or below it.

Coulomb scattering, although not very accurate a method, is independent of the fading of the latent image in photographic emulsions and hence is suited for work with particles occurring in events of which the relationship in time is unknown. The probability of Coulomb scattering in the gas of a cloud chamber is very small compared to that in the photographic plate due to the smallness of the gas atoms in comparison with the atoms of the emulsion.

The convention has generally been accepted to represent the primary mesons by the symbol π, and the less massive secondary ones by μ. A third class of mesons, σ-mesons, is defined as those mesons which suffer capture and lead to observable nuclear disintegrations in the emulsion at the ends of their track, the charged fragments being observed as prongs of a "star." A fourth group, ρ-mesons, are those which stop in the emulsions without giving rise to any observed charged particles.

Two kinds of ρ mesons, distinguished by positive and negative electric charge, are observed in approximately equal numbers in cosmic rays. It may sometimes be a π-meson which happens to knock only neutrons out of a nucleus so that the star is not visible, or it may be a μ-meson.

Most, if not all, σ-mesons are negatively charged π mesons, although a few could be negative μ mesons or possibly positive π mesons.

π-mesons are subdivided into positive π^+ and negative π^- and also neutral π^0, although no conclusive evidence of the latter has been found. A π^+ is always produced at high energy, and hence in the ordinary photographic plates (which are sensitive only to low-energy mesons) its birth cannot be observed. A π^- can be produced at sufficiently low energy to be visible as one prong of a star and, if it encounters a nucleus, it may disintegrate it and produce a star.

A π^--meson may be captured by a light as well as a heavy nucleus; μ^--mesons are captured only by heavy nuclei.

If a π^- does not encounter a nucleus, it decays into a μ^- and a neutrino. A π^+ may also decay into a μ^+ and a neutrino. If it does not approach too near a nucleus, the μ-meson in its turn also decays, the products of the disintegration being two neutrinos and an electron which is either positively or negatively charged according to the charge of the meson. The neutrinos are not observed, but their presence is inferred from the fact that the decay electrons observed

in cloud chambers appear to have a uniform distribution in energy up to a maximum at about 55 Mev. If only a single neutrino were emitted, the electron would have a fixed energy.

Mesons of mass approximately 700 m_e to 800 m_e have been detected and are called τ-mesons. These stop in the emulsion without any observable decay particles, the latter particles perhaps being of high velocity and undetectable. Mesons of approximate mass 1000 m_e have been labeled K^+ and K^- by some as is shown later. The existence of neutral mesons (neutrettos) has also been postulated (147). Various properties of the neutretto have been predicted, as the existence of a finite cross-section for the transformation of a neutretto into a charged meson and also for the reverse process. Such processes, if they occur, are detectable. Preliminary experiments of Lovell (148) failed to detect such a particle.

Although experimental evidence is lacking, the π- and μ-mesons discussed above may be the vector and pseudo-scalar (ordinary) mesons predicted by the Møller-Rosenfeld (149) theory An even better agreement is found with the modification of this theory by Schwinger (150). In the latter theory the two mesons are assumed to be of different mass. The theory of Møller and Rosenfeld predicts also the occurrence of charged and neutral vector mesons.

I. COULOMB SCATTERING

Discussion of the method and equations involved. A

charged particle traversing a medium suffers frequent small-angle deflections in elastic collisions with the nuclei of the atoms composing the medium. The track has a curved appearance due to many such small deflections as shown in Fig. 7.

The mean ionization along a long meson track and its curvature due to multiple scattering are determined. The average number of silver grains deposited per unit length of the meson track is assumed to be proportional to the initial kinetic energy of the particle. It is further assumed that both the meson and the proton carry one unit of charge, so that when these two particles start with the same velocity, the mean grain number, which is inverse to mean grain spacing, deposited along their tracks in a given emulsion will be the same. The mean kinetic energy of the meson can be deduced from the mean curvature of its tracks in the photographic emulsion due to multiple scattering. In this method the ratio of the mass of the unknown particle to that of the proton is determined from the ratio of the kinetic energies of these two particles which have the same mean grain spacing along their respective tracks in similar photographic emulsions. The mean grain spacing is taken to vary inversely as the mean ionization. The protons are produced in an emulsion as recoil particles by using neutrons of different energies produced by a source such as radium-beryllium.

The theory of multiple scattering as developed by Williams(151) for fast particles enables the determination of the

energy of incident mesons from their mean scattering. Bose and Choudhuri (152) considered the scattering to be due only to Coulomb forces since the nuclear charge of the photographic emulsion through which a meson passes is low. Finding the energies of such mesons to be between 0.4 and 1.6 Mev, they used non-relativistic equations and Born's approximation, writing the mean scattering angle $\bar{\theta}$ suffered by the mesons in passing through a thickness t of a medium of nuclear charge Z'e and containing N atoms per cubic centimeter as follows:

$$\bar{\theta} = 3.69 + 0.28 \log_{10}\left[(Z')^{4/3}\left(\frac{dt}{A\beta^2}\right)\right]\frac{Z'Ze^2}{W}\sqrt{Nt}, \qquad (12)$$

where W is the mean energy of the mesons and d the emulsion density. The assumption was made that the actual distribution of atoms of different kinds in the photographic emulsion is replaced by one kind of atom of mean nuclear charge Z'e and mean atomic weight A. The density d of the emulsion and its percentage composition enables an estimate of Z' and A as given by Wambacher (153). The equation was then written

$$\bar{\theta} = \psi\frac{Z'Ze^2}{W}\sqrt{Nt}\ , \text{ where } \psi \text{ is a constant.}$$

The mean value Z' defined by Bose and Choudhuri (154) in summing up for the scattering due to the different kinds of atoms with different values of nuclear charge is

$$\bar{Z}'N = \sum_{1}^{k} Z_k' N_k.$$

They found, however, that the value of Z' they should have used

was the root-mean-square of Z', namely,

$$(\overline{Z}')^2 N = \sum_{1}^{k} Z_k^{\,2} N_k,$$

since the value of $\overline{\theta}$ was deduced from that of $\overline{\theta}^2$ which is defined as $2/\pi$ times the mean square of θ. The value of $\overline{Z}^2$ is given as $\sqrt{\overline{Z}^2} = 11.3$, and that of A as 3.69 for the Ilford New Halftone plates used by them.

The value of $\overline{\theta}$ may be determined by using individual values of θ (see Appendix IV) in order purposely to get a statistical distribution of the meson mass values about the true value, or by measuring the total deflection θ suffered by a group of particles having a given mean energy and traversing a varying thickness of emulsion.

Bose and Choudhuri (155) found, for the large number of encounters which take place,

$$\frac{|\theta - \overline{\theta}|}{\overline{\theta}} \ll 1,$$

that is, θ could be written for $\overline{\theta}$ in Eq. 12.

Thus the mean energy of the mesons corresponding to a given mean grain spacing, namely $W = 1/2\ M\ \overline{v}^2$, may be determined.

To determined the kinetic energy of protons having the given mean grain spacing along their tracks in the same kind of emulsion, the protons must have the same initial velocity as the meson, as previously pointed out. The ionization loss of different particles with the same charge in a given medium depends only on their velocities. Such particles may have

different ranges, but the mean grain spacing along their tracks will be the same if they start with the same initial velocity. A calibration curve showing the mean grain spacing along the tracks of protons as functions of their initial energies is usually plotted. It has been found (156) that for energies above 4 Mev the mean grain spacing bears a linear relation to the energy of the protons. Extrapolating this curve, energies of protons corresponding to different values of mean grain spacing can be obtained provided the linear relation holds good for higher proton energies.

If, then, two particles like a proton and a meson carrying the same unit charge, have masses M_p and M respectively, and have the same mean grain spacing along their tracks in similar emulsions, the ratio of their kinetic energies (K.E.) is

$$\frac{(K.E.)_{proton}}{(K.E.)_{meson}} = \frac{M_p}{M}.$$

A usual method of determining θ has been by measuring the angle between two successive tangents drawn at the beginning and the end of the track. However, since the track is defined by a small number of grains, it is very difficult to draw accurate tangents. Therefore, Lattimore (157) measured the angles ψ between consecutive chords along the track. The advantages of this method are that the chords are easy to draw and the observations repeatable. The method is illustrated in Appendix IV.

Goldschmidt-Clermont et al. (158) magnified a large scale drawing of one of their tracks, divided it into a series of segments, and measured the changes in the direction between the middle points of alternate segments. The distances (t) between these middle points are called cell lengths. A small systematic error was deliberately introduced into the measurements by measuring angles between mean lines drawn through grains over certain segments of a track, the length over which this mean line is drawn being chosen as half the cell length. The mean line will generally be intermediate between a chord and tangent [see Fig. 31a (159)] .

The effective number of measurements on a single track was increased by the same group as used the above method by dividing the track into overlapping half cells 1, 2, 3, etc. as shown in Fig. 31b (159). In each cell, a straight line is drawn to pass, as closely as possible, through the centers of gravity of the grains, the angular deviations between the lines in 1 and 3, 2 and 4, 3 and 5, etc. then being measured.

Of the mesons observed in photographic plates, the particles considered are usually found to have different track lengths and/or different mean grain spacings. Hence, the particles with energies lying within certain limits must be sorted out and grouped together, that is, a classification of the particles according to their mean grain spacing which is a measure of their energy is required. Due to differences in the inclinations of the tracks to the plate, the tracks in any single

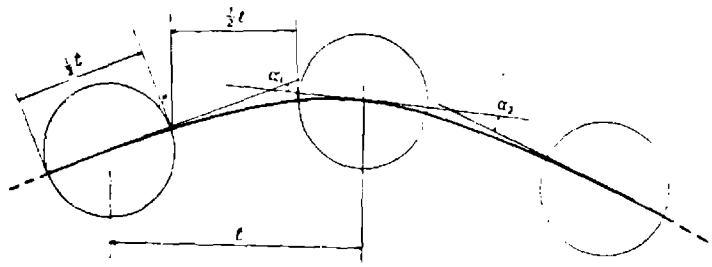

Figure 31a. Method of measuring angular deviations.

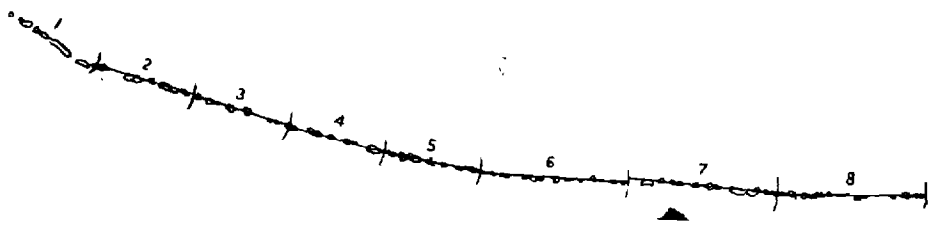

Figure 31b. Reproduction of a section of drawing made on a typical meson track, showing lines drawn through grains in successive segments.

group thus formed may not have the same length. Therefore, the track lengths in each group, as well as the angles of deflection suffered by these tracks, are summed up. Now the energy of a particle of track length and scattering angle equal to the mean track length and mean scattering angle, respectively, of a group is determined by using Eq. 12.

Types of apparatus used. The large-scale drawings referred to were made with the mechanized projection microscope (160) devised by Occhialini, Payne, and Powell. The method of drawings has the advantage over direct measurements in that spurious scattering can be accurately evaluated, and a permanent amplified trace of the track for study is made available. The actual drawing is usually magnified about 4000 times.

Specific experiments. Bose and Choudhuri (154) made three determinations of the meson mass (see Table VIII), the first being made with the photographic plate in air, the second with the plate in water, and the third with the plate under 2 1/2 ft. of mud and wood. The values obtained from the latter two positions of the plate are considered high due to the presence of proton tracks in the plates because of the collision of primary cosmic-ray components with hydrogenous matter. It is interesting to note that a mass of 186 m_e was determined from the curvatures of the pair tracks in the emulsion.

In the experiments of Goldschmidt-Clermont et al. (161)

the tracks of cosmic-ray particles on the photographic plates were divided into four groups to represent the four types of mesons mentioned in the discussion preceeding this section. Only those π-mesons were accepted for measurement of which the track of the associated μ-meson was of a sufficient length to allow a definite identification. No μ-meson tracks were accepted which were unaccompanied by the track of the primary π-meson, and then only if the track of the μ-meson were of length of the order of 600 microns and terminated in the emulsion.

Meson mass values. Table VIII contains a summary of the values of meson mass obtained by various experimenters employing Coulomb scattering.

II. GRAIN COUNTING

Discussion of the method and equations involved. The assumption is made that a particle carrying one unit of charge, with energy E, and range in the emulsion R, loses energy at a rate which depends only on its velocity and is independent of its mass (see Eq. 34). If N(R) is the total number of grains in the track of a particle of range R, it is further assumed that the number of grains per unit track length, in an element of length of the trajectory, is a function only of the rate of loss of energy of the particle. That is,

$$\frac{N(R)}{R} = f\left[\left(\frac{-dE}{dx}\right)\right].$$

TABLE VIII

MESON MASSES FROM THE COULOMB SCATTERING METHOD

Mass ($\times 1/m_e$)	Type Meson	Reference
1,800±400		Brown, et al. (162)
200 (?)	σ	Lattimore (163)
>400 (?)	σ	
290±80		
260±30	π	Goldschmidt-Clermont, et al. (164)
205±20	μ	
275±15	σ	
200±10	ρ	
217±30		Bose and Choudhuri (154)
336±19.5		
313±18.5		
1500±1000	τ	Wagner and Cooper (165)
221	Average	Bose and Choudhuri (166)
160	214	
263		
180	Average	
257	219	
328	Average	Choudhuri (167)
355	314	
440	Average	
588	514	
276	Average	
386	331	
332		
258	Average	
331	331	
404		
552	Average	
478	515	
404	Average	
736	607	
350	Average	
552	450	

TABLE VIII (continued)

MESON MASSES FROM THE COULOMB SCATTERING METHOD

Mass ($\times 1/m_e$)		Reference
380 333	Average 356	
400 282	Average 341	
350±100		Occhialini and Powell (168)
100 - 300		Perkins (169

Lattes, Occhialini, and Powell (170) give the energy loss to be a function of R/M. Hence, the number of grains per unit track length, which may be written as dN/dR, is a function of R/M:

$$dN/dR = f(R/M).$$

Integrating,

$$N = M\int_{o}^{R/M} f(R/M)d(R/M).$$

Since the integral on the right would have a unique value, starting from a point on the track where the velocity has a given value (given R/M value), then, for two different particles having different masses the total numbers of grains, N_1 and N_2, in the residual paths, R_1 and R_2, in a given emulsion will be in the ratio of the masses, M_1 and M_2. Thus,

$$R_1/R_2 = N_1/N_2 = M_1/M_2. \qquad (13)$$

The procedure is to find points along the paths of the two particles for which the grain densities are equal. Then the relative masses of the two particles will be in the ratio of the two residual paths, or, alternatively, in the ratio of the total numbers of grains in the two residual paths as given by Eq. 13.

We see then that by counting grains in meson tracks and proton tracks found in the similar plates, the mass ratio of meson to proton can be found. This method has also been

employed to determined the ratio, M_{π}/M_{μ}, of the masses of the π^- and μ-mesons from the observed numbers of grains.

Since at the end of the range of a meson an unresolvable continuous succession of grains is found due to the intense ionization, the number of grains in a segment of the path of length r, in which there is a contiguous succession of grains, is taken as r/a, where a is the mean diameter of the grains. The difficulty mentioned, referred to as "clogging," may not be serious in a certain part of a track; however, the grains may still be unresolvable. "Clogging" is usually found to be bad only in the last 50 microns of meson tracks. Due to the possible unresolvability of the grains elsewhere, however, different observers apply possible statistical errors previously determined by others to their measurements of the number of grains in a track to obtain consistent results.

The number of grains in a track length are usually determined by counting the number of grains in successive intervals along the trajectory of length 50 μ. These intervals are measured along the projection of the track on the plane of the emulsion. Over-estimation of the grain-density in a track which dips relative to the plane of the emulsion is possible with this procedure. Ilford C2 or Kodak photographic plates with emulsion thickness of approximately 50 μ are most often employed. The track grains may be about 0.35μ in diameter. Optical equipment giving large magnification (2000 times) and the highest available resolving power

is employed.

Specific experiments. In determining the ratio M_π/M_μ, Lattes, Occhialini, and Powell (171) made a logarithmic plot of the number of grains N in a residual range R. They then multiplied the number N for the different events on their graph by a normalizing factor defined as the ratio of the average number of grains in the last 400μ of the different μ-meson paths to the number of grains in the same length of the particular μ-meson under consideration. The values deduced from the observations on the individual events are not changed by the use of the normalizing factor.

The results (obtained in observations on the tracks of four protons and four μ-mesons occurring in the same plate) by Brown, et al. (172) are represented in Fig. 32a. In this figure the number of grains per unit length in the tracks is plotted for different values of the residual range, the full lines indicating the mean values for tracks of the same type. The ratio of the masses of the two particles is found by comparing the values of the residual range at which the grain densities have the same value. The result thus obtained is $M_\mu = (220 \pm 20)\ m_e$.

Fig. 32b (173) contains a reproduction of a mosaic of photomicrographs showing a primary meson (labeled m_1) coming to the end of its range in the emulsion. The track of a secondary meson (labeled m_2) starts from the point where the first one ends. Grain counts indicate the masses of m_1 and m_2 to be

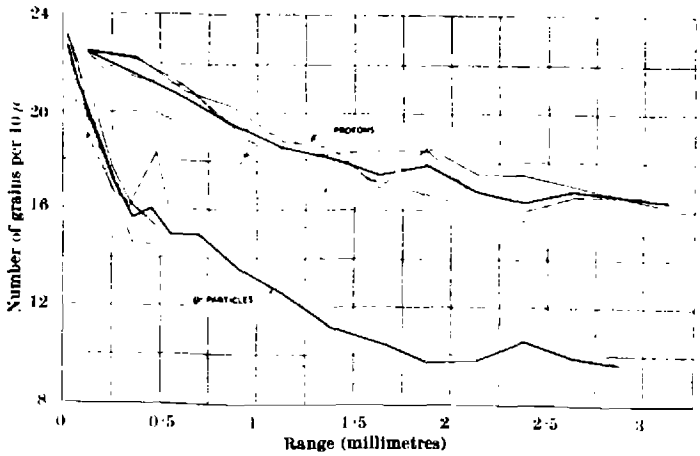

Figure 32a. Graph of tracks of four protons and four μ-mesons in the same photographic plate.

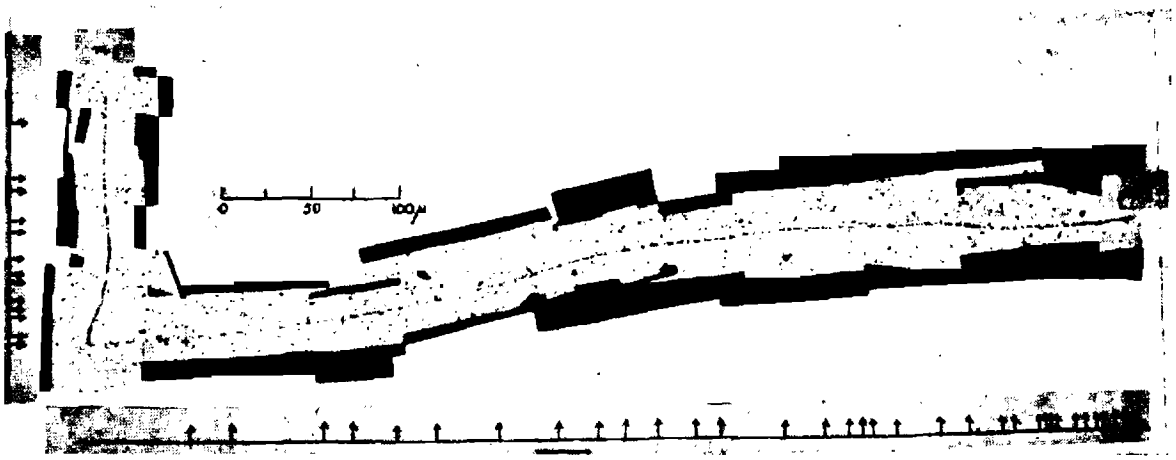

Figure 32b. Photomicrograph of a primary meson (m_1) and a secondary meson (m_2) in an Ilford "Nuclear Research" boron-loaded C2 emulsion. The arrows indicate points where changes in direction greater than 2° occur as observed under a microscope.

$(350\pm80)m_e$ and $(330\pm50)m_e$, respectively, the limits of error corresponding only to the standard deviations associated with the finite number of grains in the different tracks. The above mass values were deduced from calibration curves corresponding to an average value of fading in the plate. The assumption was made that the two tracks were produced in quick succession and were, therefore, subject to the same degree of fading. That the observation corresponds to a chance juxtaposition of two tracks from unrelated events is very doubtful, the probability of such an occurrence being less than 1 in 10^9.

Meson mass values. Table IX contains values of meson mass for different types of mesons obtained by several experimenters employing the method of grain counting. The type of meson investigated is also listed.

III. MAGNETIC DEFLECTION

It has not been possible thus far to make observations on the curvature, due to a magnetic field, of the trajectory of a meson in a photographic emulsion. A measurable deflection at high magnification would correspond to such a small value of the radius of curvature that a field of 10^6 gauss would need to be maintained over a long period of time. Small-angle Coulomb scattering would greatly complicate the interpretation of the results. Thus, observations are made on the meson's change in direction in its passage through a gas, or a vacuum, in a magnetic field. Many possible geometrical dispositions of the photographic plates relative to the field are possible.

TABLE IX

MESON MASSES FROM THE GRAIN COUNTING METHOD

Mass ($\times 1/m_e$)	Type Meson	Reference
305	Heavy	Barkas, Gardner, and Lattes (174)
202	Light	
220±20	μ	Brown, et al. (162)
100 - 230		Occhialini and Powell (175)
330±50		Lattes, et al. (176)
350±80		
330±50	Secondary	
375±70	Secondary	
240±50	Secondary	
725±40	τ	Wagner and Cooper (165)
205±50	μ	
330±30	π	Occhialini and Powell (177)

A decided advantage in the method is that it is applicable to mesons of lifetime of the order of 10^{-10} sec.

Discussion of the method and equations involved. If two separate photographic plates are placed with their emulsions face to face and perpendicular to a magnetic field, a meson, moving with sufficient energy to reach the opposite emulsion and emerging from the one emulsion at a small glancing angle ϕ', will cross the narrow air-gap between the plates and be recorded in both. In the space between the plates the meson moves in a spiral path lying on a circular cylinder of which the radius, ρ, will depend on the component of the momentum of the particle in the plane perpendicular to the field. If the track of the same meson can be identified in the two emulsions, then the observed change in the direction of motion in traversing the air gap, and the distance between the points of exit and entry of the meson in the emulsions, allows the $H\rho$ for the meson to be calculated. If the particle stops in the second emulsion, its residual range R can also be measured.

The component of meson momentum in the plane perpendicular to the field is $p' \sin \phi$, where p' is the momentum at an angle of ϕ' with the initial plate. Hence, from Eq. 24 (momentum of a particle in terms of $H\rho$),

$$p'c \sin \phi = Ze\, H\rho \ ,$$

where ϕ is the complement of ϕ', and

$$p' = (Ze/c)\, H\rho / \sin \phi \ . \qquad (14)$$

If the charge Ze is known, p' can be determined, having obtained $H\rho$ from a measurement of ϕ as described. Since the momentum is a function of the mass and the velocity, the mass can be obtained by determining the velocity. Appendix III shows the velocity to be a function of the range, which can be measured.

Franzinetti (178) expresses the range-energy relationship for particles in a photographic emulsion as follows:

$$E_p = KR_p^n, \qquad (R_p > 200\mu),$$

where E_p is the energy of say a proton of range R_p. This equation holds for mesons as well. The ranges R and R_p of a meson and proton, respectively, with the same initial velocity, with masses M (of a meson) and M_p (of a proton), and charges Ze (meson charge) and ze (proton charge) are related by the equation (178)

$$R_p = R\frac{M_p}{M}\left(\frac{Z}{z}\right)^2 - c,$$

the constant c taking into account the capture and loss of electrons in the last part of the range, particles of different charges being affected differently. Since c is negligible compared with the usual meson ranges considered, it may be neglected. Also, z = 1 for protons.

Since the energy of a charged particle is a function of its mass and velocity, and since the velocity may be expressed as a function of the energy, charge, and range

(see Appendix III), the energy of a meson may be written

$$E = f(R, M, Z). \tag{15}$$

The explicit form of this equation follows from the two relations given prior to Eq. 15, that is

$$E = K(M/M_p)^{1 - n} Z^{2n} R^n. \tag{16}$$

Solving Eqs. 14 and 16 simultaneously,

$$\frac{M}{Z^{\alpha}} = A\left(\frac{H\rho}{\sin\phi}\right)^{\frac{2}{2 - n}} R^{\frac{n}{2 - n}}, \tag{17}$$

where

$$\alpha = \frac{2(1 - n)}{2 - n} \quad \text{and} \quad A = \left\{\frac{e^2}{c^2} M_p^{1 - n/2K}\right\}^{1/2 - n}.$$

If the logarithm of the residual range of a meson is plotted against the logarithm of its measured radius of curvature, Eq. 17 shows that mesons of equal masses should be represented by points lying on straight lines of slope Φ given by

$$\tan \Phi = n/2.$$

Such a plot is shown later in Fig. 35 (179). For particles of ranges shorter than 200 μ, the range-energy relation given in Eq. 17 is no longer valid.

To establish the geometrical relationship of the two plates during the exposure, the plates in their holder are

exposed to a fine pencil of X-rays perpendicular to the plane of the emulsion. A screen of lead a few mm. thick is placed between the plates and the X-ray source thus "printing" a grid of lines on both the plates in such a way that corresponding points on the grids printed on the plates represent the same coordinates. Determinations are then made on a single meson by observing its trajectory in its two portions relative to the common grid.

If angles of dip of the trajectory of a meson and the surface of the emulsions are equal, the identification of the two portions of the track is made easier and the probability of attributing two unrelated tracks to the same particle is greatly reduced. Furthermore, by observing the direction of the projection of the trajectory on a plane parallel to the emulsion surface at the point of entry into one emulsion, the corresponding direction at a given point of exit in the other is determined. Meson tracks for mass determinations are usually chosen as those extending a distance between 100μ and 400 μ in the second emulsion and indicating an angle of dip of less than 15°.

Types of apparatus used. A schematic diagram of the arrangement employed is shown in Fig. 33 (180). Emulsions of 50μ, 100μ, and 200μ are most often used. Thicker emulsions show distortion in the processed plates. Relative movements of the plates is excluded by attaching the plates to a frame which is then covered with a thick layer of liquid rubber and

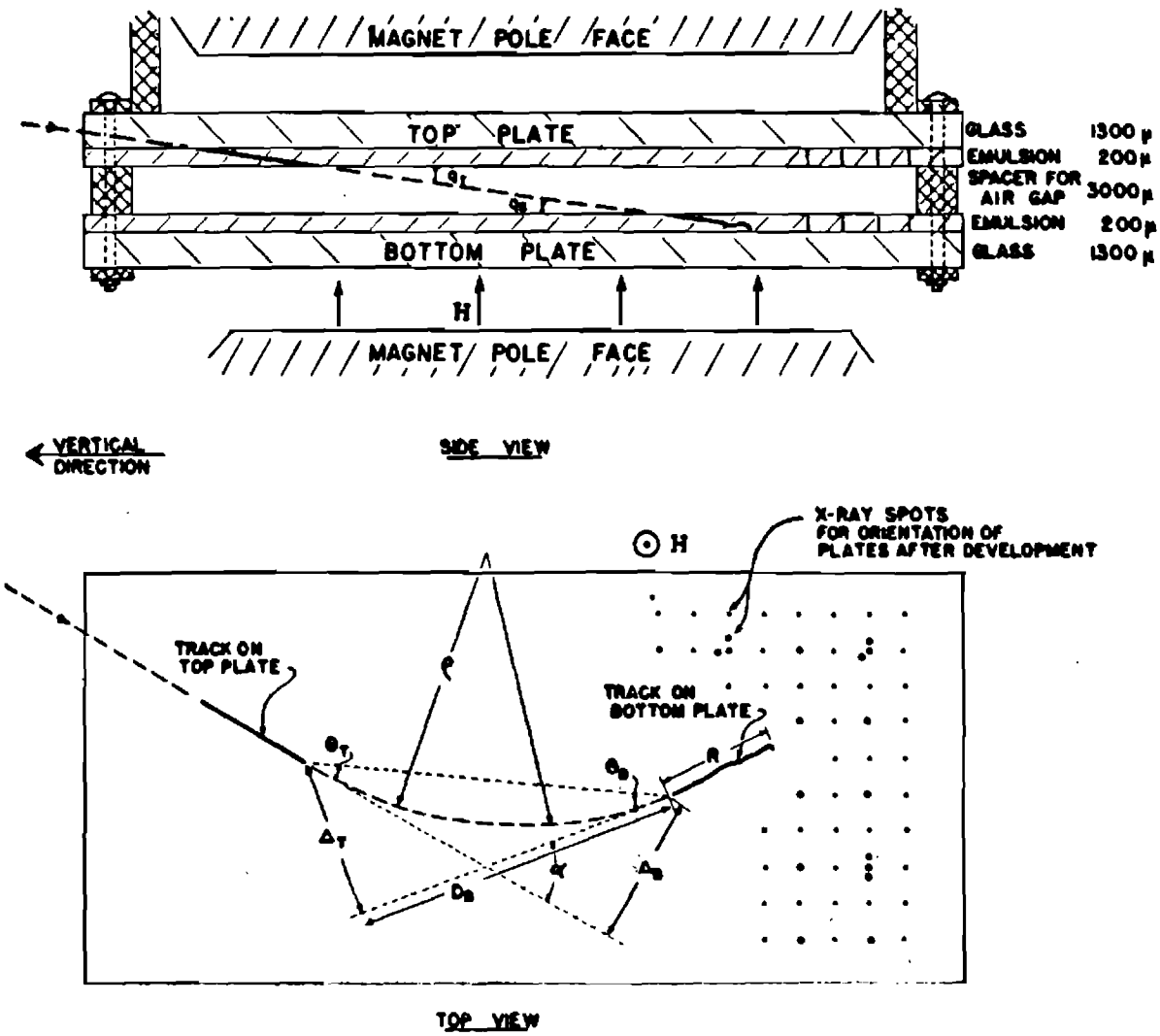

Figure 33. Side and top view of plate assembly for magnetic deflection experiment.

allowed to dry, thereby holding the plates firmly in place.

Specific experiments. In the experiments of Powell and Rosenblum (181) the emulsions were separated a distance of 3 mm., the whole being placed normal to a field of 8600 gauss. Franzinetti (182) employed a field of 29,180 gauss which was maintained constant during the exposure time to within 300 gauss.

The former experimenters analyzed a meson of 200 μ-range in one emulsion, the value of $H\rho$ being 70,000 gauss cm. and the angle of dip 10^{o}. From the observed range, a curve showing the relation of mass and velocity was drawn, the line so plotted being immediately replaced by a band to allow for straggling. Another curve was then drawn relating momentum and the calculated $H\rho$ from observed curvature measurements. Since there is an uncertainty involved in determining the change in direction of the meson between the plates (estimated as $\pm$1 per cent), this curve must also be replaced by a band. The mass of the meson is determined within the limits corresponding to the region of overlap of the two bands.

Photographs of the tracks of a particle at its exit from the first emulsion, at the entry into the second emulsion, and at the end of its range are shown for a μ^{-}-meson in Fig. 34 (183). The blob at the end of the range seems to be a characteristic of negative mesons.

Meson mass values. Fig. 35 contains the results of measurements on 150 particles by Franzinetti, the probable

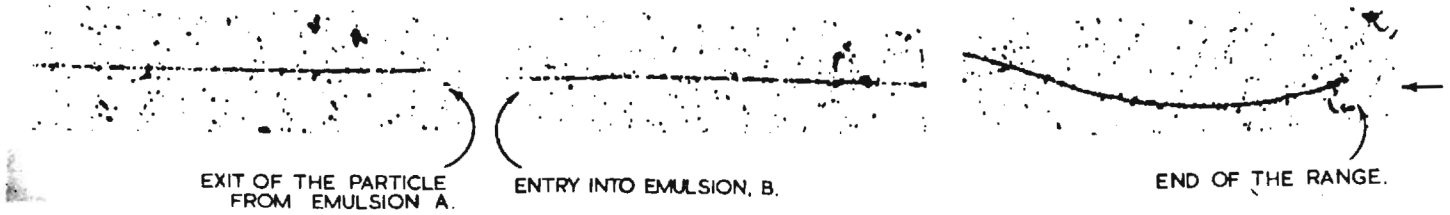

Figure 34. μ^--meson of mass $(220 \pm 5)\ m_e$.

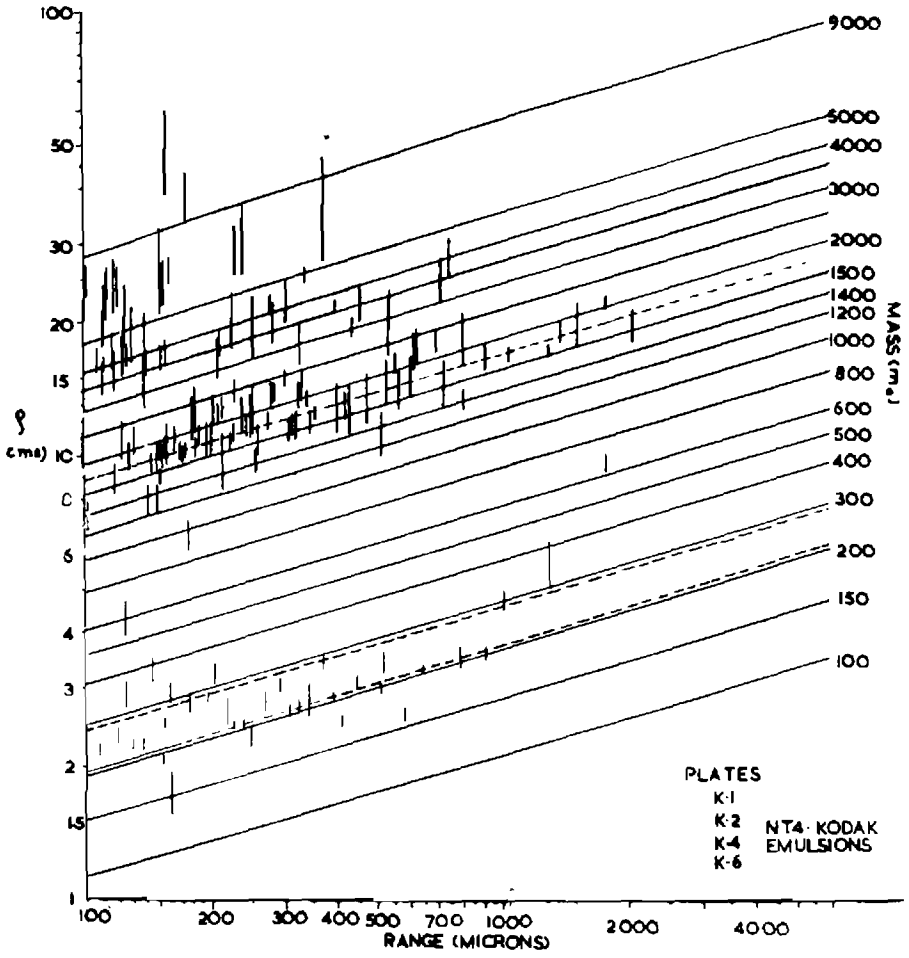

Figure 35. Logarithm of the radius of curvature ρ (cm.) versus logarithm of residual range r for mesons. The lines represent the function with slight corrections to allow for deviations of the range-energy relation from the power law for short ranges.

error in the curvature measurement being indicated for each point. Mesons, protons, and deuterons are all present.

Table X contains a list of the average meson mass values obtained by various research workers employing magnetic deflection methods.

TABLE X

MESON MASSES FROM THE MAGNETIC DEFLECTION METHOD

Mass ($\times 1/m_e$)	Type Meson	Reference
219 ± 26	Combining μ and ρ values	Barbour (184)
270 ± 23	Combining π and σ values	
150 - 250		Powell and Rosenblum (181)
217 ± 4	μ^+	Franzinetti (185)
281 ∓ 7	π^+	
288 ∓ 13	π^-	
236 ∓ 8	μ^-	
220 ± 5	μ^-	Franzinetti (183)

CHAPTER VIII

OTHER METHODS OF MESON MASS DETERMINATION

I. NEUTRON-PROTON EXCHANGE FORCE

A self-consistent method is developed by Kar and Roy (186) to determine the meson mass, the accuracy of which depends on the accuracy of the deuteron binding energy data.

The neutron-proton attractive force in a deuteron is taken by Kar and Roy to be of the Yukawa type and derivable from a potential. An exchange type of attractive force is observed between the particles, the meson evidently taking part in the exchange. Assuming a spherically symmetrical potential of the Yukawa type and referring the motion to the center of mass of the interacting neutron and proton, the wave equation of the neutron or proton due to a displacement after exchange is written and solved, giving an equation of the wave statistical binding energy of the deuteron in terms of the meson mass.

Calculations by this method gave a meson mass of 110 m_e. From the theory of proton-proton scattering developed somewhat similarly by Kar (187), the mass value was found to be 110.8 m_e, which was in unusually close agreement. It is unfortunate that experimental verification has not been obtained.

II. DEFLECTION IN COMBINED ELECTRIC AND MAGNETIC FIELDS

Many experiments have been carried out on the deflection

of charged particles in known uniform electric and magnetic fields with very consistent results. However, until the present time no experiments to determine meson masses have been undertaken since it has been practically impossible to control the mesons at will. The 184-inch Berkeley cyclotron, wherein mesons have recently been produced as mentioned earlier, perhaps will enable mass measurements of this type to be made in the future. Excellent opportunities for meson work have been made available by the latest development at Berkeley (188), namely, the production of variously charged mesons of the different types by exposing photographic plates to high-energy neutrons produced in the cyclotron.

One possible method of measuring the mass of these meson by means of combined known electric and magnetic fields would be to place the plates at right angles to crossed electric and magnetic fields so adjusted that no meson deflection is produced. This can only be done by previously taking many exposures of one kind of meson subjected to various values of the electric and magnetic fields. This, in turn, would only be possible if a meson of a definite type could be produced at will. With no meson deflection, the acceleration (f) of the meson due to the fields is zero and, from the well-known equation for motion of ions in combined fields such as this

$$Mf = ZeE' + HZev, \qquad (18)$$

we have

$$v = E'/H \qquad (18')$$

where Ze is the charge of the meson and E' the value of the electric field. If, now, the electric field is suppressed and a stream of mesons with the same velocity may be produced on the plates at right angles to the lines of force of the remaining magnetic field, the observed deflection would give the radius of curvature ρ in the magnetic field.

Letting E' = 0 in Eq. 18 we have

$$Mf = HZev. \qquad (19)$$

Since the path of the meson in the magnetic field will be a circle, its angular velocity about the center of this circle may be represented by ω, the centripetal acceleration then being $v\omega$. Substituting in Eq. 19,

$$Mv\omega = HZev,$$

and

$$\omega = HZe/M.$$

The radius ρ of the circular orbit is v/ω. Hence,

$$\rho = Mv/HZe.$$

But Eq. 18' gives the value of v; then

$$\rho = ME'/H^2Ze, \text{ or}$$

$$M = H^2\rho Ze/E',$$

which gives the meson mass if the charge Ze is known. The charge is usually taken as that of the electron, namely, e. Replacing Z by unity,

$$M = H^2 \rho e/E'.$$

Methods of this type, first employed successfully by J. J. Thomson, have given accurate ratios of charge to mass of the electron.

III. DISINTEGRATION

Photographic Technique

The observation of the transmutations of nuclei by charged mesons has led to the suggestion of a method for determining the mass of these particles based on observations of the total energy released in the disintegration. It is known that positive mesons decay with the emission of a positive or a negative electron which can be detected by delayed coincidence experiments, while negative mesons, at the end of their range, have a high probability of being captured by nuclei. The entry of the negative particles into the nucleus is assumed to produce nuclear excitation energy due to their annihilation, which is followed by the emission of heavy particles.

It is assumed, by regarding the momentum of the incident meson producing the disintegration and the observed directions of ejection of the disintegration particles, that neutrons or other particles unrecorded are also emitted in many cases. The

most favorable conditions of observation for the determination of the mass of the particles producing the disintegration is provided by using thick emulsions loaded with the light element Reactions involving the ejection of two particles of equal rang moving in opposite directions from the disintegrating nucleus are particularly easy to identify.

In attempting to apply the method, the particular nucleus undergoing disintegration must be identified. In the photograph of Fig. 36 (189) an incident meson (labeled m) causes a nucleus to disintegrate producing tracks of four heavy particles, of which the short tracks α_1, α_2, and α_3 end in the emulsion; α_1 and α_2 are found to be produced by α-particles, while grain-counts show that α_3 is due to a proton. Grain-counts on the track of the particle of long range, d, give the energy of the particle. The minimum energy which must be attributed to emitted neutrons if energy is going to be conserved in the disintegration has been determined, which allows a minimum mass value to be given the primary meson. The value established for m in this photograph is 240 m_e, agreeing very closely with the value, (240 ± 50) m_e, determined by grain counts.

The above value of the meson mass depends upon the assumption made by Lattes et al. (189) that the disintegration represented in Fig. 36 was of a nitrogen nucleus. That the nucleus was one of silver or bromine instead is probable on the basis of delayed coincidence experiments.

Perkins (169) observed a process in which it was

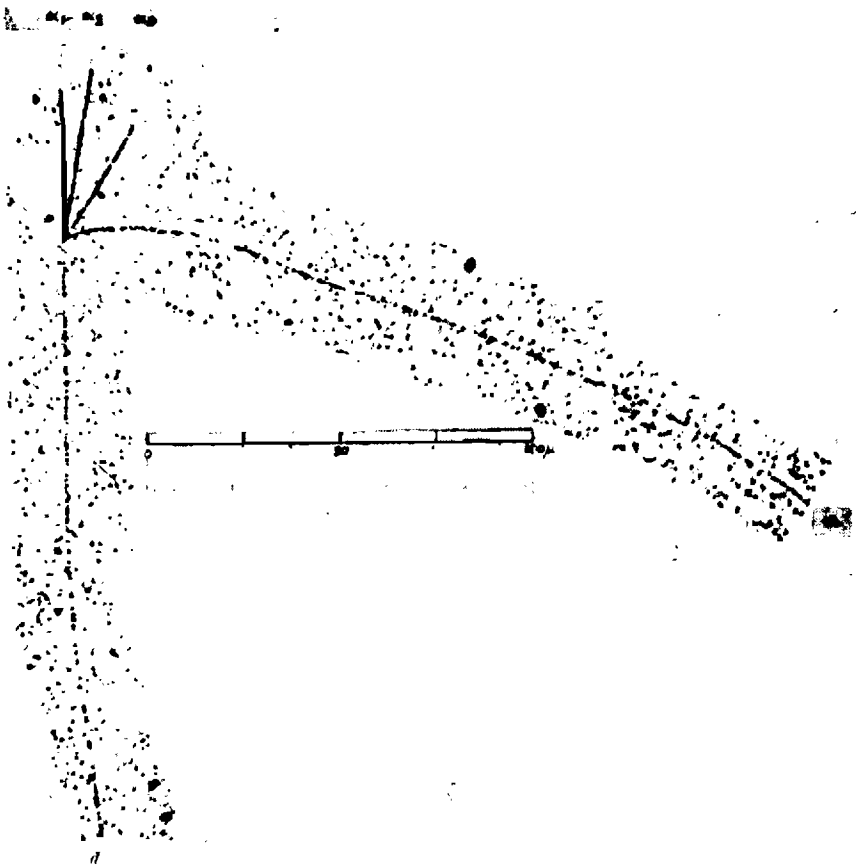

Figure 36. Disintegration of a nucleus by a meson as observed in an Ilford "Nuclear Research" emulsion, type C2, lithium-loaded.

established that the disintegrating nucleus could not be that of silver or bromine. Since the emitted particles had to have sufficient energy to surmount the potential barrier, the nucleus had to be either carbon, oxygen, or nitrogen, which all appear in the gelatin. Perkin's photograph was that of a star of five tracks, two due to protons of different energy, one due to a triton, one due to the incident meson, and one short track apparently due to the residual recoil nucleus.

To conserve momentum at least one neutron had to be postulated in view of the calculated momentum of the recoil nucleus. Further, the assumption is made that a negative meson nearly at the end of its range is captured and completely annihilated, its rest energy becoming nuclear excitation energy. With the limitation that the recoil nucleus probably has a fairly high excitation energy above the ground state (5 - 10 Mev) and is, therefore, relatively stable against further disintegration into charged particles, a large number of reactions are still possible considering all the isotopes of carbon, oxygen, and nitrogen. However, the mass excess of the recoil nucleus is generally considered to be a given value and, knowing that of the initial nucleus, by finding the negative Q value of the reaction (allowing for excitation energy) and the total kinetic energy of the ejected particles, the total excitation energy of the original nucleus may be found. On this hypothesis the rest energy of the incident meson was determined and the corresponding mass found to be between 120 m_e and 200 m_e.

From a rather complicated decay photograph, Brown et al. (190) concluded that a meson approached a point A, where it neared the end of its range, was captured by a nucleus or decayed spontaneously, and formed two tracks of either electrons, μ-mesons, or π-mesons. Considering a spontaneous decay and the resulting particles to be mesons only, they found the rest mass of the incident meson to be 869 m_e for two resulting μ-mesons and 985 m_e for two resulting π-mesons. Another particle emanating from A ended its range at another point and produced a disintegration there, emitting protons or heavier particles. Since this particle was frequently scattered in passing through the emulsion it was of low velocity and, due to the type of disintegration it produced, was considered a π^--meson. Its mass was determined to be 286 m_e. The original meson was assigned a mass of 1100 and labeled a K^+-meson.

To see how this π-meson mass value compares with another recent value, consider that obtained by Brode (191). Observing the kinetic energy of a μ-meson to be about 4 Mev and taking its mass as (215 ± 5) m_e, he calculated the mass of the π-meson to be (283 ± 7) m_e.

Leprince-Ringuet et al. (192) observed in an Ilford plate two stars linked together by a σ'-meson. The meson emerged from the one star and produced the other; it was assumed to be a σ'-meson of mass 300 m_e. The mass of the incident meson was computed as being greater than 700 m_e by calculating the energy of the meson emitting star, taking into account the neutrons

as well as the σ meson. A determination by grain counting leads to an agreement with the above mass value, the meson being considered as negative. This meson perhaps is a K^-.

For a μ-decay, in which the π-meson decays with a mean lifetime between 10^{-6} and 10^{-11} second into the μ-meson, Lattes Occhialini, and Powell (193) applied the conservation laws of energy and momentum in conjuction with the calculated energy of the secondary μ-meson obtained from a range-energy calibration and found that a balance in the process was provided by assuming the emission of a neutral particle of mass (115 ± 30) m_e, which they called the neutretto. The variation in the length of the track of secondary mesons produced in different events was found to be small and is attributed to straggling. This strongly suggests that, in μ-decay processes, the secondary mesons are always emitted with constant velocity.

Since π-mesons, of charge either positive or negative, are formed during nuclear disintegrations, and the π-meson decays spontaneously into a μ-meson, the postulated neutretto enables better interpretation of disintegrations and will no doubt account for more accurate meson mass values by the disintegration method.

Cloud-chamber Technique

By assuming a particle of mass M and initial momentum p to be transformed spontaneously into two particles of masses m_1 and m_2 of momenta p_1 and p_2 at angles of θ_1 and θ_2 with the direction of the incident particle, we may obtain the mass of

the incident particle, assuming the masses m_1 and m_2, from the following relations due to the laws of conservation of momentum and energy:

$$\sqrt{M^2c^4 + p^2c^2} = \sqrt{m_1^2c^4 + p_1^2c^2} + \sqrt{m_2^2c^4 + p_2^2c^2} ,$$

$$p = p_1 \cos \theta_1 + p_2 \cos \theta_2,$$

and $$p_1 \sin \theta_1 = p_2 \sin \theta_2.$$

The value of M must be greater than that obtained by taking the rest masses of the secondary particles as small compared with their momenta. Thus, the minimum value of M is given by

$$M_{min}\, c^2 = c\sqrt{(p_1 + p_2)^2 - p^2} \qquad (20)$$

In the special case where the incident particle disintegrates transversely into two particles of equal mass m_o, giving a symmetrical fork, the first of the above equations reduces to

$$\frac{M}{m_e} = \frac{2m_o}{m_e}\left(1 + \frac{p_{1,2}^2c^2}{m_o^2c^4} \sin^2 \theta_1\right)^{1/2}, \qquad (21)$$

where $p_{1,2}$ is the momentum of each of the secondary particles.

Applying Eq. 20 to a forked track in a cloud chamber, Rochester and Butler (1944), after calculating the values of p from the observed values of p_1 and p_2, found M_{min} for a neutral meson to be $(770 \pm 200)\ m_e$. Ionization and momenta showed the maximum value of M, M_{max}, to be 1600 m_e. The application of

the same equation to the forked track ab shown in Fig. 37 (194) by these men showed $M_{min} = (1,700 \pm 150)\ m_e$. By assuming different values of p, different values of M_{min} were found, the lowest of which was $M_{min} = (980 \pm 150)\ m_e$. They recalculated the mass of the incident meson by assuming various equal values of the masses of the secondary particles and using Eq. 21. The value was found to be about 1000 m_e. Fig. 37, then, was explained as the photograph of a charged incident meson, of mass greater than 980 m_e and less than that of a proton, which decayed into a penetrating particle and a neutral particle.

IV. MESO-STATES

Barnothy has developed a theory (195) to solve the problem of elementary particles with the help of four-dimensional space. The theory assumes electrons and protons to exist in unstable "meso-states" as well as in their normal stable state. The theory provides one solution for the meso-state of the electron (meso-electron) and eighty-two solutions for the meso-protons. Meso-electrons are identified with the ordinary mesons in cosmic rays. A mass value of $(250 \pm 10)\ m_e$ is assigned to the meso-electron by Barnothy (196), the mass values of the meso-protons being given as follows: (a) one meso-proton mass is 995.8 m_e, corresponding perhaps to the mesons of mass $(990 \pm 100)\ m_e$ observed by Leprince-Ringuet and Rochester and Butler; (b) another meso-proton mass is 481.8 m_e,

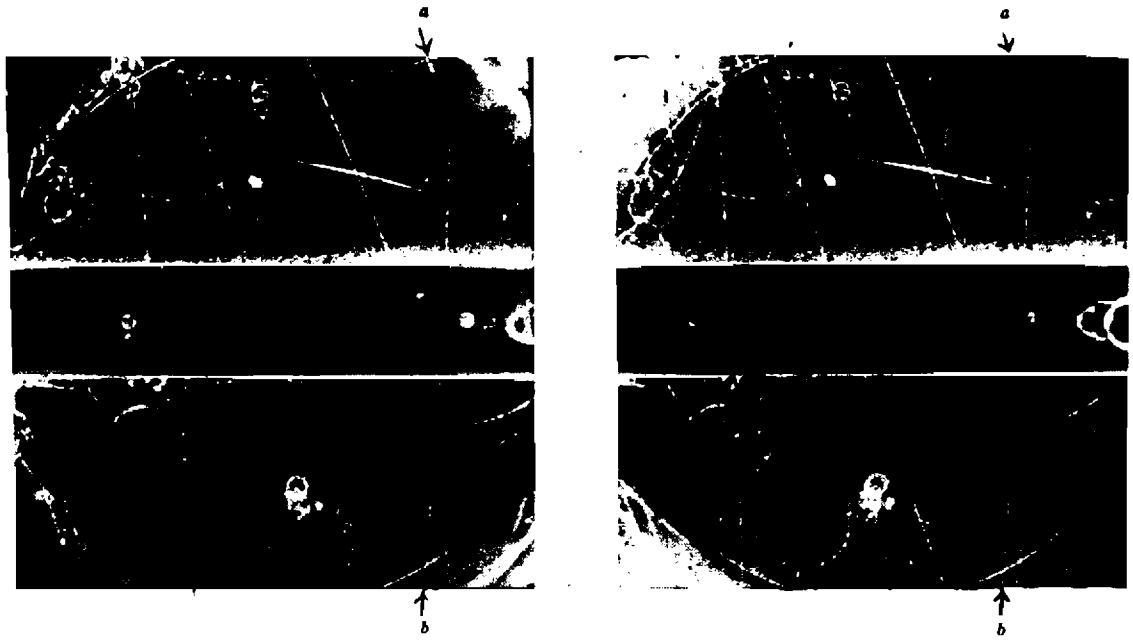

Figure 37. Stereoscopic photographs of the transformation of a meson into two light particles. The direction of the magnetic field is such that a positive particle coming downwards is deviated in a clockwise direction.

being perhaps the π-meson; (c) a third meso-proton mass is 217.8 m_e, possibly identifiable as a μ-meson. Many other meso-proton masses are given as well as an indication of the existence of a neutral meso-electron, corresponding perhaps to a neutral meson of mass only slightly smaller than that of the charged particle.

CHAPTER IX

DISCUSSION

I. GENERAL CAUSES OF INACCURATE MASS DETERMINATION

Distortions. Track distortions in cloud chambers may be caused by the optical system, the front glass plate of the chamber, or by the gas motions inside the chamber.

Optical or lens distortion is caused by the fact that large aperture lenses must be employed to get longer tracks when the tracks are photographed through a hole in the pole piece of the magnet and to get sufficient illumination. Distortions, which may be negative or positive, are found in even the very highest quality lenses. Blackett and Brode (197) have geometrically determined the distortion produced by a lens and experimentally verified this.

To determine experimentally the distortion due to the lens used, several parallel wires are photographed and the curvature of the images measured. The curvature of a track on a plate is the sum of the true curvature of the track and the distortion produced by the lens. Subtracting the distortion curvature from the total curvature gives the true curvature of the track. The distortion may be minimized by designing a special lens system to go with the particular front plate of the chamber.

Front plate distortion can be determined by the laws

of optics knowing the thickness and refractive index of the plate, the image distance, and the angle the axis of the camera makes with the plate. The distortion of the glass plate may be determined experimentally by measuring the image curvature of a straight wire, with and without the glass plate between the wire and the lens. Since the plate introduces positive distortion, a small negative distortion of a lens would possibly be compensated for if it were used with a proper front plate.

Chamber distortions due to irregular gas motions take place during the interval (about 10^{-2} sec.) between the passage of a ray and the instant of photographing while the chamber is being expanded. The tracks will also be distorted if any convection current exists before expansion. The fall of drops through the gas, the turbulent motion of the gas, vortices produced at the expansion, and variations in the room temperature surrounding the chamber are other causes of this type of distortion. The chamber distortion increases not only at distances away from the lens axis, but also as the inclination of the tracks to the vertical increases. For good results the tracks should be limited to the vertical direction as much as possible. Since the distortion is higher at higher room temperatures, some method such as enclosing the metal casings of the cloud chamber in a box cooled with running water should be employed. Convection currents may develop after expansion if a temperature difference between the chamber wall and the adiabatically cooled gas exists.

Illumination. It is often experienced that although good tracks are visible inside the cloud chamber, these do not appear in the photographs. This may be caused by improper illumination, wrong adjustment of magnification, or small depth of focus of the camera lens. The critical aperture to use must be determined so that the breadth of the average image is neithe increased nor decreased. Since the tracks in a cloud chamber are only visible due to the light scattered by the droplets and the intensity of the scattered light at 20° to the beam is about 100 times that at 90° for water and 50 times that at 90° for water-alcohol, the axis of the camera should be inclined at a small angle to the direction of the light for greater illumination. However, the camera axis must be placed normal to the direction of illumination when the depth of the chamber used is small since there is no alternative. This demands strong illumination for clear tracks, but strong illumination may also produce convection currents. Hence, the best illumination must be chosen with care.

Magnetic field. The magnetic field to be used in connection with a cloud chamber must be selected very carefully so that the curvature produced is neither very large causing the meson to revolve several times nor very small that the meson will pass undeflected. When the chamber is very deep ($\sim$30 cm.) the electromagnet needed to yield a large field strength will also require very high power for its operation. The field in these cases is uniform only over the region used

to photograph the meson tracks. The warming up of the magnet utilizing large amounts of power will increase distortion unless the chamber is properly temperature-controlled.

Photographic system. Investigations of a meson track in a cloud chamber require the track to be photographed from two different directions. For the sake of easier computations and accuracy in the determinations of the angle between various particles in the chamber, two cameras perpendicular to one another are employed. Many errors, which might arise because of bad alignments of the different parts of the cameras, are eliminated by replacing the developed negatives in the film holders of the camera in the exact positions in which they were when the photographs were taken and reprojecting the two images back in the object plane as previously described. However, the relative positions of the two cameras must be maintained at all times and some method devised to facilitate replacing the negatives in the exact positions they occupied at the time of exposure. Care must be taken to avoid distortion due to change of size and shape of the film at development. Speedy photography, as well as the use of superior photographic equipment, may reduce distortions developing after expansion.

Multiple scattering. At sufficiently low velocities, the effect of multiple scattering on cloud-chamber tracks will always be greater than the curvature of the meson in the magnetic field. This is especially true for a gas of high atomic number such as argon or a small magnetic field of the order

of 1000 gauss.

Multiple scattering has such a large effect because of the extremely low energy of any particle which can be stopped in the cloud chamber gas. The mean angle of deflection due to multiple scattering in a given thickness of material is inversely proportional to the particle's kinetic energy while the deflection produced by the magnetic field is only inversely proportional to the momentum.

Observers sometimes maintain that cloud-chamber tracks having a large curvature should yield accurate results since very exact measurements of ρ may thus be made. This is erroneous. It must be remembered that the normal, nearly straight tracks may not have been affected by scattering. Scattering causes a smooth circular arc rather than an erratic path because of effects such as the combination of magnetic and scattering curvature. If an already short track is broken into sections, the curvature in each section is relatively even more influenced by scattering than that of the entire track.

Williams (198) has given a rough formula for the apparent radius of curvature due to scattering as follows

$$\rho_s/R = 1.3(M/m_e Z')^{1/2}.$$

Bethe (199) gives the expression as

$$\rho_s = 103 \frac{M\beta^2}{Z'}\left(\frac{X}{BP}\right)^{1/2},$$

where M is the mass of the particle (including relativistic

correction) in units of the electron rest mass, X is the thickness traversed by the particle, P is 2 for air at NTP and 1 for argon at NTP, and B is a correction factor close to unity given by

$$B = 1 + 0.444 \log_{10} \frac{p}{m_e c} \theta_{max} (Z')^{-1/3},$$

θ_{max} being the maximum single angle scattering.

Discrepancies in the two equations are caused by different definitions of ρ_s, different definitions of the actual radius of curvature, differences in the range-energy relations used in deriving each equation, and differences in the treatment of θ_{max}.

Others. If the rate of expansion of a cloud chamber is slow, the amount of heat flow during the finite time of expansion must be taken into account. Allowance may be made for this heat flow during expansion by producing a little extra expansion. For sharp tracks, the distance moved by the piston should be as small as possible, the mass of the piston should be as light as can be managed, and the pressure inside the chamber should be as large as practicable. Non-axial movement of the piston may give rise to a distortion; however, this distortion may be modified by eddy currents in the piston due to the magnetic field or it may be mapped out in a way similar to that used for the distortions due to photography, except that the distortions due to movement of the piston are determined from the images of tracks in zero field and not from

the images of straight wires. The eddy current distortion can be determined only by noticing its effect on the change of curvature of particles passing through a metal plate placed in the chamber.

Apart from actual distortion, the measured curvature of a track in a cloud-chamber may be influenced by undue weight given to dense groups of ions, from ionization by low energy secondaries, which may be centered appreciably off the line of the trajectory. If the photographic exposure has been sufficient to record clearly the normal single drops of primary ionization, these groups may be ignored.

When all possible sources of curvature error are eliminated, residual random errors of curvature are expressed either directly or in terms of the maximum detectable momentum (that momentum which would give curvature equal to the probable curvature due to residual random distortion), which, in a single compartment chamber, can be measured only in zero magnetic field. In a chamber separated into two halves by a metal plate, it is possible to make a comparable determination of maximum detectable momentum in the full magnetic field (200). Values so obtained have agreed well with those measured in zero field.

In many cases distortion is encountered without external indication that error has been introduced. Therefore, a set of track photographs is usually cross-checked in all possible ways. At present, it is unlikely that any significant improvement in precision and elimination of errors can be made in

cloud-chamber measurements by further attention to detail. Greater precision must now probably be sought in the use of larger equipment and stronger magnetic fields.

For photographic plate methods. The task of finding and measuring meson tracks on photographic plates is made exceedingly difficult if a heavy background of silver grains is present. Since each track consists of a row of discrete silver grains whose average distance apart is several times the diameter of the grains, a stray silver particle at the beginning or end of a track will increase or decrease its apparent length, leading to an uncertainty regarding the terminals of a track.

Determinations of track length for particles which enter the emulsion at steep angles rather than at grazing incidence are done by measurement of depth. The process, called differential focusing, by which this is done is less accurate than the measurement of a track's horizontal projection with an eyepiece scale.

Spurious appearances, which are easily mistaken for real tracks, may be produced by the presence of foreign matter in the emulsion, by contractions of the gelatine during processing, or by scratches on the plates. Scratches may often be distinguished from real tracks because they usually lie entirely on the surface of the emulsion.

Using a dark-field illumination to allow the meson tracks to stand out more clearly enhances the visibility of

the many stray silver grains. Thus observational errors due to eye strain must be expected. Also, for fairly large grains, the center of a grain may be appreciably displaced from the true path of a particle.

The grain-spacing of a track increases as the temperature falls (214). This effect introduces another uncertainty in experiments in which it is difficult to maintain temperature control during say a prolonged exposure of the photographic plates.

II. EXPERIMENTAL ERRORS INVOLVED IN THE METHODS

Direct Methods

Elastic collision. The main source of inaccuracy lies in the uncertainty of $H\rho$ which is due, at $H\rho = 10^5$ gauss cm., about equally to scattering and to experimental error in the actual curvature measurement due to distortion. The elastic collision method requires a higher magnetic field for more precise $H\rho$ measurements in order to utilize the higher momentum tracks which are otherwise suitable for this method.

Multiple scattering introduces errors in the measurement of the momentum of the primary meson, the momentum of the electron, the angle, ψ_1, between electron and primary particle in the plane perpendicular to the magnetic field, and in the angle, ψ_2, between these particles in a plane parallel to the magnetic field.

The first error due to multiple scattering is usually quite small because a long track is available for curvature

measurements. The error in the radius ρ and therefore in E' and that in the sagitta f and therefore in ψ_1 (see Fig. 10a) are related. The error in f due to multiple scattering is calculated in Appendix V. Taking α (one half the angle subtended by the measured track length) to be 45° and β (see Appendix V) to be 45°, the probable error in f is given by Bethe (59) as

$$f = 0.722\,\Delta\rho,$$

where $\Delta\rho$ is the probable error of the radius of curvature.

In Eq. 3, if the actual radius in the magnetic field is greater than the apparent radius of the track (between A and B in Fig. 10a), the true path will have a greater sagitta than f and therefore a smaller cos ψ_1 than the true value. This means that the energy E' is greater than estimated and cos ψ_1 smaller than estimated. The actual mass of the primary will be less than the estimated one since both errors tend in the same direction.

The measurement of the angle ψ_2 will be affected by multiple scattering in that a mean square deflection will be produced as given by the following equation (201) with $x = \pi/2$:

$$\theta^2_{av}]_{pl} = \frac{4\pi e^4 Z'^2 Nx}{p^2 v^2} \ln \frac{\theta_{max}}{\theta_{min}}, \qquad (22)$$

where θ^2_{av} is the mean square average angle of scattering in a thickness x of a substance of atomic number Z'. The subscript pl indicates that the projection of the scattering on

a plane is meant, N is the number of atoms per cubic centimeter in the substance, and θ is the scattering angle. The minimum scattering angle θ_{min} is given as

$$\theta_{min} = (m_e c/p)[(Z')^{1/3}/181] ,$$

and the maximum angle, θ_{max}, is taken for cloud chamber tracks as that angle which can easily be recognized as single scattering (normally about .1 radian).

According to a scattering analysis given by Bethe (202), if all the probable errors are doubled and added together with the same sign, the upper limit of the mass $M = (990 \pm 120)\ m_e$ given by Leprince-Ringuet and Lheritier (203) could reach the proton mass while the lower limit cannot be less than 600 m_e. The ejected electron is at its minimum of ionization, which favors the primary to be a very heavy meson since a primary proton would produce an ionization 2.4 times the minimum. But estimates of ionization without droplet counting are qualitative and often incorrect. Bethe gives the probable error in the measurement of the momentum of the primary particle as 5 per cent due to multiple scattering.

The meson track reported by Leprince-Ringuet and coworkers (62), which gave a mass of $(240 \pm 20)\ m_e$, has an error due to measurement given by the authors as 10 per cent. Bethe (202), in analyzing the track with regard to scattering, gives the probable error of the meson mass (adding the squares of the individual errors) as 16 per cent and a mass of 200 m_e as

within the probable error. He determines a probable error in the meson momentum of 3 per cent, in the electron momentum of 8.4 per cent (causing a probable error of 8.6 per cent in the expression $[E' + m_e c^2]/[E' - m_e c^2]$ in Eq. 4), in f of 0.061ρ (the error in cos ψ_1 then being 0.061), and in cos ψ_2 of 2.4 per cent (the probable angle of scattering being given as 4.6°).

An error of ± 22 in the mass value of 240 m_e given by Leprince-Ringuet et al. (204) was obtained by computing a 2 per cent error in the ρ_1 measurement, a 2 per cent error in the measurement of θ, a 2.5 per cent error in determining ρ_3, a 2 per cent error in determining f, and a 1 per cent error in H.

Indirect Methods

Range and curvature. A drawback of this method is as follows: as the meson slows down it is subject to increasing amounts of scattering for which it is difficult to allow. However, this is the most accurate of all the methods with the possible exception of the photographic method, as both the curvature and the range may be measured fairly accurately from sharp tracks. Often, though, only a lower estimate can be made of the range, in which case this method gives an upper limit of the mass of the particle.

Williams's formula for the average spurious radius, ρ_s, caused by scattering which must be added to the uncertainty of measurement of the Hρ value has been reduced by Hughes (205)

to a simple form applicable to his chamber. The formula can be made to apply to any chamber if the differences in chamber gas and magnetic field are taken into account.

For H = 1165 gauss, argon gas at a pressure of 80 cm., and a track length of 16 cm.,

$$\rho_s/\rho = 15.0\,\beta\,, \qquad (23)$$

which shows a 7 per cent error in ρ due to ρ_s when fast particles are involved and a spurious curvature equal to the magnetic curvature for $\beta = 0.067$. Hence, even though the lower momentum particles enable easier curvature measurements, the error due to scattering will be greater and the accuracy of mass determination less.

For a given chamber gas, magnetic field, and meson mass there is a certain curvature value for which the accuracy of mass determination is a maximum. In Fig. 38 (206), Hughes shows the accuracy of mass determination as a function of ρ for his chamber. He assumes that the error (due to convection currents, etc.) in measuring radius of curvature is equal to a displacement of the center of the track of 0.05 cm., basing this value on tracks measured with no magnetic field in the same chamber. The curves marked "fixed R" are the probable error when mass is determined from measured range (assuming no error) and curvature. The results were calculated from the nomograph in Fig. 1 and Eq. 23.

From Fig. 38 it can be seen that the accuracy in mass

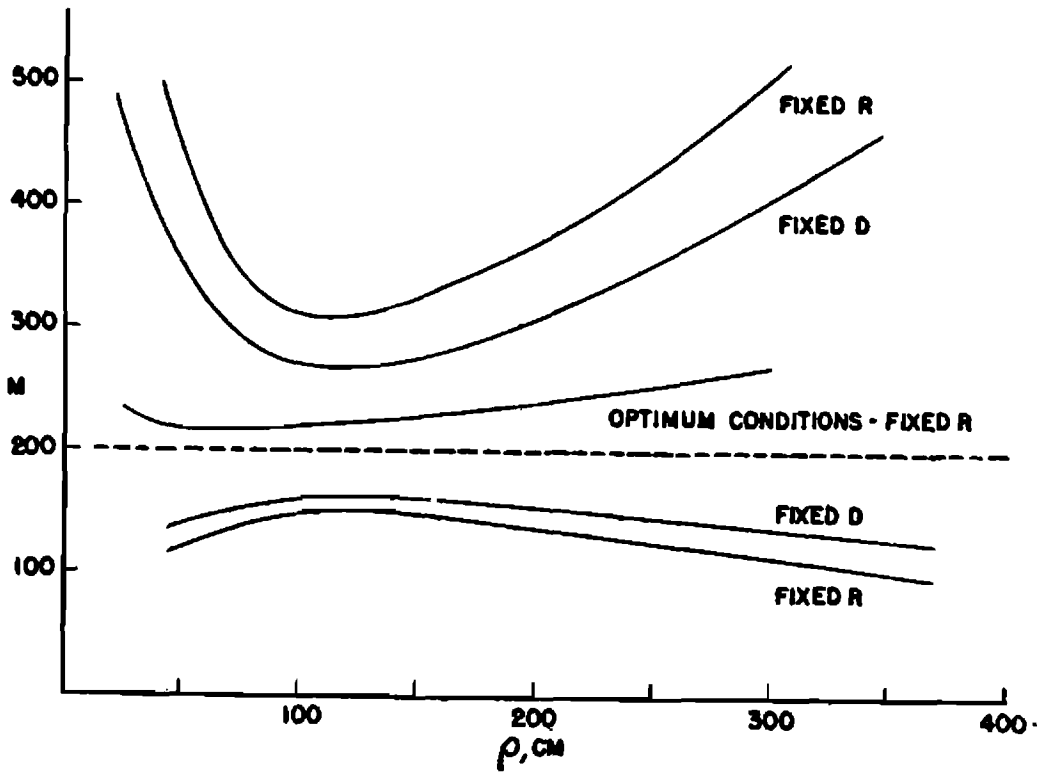

Figure 38. Variation in meson mass (M) as a function of radius of curvature (ρ) for an assumed true mass of 200 m_e. Curves labeled "fixed R" and "fixed D" refer to measurements based on range and on ionization density. The curve "optimum conditions" is for the highest accuracy to be expected from the chamber used to make the other measurements.

determination with Hughes's chamber is greatest for a radius of curvature of about 125 cm. corresponding to a range of 500 cm. and that the accuracy is greater for a determination based on a measured D than on a measured R, assuming no error in the measurement of each. Even at best, Hughes gives the mass as 200(+50, -32) m_e, the accuracy at best being only about 20 per cent.

If the operating conditions of Hughes's chamber were to be improved, the highest accuracy that could be expected is shown as the curve marked "optimum" conditions in Fig. 38. The "optimum" conditions refer to the same magnetic field of 1165 gauss, substitution of helium for argon as the gas in the chamber, measurement of range in the chamber with negligible error, and reduction of chamber distortion to the extent that the magnetic displacement of the center of the track can be determined to 0.02 cm. Under such conditions the minimum error in the meson mass is given as 8 per cent, attainable only at a radius of curvature of 65 cm. Plotting a similar graph for a different chamber, one could determine the curvature for the best value of mass.

If the magnetic field were doubled, the most accurate point would occur at half the radius of curvature, the same $H\rho$ value, and the same range, doubling the accuracy. A four-fold increase of H for the optimum conditions mentioned above would lower the error in mass to 2 per cent, reducing the radius of curvature to 16 cm. Mesons with such small radii of curva-

ture, however, would tend to be deflected away from the cloud chamber by the magnetic field being produced. The higher magnetic field would give an accuracy of about 8 per cent, the same as the optimum for the lower field, but for particles of four times the momentum. These mesons will have the same radii of curvature as those of one-fourth the momentum and therefore will have the same probability of reaching the chamber. Hence, in such a case, equal accuracy is attained for the high-momentum particles. The high field, though, causes the particles to have greater ranges requiring more absorbers in the chamber and, consequently, making range measurements more difficult. If the particles are produced artificially in the chamber, a high magnetic field and the optimum curvature may be employed since the increase of optimum curvature with the magnetic field does not apply in this case.

Change of chamber gas, change of pressure, use of absorbers in determining R, etc., will all change the accuracy somewhat as follows:

ρ_s/ρ changes very nearly as $l^{\frac{1}{2}}$ (where l is the track length,

ρ_s/ρ changes as Z^{-1} (where Z is the atomic number of the chamber gas),

ρ_s/ρ changes as $p^{-\frac{1}{2}}$ (where p is the chamber pressure), and

ρ_s/ρ changes as H (where H is the magnetic field strength)

Summarizing, the highest accuracy is obtained for a high magnetic field, a particular curvature value, a gas of low atomic weight and low pressure, and a rather long track length.

A curvature correction of 0.3 ± 0.04 meter^{-1} with a cloud chamber filled with air at 1.13 atmospheres was derived by Retallack and Brode (207) from the measurement of 60 no-field tracks of mesons. The field employed for the measurement of curvature was 4750 gauss. The probable errors due to scattering were found to be from 1.5 to 2.5 per cent for mesons of energies from 50 to 600 Mev, but the probable errors due to turbulence from 3 to 8.5 per cent for this range.

The track of Fig. 13 was that of a meson of mass 250 m_e, the mass giving a range in $H\rho$ due to ρ_s of 0.82 to 1.46×10^5 gauss cm. This range in $H\rho$ is about the minimum to be expected, for the track has a radius of curvature of 90 cm. from Fig. 38. However, the corresponding uncertainty in the meson mass is still about 150 m_e, the actual value being anywhere between 200 m_e and 350 m_e.

If the effect of ρ_s on the track of Fig. 14 is now calculated, it is found to be very large due to the small $H\rho$ value and short track length. Bethe corrects this value by taking into account the multiple scattering due to the atoms of the cloud-chamber gas and shows it to be consistent with a mass of about 200 m_e (see Chapter X).

Momentum loss. It is important to avoid large scattering in determining the mass of the meson by the method of momentum loss. If the momentum of the meson after traversing the plate is considerably less than that before traversal, the momentum change measurement can be made accurately. However,

the momentum of the particle after traversal must not be too small to insure small scattering. If the momentum decreases in the plate by a factor of the order of 1/2, both conditions will be satisfactorily fulfilled.

Large errors in employing this method are due to turbulence in the upper chamber, distortion of the track by the glass of the chamber through which track photographs are made and the camera system, and errors in the measurement of the track.

The probable error due to scattering (208) depends on the length of track, the magnetic field, and the velocity of the mesons. The error in magnification due to the plane in which the meson passes through the illuminated region introduces an error proportional to the curvature. It is usually estimated from the depth of the illumination. Uncertainty in the measurement of the magnetic field is due to calibration, current measurement, flip coil, etc. The usual procedure in determining turbulence errors is to observe the appearance of other tracks on the same strip of film, since turbulence is obvious in tracks that are bent very little by the magnetic field. Since the displacement of the track, when plotted on a large scale, should be nearly parabolic, a displacement plot compared with true parabolas reveals any skew or off-center motion before the picture was taken.

Chamber distortions are greatly increased by the insertion of one or more plates inside the chamber. To determine

the corrections for distortion, during each run no-field tracks, interspaced in time with the field tracks, are photographed. The pictures are made simultaneously for each half of the chamber. From these no-field tracks, distortion curves giving the curvature correction for each half of the chamber and for each separate run versus position in the chamber are constructed. Since it is possible for photographs to indicate that the meson has gained momentum after emerging out of the plate due to curvature errors, the determination of such errors are of primary importance.

It was generally concluded by Fretter (209) in his experiments employing momentum loss methods that the uncertainty in $H\rho$ in the majority of tracks varied from ± 5 per cent to ± 10 per cent. He rejected tracks with an uncertainty greater than this in plotting his mass values (Fig. 21a). He arrived at this error by estimating the uncertainty in measuring the magnetic field to be about 2 per cent, in measuring the magnification factor less than 1 per cent, in measuring track curvature about 2 per cent, and the uncertainty caused by scattering in the argon of his chamber about 2 per cent. The latter was determined by means of the formula for the spurious radius of curvature produced by scattering in the gas of the upper chamber given by Williams (198) and mentioned previously.

Retallack and Brode (210) obtain a probable error in curvature of 0.04 meter^{-1}, which is derived from the measurements on 60 no-field tracks. This gives an error in C, the

curvature in unit field x 10^6, plotted as abscissa in Fig. 24, of 0.084 cm.$^{-1}$ gauss^{-1}. The other errors were determined as follows: estimated error in magnification, 0.01 C; estimated probable error in measurement of the magnetic field, 0.01 C; probable error due to scattering (on the assumption of a mass of 200 m_e), 0.02 C. The total error in the curvature, C, is compounded from these errors: $[(0.084)^2 + (0.025)^2C^2]^{1/2}$. The probable error in range is given as 0.17 cm./cos θ, that is, one fourth the plate thickness divided by the cosine of the angle of the track with the vertical as it enters the last plate.

For mesons that remain in the illuminated area, the uncertainty in range as determined by Fretter (211) is given as 0.25 inch of lead for particles that appear to ionize heavily before entering the plate and 0.5 inch of lead for those that appear to ionize normally. Since the average angle of scattering for the latter as they enter the lead is about 8°, the correction due to this is neglected since it is not large. The maximum value of mass for a given set of data was calculated using the maximum $H\rho$ and minimum range, while the minimum $H\rho$ and maximum range gave a minimum mass value. Fretter assigned to the probable error of each observation of mass a value about 30 per cent less than the maximum error since he considered it unlikely that the uncertainties in $H\rho$ and range would add in the way described.

In the experiments of Fretter and Brode (86), the

uncertainty in $H\rho$ is given as approximately 10 per cent and the uncertainty in range as about 1/2 inch of lead. These lead to an uncertainty in the mass of $\pm 30\ m_e$. The straggling in range found by Street (212) in a similar experiment was not in evidence.

Fig. 39 shows the relationships between meson mass M, range R, and $H\rho$ as determined by Hughes (213) to obtain the error in M due to a certain error in $H\rho$. The error for $M = 200\ m_e$ at an R of 50 g./cm.^{2} in lead represents a 10 per cent error in $H\rho$. Hughes gives the corresponding error in M to be 20 per cent.

Ionization and curvature. Fig. 38 (curves marked "fixed D") shows the probable error of mass values for an actual mass of $200\ m_e$ by the ionization and curvature method.

The probable errors which were predominant in all the determinations made by this method were those due to chamber distortion of curvature and the statistical uncertainty arising from droplet counting. Nielsen and Powell give the statistical error in their counts of 335 droplets as approximately 5 per cent. They determined curvature by plotting micrometer readings of coordinates along the track and fitting a curve to the points by the method of least squares, giving a probable error in one curvature determined from 13 points of 3.5 per cent.

Williams, from tracks of fast particles in the same part of the chamber at the same time as the meson of mass

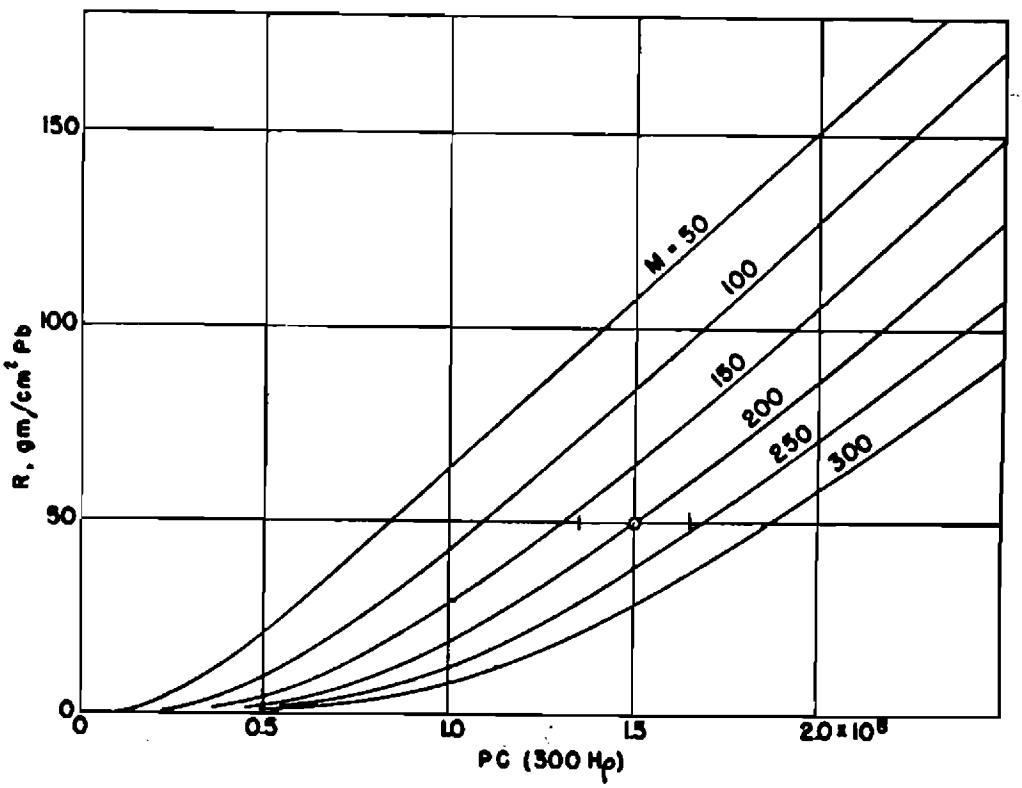

Figure 39. The relationship between momentum and range for different values of meson mass M. Assuming R measured accurately, the error in M is considered to be 1.5 times the error in $H\rho$ for low velocities and a mass of 200 (see Fig. 1) and 2 times at an $H\rho$ of about 5×10^5 gauss cm. (point indicated).

(160±30) m_e, found the spurious curvature to be less than about one-twentieth the curvature of the track and in the opposite direction. The extent of the spurious curvature corresponding to distortion was small and also in the opposite direction to that of the track.

Ionization and range. This method is limited to mesons of rather low energy and has been predominantly applied to the positive mesons. The errors involved are generally the same as those cited in the other methods involving ionization and range measurements.

Photographic Plate Methods

Coulomb scattering. The errors arising by employing multiple Coulomb scattering theories to determine meson masses give a spurious scattering superimposed on the Coulomb scattering. These errors are due to the size of the grains, the distortion of the microscopic field, the errors in measuring, and, if the tracks are redrawn for better determinations, errors in drawing.

Goldschmidt-Clermont, et al. (215), have evaluated the spurious scattering in their experiments mentioned previously by means of observations on the tracks of very fast protons, these tracks having a negligible multiple scattering and the same grain density at corresponding points in the tracks as mesons of the same velocity. Almost all the observed changes in direction were due to the sources of error mentioned above.

Spurious scattering may be determined by measuring the displacements from gravitational centers of the grains in a proton track from a line running roughly parallel to the direction of the track. A factor is then obtained which indicates the mean displacement of the individual grains about the path of the particle. This factor provides a useful indication of the spurious scattering on all types of track, even those with large multiple scattering.

From measurements on 10 mesons, Goldschmidt-Clermont, et al. (216) give the correction for spurious scattering over a whole track to be less than 3 per cent. They also find that the spurious scattering decreases the longer the length of the cells they draw on the tracks. Since the Coulomb multiple scattering increases with longer cells, they find that by choosing proper lengths for the successive cells, spurious scattering can be made less than one-quarter of the true Coulomb scattering. They give the systematic experimental error as about ± 7 per cent. Although their experiments indicated the existence of mesons of mass approximately 80 m_e, their statistical errors are too great to accept the observations as reliable evidence for mesons of this mass value.

Choudhuri (217) gives the theoretical drawbacks in her method as (1) the procedure of adding together the individual track deflections, if this is done, and (2) the substitution of the resultant track deflection thus found for $\bar{\theta}$ in Eq. 12 for determining the average energy for a meson

producing tracks with a certain value of mean grain spacing. She compares her data as shown in Table VIII (Chapter VII), where the meson masses are given for tracks grouped together under defined limits, with the values obtained when the tracks belonging to the same mean grain spacing group in two plates are combined together. The mass determined in this latter way always was smaller than that estimated from the two plates separately.

Grain counting. The main source of error in determinations by grain counts arises from the fugitive nature of the latent image produced in the silver halide granules by the passing of the particle. In a case such as the μ-meson decay, it is assumed that the two meson tracks are formed in quick succession and are subject to the same degree of fading. Also, in such an event, both tracks are completely contained in a very small volume of the emulsion, the processing conditions therefore being identical for both tracks, apart from the variation of the degree of development with depth. This requires contemporaneous tracks, which would ordinarily result in a short track for one of the components. However, if short exposures are employed, the effects of fading may be considered negligible, and by developing the plates by the method employed by Dilworth, Occhialini, and Payne (218), nearly uniform degree of development with depth is obtained. In the plates obtained by these methods, it is legitimate to compare the grain-density in the tracks of unrelated particles.

Further difficulties arise in grain counting from the fact that in addition to the standard deviations in the number of grains counted, places exist in the emulsion in which the concentration of grains is significantly higher, or significantly lower, than the average values. It is found, however, that the influence of this factor on the total number of grains in relatively long tracks is not more serious than the purely statistical fluctuations associated with the finite number of grains in a track.

The above errors will be small if the measurements are made on a sufficiently large number of mesons. They contribute however, to the variations in the individual mass values.

Magnetic deflection. Probable errors in angular deflection are due to errors in the theoretical average scattering angle, for a meson of the range and mass considered; emulsion distortion (Barbour (180) measured deflections of protons with no field and found a standard deviation of $1/2^{o}$); and instrumental errors. Since scattering introduces the greatest uncertainty, it is highly desirable to make measurements on particles with range 500 μ or greater. Mesons with small dip angles will have a small per cent of error due to an increase in the deflection angle with the path length in the air gap, the curvature remaining the same.

The scattering is the result of elastic collisions of mesons with oxygen or nitrogen nuclei in passing through the gas between the plates. If the nuclear collision occurs near

the mid-point of the trajectory of the meson in the air-gap, the deviation is of such a nature that the meson track can still be accepted. The observed deflection will be either greater than or less than that due to the magnetic deflection alone, and the calculated mass values correspondingly greater or less than the true value.

Inelastic scattering of protons in the emulsion tends to lead to an overestimate of the mass. Also, in the emulsions, the individual grains in the track may be displaced from the true line of the trajectory. However, the error from spurious scattering may be neglected in experiments with C2 Ilford plates, the effect having been found by Goldschmidt-Clermont, et al. (216) to be less than 3 per cent of the real scattering for tracks of range less than 2000 μ .

Near the edges of the plates, and confined to these regions, serious distortion of the emulsion extending over large areas has been found. This effect may change the coordinates of a point by more than 10 μ . The affected area extends inwards from the edges of the plate for 2 mm. in the case of emulsions 50μ thick and for 1 cm. for 200 μ emulsions. If special care is not taken in processing, local distortions occur which may alter the direction of a track considerably. Differences in the general background of grains often accompany local distortions and hence they may be detected, with the naked eye, in the form of slight imperfections in the smooth surface of the emulsion.

Errors due to scattering in the surface layers of the emulsion depend on the method of defining the direction of the track. Franzinetti (219) defines the direction of the track to be the direction of the chord in the last few microns as the track approaches the surface of the emulsion. The angle ξ between the chord and the trajectory as given by Rossi and Greisen (220) is

$$\xi^2 = 4/3(t/w^2),$$

where t is the length of the chord in radiation units and w is a function of the momentum and velocity.

The total angular deviation θ of a track from its original direction, after a path t, is given by Franzinetti as

$$\theta^2 = 2t/w^2 = 1.5\,\xi^2.$$

From experimental values of θ, ξ is easily evaluated.

III. GENERAL CRITICISMS OF THE METHODS

At present, it seems that the elastic collision method affords a more accurate means of determining meson mass (when a picture of a head-on collision, or nearly such, can be obtained) than do the indirect methods. Although mesons of very high primary momentum may be used on which to make mass measurements, a rather high magnetic field is required to determine

accurately the curvatures of recoil electrons. Curvature measurements, too, are always susceptible to errors due to distortion and scattering. The primary meson is also subject to scattering.

Mass determination by range and curvature is probably the most accurate of the indirect methods provided the same accuracy in data exists throughout the various methods. This may be due to the fact that it does not involve measurement of specific ionization and is therefore independent of any assumptions underlying the theoretical ionization loss formulae. Here, again, spurious curvature gives erroneous effects which must be corrected. Range measurements afford no great difficulty if the meson stops in the cloud chamber. If it does not, only an estimate of its range can be made or a value of $H\rho$ and a minimum range assigned the meson, thus setting its upper mass value.

The momentum loss method also avoids measurement of the density of ionization and, since the thickness of a material can be very accurately measured, this method should be quite dependable taking into account the $H\rho$ corrections. Of course, the reliability of the energy loss formulas applied is questionable and the resolving power of the method is found to be poor for $H\rho >> 4 \times 10^5$ gauss cm. This method fortunately has few limitations and, hence, an abundance of data can be obtained. Scattering again must be avoided.

Ionization and curvature presents a fairly good method

of determining meson mass. However, which of the theoretical expressions mentioned actually holds, if either does, seems to warrant further investigation and experiment. Droplet counting and curvature distortion appear to be the greatest setbacks of this method.

A method of not too great an accuracy is that of ionization and range since both measurements are likely to be underestimated and the ionization determination presents a particular problem. The method fails almost entirely for mesons that do not stop in a cloud chamber.

Photographic plate methods afford the easiest and most reliable mass determinations, especially of the various types of mesons practically unknown until recent investigations on cosmic rays were undertaken with photographic plate methods. Even though heavy backgrounds may seem to indicate that accurate measurements on mesons cannot be made, the contrary has been established. In fact, plates have been devised which nearly eliminate this background. The errors due to scattering can be determined much more easily than scattering errors in the other mass determination methods. Fading in the grain counting method presents a problem as does emulsion distortion in the magnetic deflection method. Both, however, may well be compensated for.

CHAPTER X

SUMMARY AND CONCLUSIONS

I. SUMMARY

A discussion of the various methods of measuring meson mass, the laws and equations involved, and the apparatus necessary has been presented together with a survey of the work of many experimenters and the mass values that have been published. Also, general causes for inaccuracy in the mass measurements and experimental errors that arose in the various methods were presented with criticisms.

In view of the previous mass determinations, it is the writer's opinion that mass of the μ-meson is between 210 m_e and 225 m_e and that of the π-meson between 270 m_e and 290 m_e. The best mass values, then, are given as follows. Only those values are considered whose limits are in the ranges given above. The date of the published data is given after each reference.

Range and curvature method

Mass	Type	Reference
285 m_e	π	Bishop (89) (1949)
286 m_e	π	
216 m_e	μ	

Momentum loss method

Mass	Type	Reference
215$\pm$4 m_e	μ	Retallack and Brode (116) (1949)

Momentum loss method (continued)

Mass	Type	Reference
218±5 m_e	μ	Brode (118) (1949)
215±2 m_e	μ	

Ionization and curvature method

Mass	Type	Reference
210 m_e	μ	Williams and Pickup (137) (1938)
214 m_e	μ	Hughes (65) (1941)

Coulomb scattering method

Mass	Type	Reference
214 m_e	μ	Bose and Choudhuri (166)
219 m_e	μ	(1944)

Magnetic deflection method

Mass	Type	Reference
220±5 m_e	μ	Franzinetti (183) (1950)
217±4 m_e	μ	Franzinetti (185) (1950)
281±7 m_e	π	

Disintegration method

Mass	Type	Reference
286 m_e	π	Brown et al. (190) (1949)
283±7 m_e	π	Brode (191) (1949)

In conclusion, a survey of the literature has been made to determine what has been done in arriving at a solution to the problem of the uniqueness of the meson mass from the many values that have been published. Some of these have been corrected and many have been collected and plotted to determine their distribution.

II. CONCLUSIONS

As can be seen from the tables presented in this thesis, wide variations in the meson mass values have been obtained by competent observers using different experimental methods. Variations in the results obtained by one and the same observer may be due partly to experimental difficulties, while variations in the results of different investigators using the same technique may be attributed to differences in experimental interpretations and observations.

But making allowances for the occurence of large experimental errors, the mass values obtained are so widely different that it has led to the question of whether a unique mass may be assigned to the different types of mesons. Let us briefly survey a few of the measurements described and listed previously to determine whether the data may be analyzed to arrive at a mass value compatible with a unique mass.

Considering the measurements involving the cloud chamber, Bethe (221) has pointed out the errors brought about by multiple scattering due to the atoms of the gas and, taking these errors into account, has shown that all the data which appear to give a mass less than 200 m_e are subject to scattering. He states that the various cloud chamber measurements not yielding a unique mass for the normal meson in the neighborhood of 200 electron masses can be made to do so by considering the scattering involved. The track of Hughes (222) which led to a mass of 10 to 50 electron masses, the track

of Nishina and collaborators (82) yielding (180±20) m_e, and Ruhlig and Crane's (223) value of (120±30) m_e are all shown by Bethe to be compatible with a mass of 200 m_e. The masses of 240 m_e (62) and (990±12) m_e (224) given by Leprince-Ringuet using the method of elastic collision are also subject to scattering errors, both values actually being about 200 m_e when the scattering errors are taken into account.

The 72 determinations made by Brode (118) to arrive at a mean meson mass value of 215 m_e are all statistical fluctuations of what appears to be a unique mass. External and internal consistency rules (225) were applied to the data to obtain the mean mass value. However, Brode also found a distribution of masses about the 500 to 800 range of mesons whose ionization above more than one lead plate and whose noticeably smaller scattering confirmed the assignment of the larger mass value to these mesons.

From 43 observations, omitting the four highest and the two lowest mass values, Retallack and Brode (226) find a consistent set of observations yielding a mean value of (215±4) m_e for the ordinary meson mass based on the rules of external and internal consistency. However, the six observations not included were taken as indicating that the mass of the meson as observed at sea level was perhaps not unique or that heavier and lighter mesons existed. Four of the six observations indicated a mass too large to be considered as statistical fluctuations in the observations of normal mesons and the

remaining two indicated too small a mass.

A unique mass of 202 m_e based on external and internal consistency was found by Fretter (209) taking the data for 26 particles. The probable error was determined to be ± 5 per cent.

Taking 47 quantitative individual meson mass determinations of the 50 believed published up to December 1, 1946, and recalculating the mass value using the nomograph shown in Fig. 1 to eliminate differences in the theoretical formulas used by different experimenters, Hughes (122) arranged the individual values in terms of increasing mass. The masses were found to cover a wide range from 30 to 1000 electron masses. However, because of the large experimental errors associated with many of the values as previously discussed, 60 per cent of the total determinations were found to be within experimental error of a single mass of 200 m_e. Evidence for a few masses of different values was also recognized.

The main differences in the mass values that Hughes's correction brings about is differences that are due to one author's use of the theoretical formula (227) for the density of ionization of electrons as a function of β(approximately $\beta^{-1.8}$ in the usual range) and another's use of experimental values for β such as the value $\beta^{-1.4}$ found by Williams (228). Mass determinations whose errors are such that only an upper or lower limit for the mass could be obtained were omitted as were those which gave only an average mass value based on some average property of mesons as the average density in photographic

emulsions. The nomograph used to calculate the mass values is based on the theoretical change of ionization with velocity. If the experiments (121) which show a different change of ionization with velocity are true, the measured masses would increase.

In order to check the possibility that only a single mass is actually involved in all the various measurements, Hughes calculated the error in the curvature measurement which would be necessary to give the observed results in each case, assuming the actual mass had a single value and assuming the entire error to be that of curvature measurement since this error is the predominant one practically without exception. The expected mean error for each curvature measurement was also calculated for the particular experimental conditions again assuming a single meson mass. Assuming true masses of 175 m_e and 190 m_e, Hughes plotted the resulting distribution of calculated errors in terms of the mean expected error and found a rather close agreement between the observed distribution of calculated errors and that expected as shown by a Gaussian plot of the distribution of errors. This means that if all the different measurements are considered as repeated trials with varying experimental conditions the distribution of results is about what would be expected. The agreement with mass 175 m_e seems better than with mass 190 m_e. Since the nomograph used to calculate the mass values is based on the theoretical change of ionization with velocity, which

experiments show to be in error, the measured masses are low.

Hogrebe (229) has taken the many values collected by Hughes and those of Fretter previously mentioned and has plotted them, arriving at two distributions of mass, one in the neighborhood of 171 m_e and the other near 237 m_e with an error of approximately $\pm$10 m_e. Two meson mass values are definitely indicated. The mass values are low for the same reason Hughes's values were considered low.

Thus we see excellent evidence for the existence of unique mass values for different types of mesons. Currently, the positive and negative π-mesons are taken to be of mass (285$\pm$5) m_e, and the μ-mesons, both plus and minus, of mass (216$\pm$5) m_e, these two being the only mesons accepted as well-attested members of the family of nuclear particles. Of course, there are probably others, as has been indicated, such as mesons of mass (700 - 1100) m_e. There are even a few scraps of evidence pointing to mesons of mass from 3 to 10 times that of the electron (called λ-mesons by some). Few physicists at present however take a positive stand one way or the other on any but the π- and μ-meson. Since all known fundamental particles have a definite rest mass, the most unambiguous and accurate experimental evidence would have to be obtained before a non-unique rest mass could be accepted.

BIBLIOGRAPHY

BIBLIOGRAPHY

1. Corson, D. R., and Brode, R. B., "The Specific Ionization and Mass of Cosmic-Ray Particles," The Physical Review 53:776 (1938).

2. Skobelzyn, D., "Über Eine Neue Art Sehr Schneller β-Strahlen," Zeitschrift für Physik 54:686-702 (1929).

3. Rossi, B., "Absorptionsmessungen der Durchdringenden Korpuskularstrahlung in Einem Meter Blei," Die Naturwissenschaften 20:65 (1932).

4. Rossi, B., "Über die Eigenschaften der Durchdringenden Korpuskularstrahlung im Meeresniveau," Zeitschrift für Physik 82:151-178 (1933).

5. Street, J. C., Woodward, R. H., and Stevenson, E. C., "The Absorption of Cosmic-Ray Electrons," The Physical Review 47:891-895 (1935).

6. Ehrenfest, P. and Auger, P., "Cliches de Rayons Cosmiques Obtenus au Laboratorie International du Jungfraujöch (3450 m), Le Journal de Physique et le Radium 7:65-66 (1936).

7. Leprince-Ringuet, L., "Etude de la Partie Ultra Penetrante Corpusculaire du Rayonnement Cosmique dans le Champ Magnetique de L'Electro-Aimant de Bellevue," Le Journal de Physique et le Radium 7:67-70 (1936).

8. Millikan, R. A., and Anderson, C. D., "Cosmic-Ray Energies and Their Bearing on the Photon and Neutron Hypotheses," The Physical Review 40:325-328 (1932).

9. Anderson, C. D., "Energies of Cosmic-Ray Particles," The Physical Review 41:405-421 (1932).

10. Kunze, P., "Magnetische Ablenkung der Ultrastrahlen in der Wilsonkammer," Zeitschrift für Physik 80:559-572 (1933).

11. Anderson, C. D., "Cosmic-Ray Positive and Negative Electrons," The Physical Review 44:406-416 (1933).

12. Blackett, P. M. S., and Occhialini, G. P. S., "Some Photographs of the Tracks of Penetrating Radiation," Proceedings of the Royal Society of London A 139:699-727 (1933).

13. Heitler, W., and Sauter, F., "Stopping of Fast Particles with Emission of Radiation and the Birth of Positive Electrons," Nature 132:892 (1933).

14. Street, J. C., and Stevenson, E. C., "Penetrating Corpuscular Component of the Cosmic Radiation," The Physical Review 51:1005 (1937).

15. Bethe, H., and Heitler, W., "On the Stopping of Fast Particles and on the Creation of Positive Electrons," Proceedings of the Royal Society of London A 146:83-112 (1934).

16. Anderson, C. D., and Neddermeyer, S. H., "Cloud Chamber Observations of Cosmic Rays at 4300 Meters Elevation and Near Sea Level," The Physical Review 50:263-271 (1936).

17. Neddermeyer, S. H., and Anderson, C. D., "Nature of Cosmic-Ray Particles," Reviews of Modern Physics 11:191-207 (1939).

18. Neddermeyer, S. H., and Anderson, C. D., "Note on the Nature of Cosmic-Ray Particles," The Physical Review 51:884-886 (1937).

19. Neddermeyer, S. H., and Anderson, C. D., "Nature of Cosmic-Ray Particles," Reviews of Modern Physics 11:197 (1939)

20. Bowen, I. S., Millikan, R. A., and Neher, H. V., "The Influence of the Earth's Magnetic Field on Cosmic-Ray Intensities up to the Top of the Atmosphere," The Physical Review 52:80-88 (1937).

21. Bowen, I. S., Millikan, R. A., and Neher, H. V., "New Evidence as to the Nature of the Incoming Cosmic Rays, Their Absorbability in the Atmosphere, and the Secondary Character of the Penetrating Rays Found in Such Abundance at Sea Level and Below," The Physical Review 53:219-223 (1938).

22. Johnson, T. H., "Evidence That Protons Are the Primary Particles of the Hard Component," Reviews of Modern Physics 11:208-210 (1939).

23. Jauch, J. M., "Cosmic Rays-II," Nucleonics 4 (No. 5):49 (1949).

24. Neddermeyer, S. H., "The Penetrating Cosmic-Ray Particles," The Physical Review 53:102-103 (1938).

25. Compton, A. H., Wollan, E. O., and Bennett, R. D., "A Precision Recording Cosmic-Ray Meter," The Review of Scientific Instruments 5:415-422 (1934).

26. Compton, A. H., and Hopfield, J. J., "An Improved Cosmic-Ray Meter," The Review of Scientific Instruments 4:491-492 (1933).

27. Froman, D. K., and Stearns, J. C., "Cosmic-Ray Showers and Bursts," Reviews of Modern Physics 10:134 (1938).

28. Geiger, H., and Müller, W., "Electronenzähl-rohr zur Messung Schwächster Aktivitäten," Die Naturwissenschaften 16:617-618 (1928).

29. Rann, W. H., "Amplification by Secondary Electron Emission," Journal of Scientific Instruments 16: 241-254 (1939).

30. Wooldridge, D. E., Ahearn, A. J., and Burton, J. A., "Conductivity Pulses Induced in Diamond by Alpha-Particles," The Physical Review 71:913 (1947).

31. Hofstadter, R., "Rise Time of Pulse in Silver Chloride Crystal Counters," The Physical Review 72:747 (1947).

32. Hofstadter, R., "Thallium Halide Crystal Counter," The Physical Review 72:1120-1121 (1947).

33. Curtiss, L. F., and Brown, B. W., "Diamond as a Gamma-Ray Counter," The Physical Review 72:643 (1947).

34. Friedman, H., Birks, L. S., and Gauvin, H. P., "Ultraviolet Transmission of 'Counting' Diamonds," The Physical Review 73:186-187 (1948).

35. Hofstadter, R., "Crystal Counters -I," Nucleonics 4 (No. 4):2-27 (1949).

36. Hofstadter, R., "Crystal Counters -II," Nucleonics 4 (No. 5):29-43 (1949).

37. Das Gupta, N. N., and Ghosh, S. K., "A Report on the Wilson Cloud Chamber and Its Applications in Physics," Reviews of Modern Physics 18:225-290 (1948).

38. Cork, J. M., Radioactivity and Nuclear Physics. New York: D. Van Nostrand Company, 1947.

39. Millikan, R. A., Cosmic Rays. New York: The MacMillan Company, 1939.

40. Wilson, C. T. R., and Wilson, J. G., "On the Falling Cloud-Chamber and on a Radial-Expansion Chamber," Proceedings of the Royal Society of London 148:523-533 (1935).

41. Maier-Leibnitz, H., "Untersuchungen mit der 'Langsamen' Wilson-Kammer," Zeitschift für Physik 112:569-586 (1939).

42. Wilkins, T. R., and St. Helens, H. J., "Grain-Spacing of Alpha-Ray, Proton and Deuteron Tracks in Photographic Emulsions," The Physical Review 54:783-788 (1938).

43. Martin, L. C., and Wilkins, T. R., "An Explanation of the Principles of Orthostereoscopic Photomicrography and Some Applications," Journal of the Optical Society of America 27:340-349 (1937).

44. Shapiro, M. M., "Tracks of Nuclear Particles in Photographic Emulsions," Reviews of Modern Physics 13:61-63 (1941).

45. Ilford, Ltd., "New Photographic Emulsions of Interest to Physicists," Journal of Scientific Instruments 12: 333-335 (1935).

46. Webb, J. H., "Photographic Plates for Use in Nuclear Physics," The Physical Review 74:531 (1948).

47. Barbour, I. G., "On the Use of Nuclear Plates in a Magnetic Field," The Physical Review 74:507 (1948).

48. Das Gupta, N. N., and Ghosh, S. K., "A Report on the Wilson Cloud Chamber and Its Applications in Physics," Reviews of Modern Physics 18:261 (1946).

49. Blackett, P. M. S., "The Measurement of the Energy of Cosmic Rays. I-The Electromagnet and Cloud Chamber," Proceedings of the Royal Society of London A 154:564-573 (1936).

50. Anderson, C. D., "Cosmic-Ray Positive and Negative Electrons," The Physical Review 41:406-416 (1933).

51. Blackett, P. M. S., "Further Measurements of the Cosmic-Ray Energy Spectrum," Proceedings of the Royal Society of London A 159:1-18 (1937).

52. Wilson, J. G., "Absorption of Penetrating Cosmic Ray Particles in Gold," Proceedings of the Royal Society of London A 172:517-529 (1939).

53. Fretter, W. B., "The Mass of Cosmic-Ray Mesotrons," The Physical Review 70:625-632 (1946).

54. Jones, H., and Hughes, D. J., "A Magnet and Cloud Chamber for Cosmic-Ray Studies," The Review of Scientific Instruments 11:811 (1940).

55. Das Gupta, N. N., and Ghosh, S. K., "A Report on the Wilson Cloud Chamber and Its Applications in Physics," Reviews of Modern Physics 18:266 (1946).

56. Hughes, D. J., "Cloud-Chamber Photographs of Heavy Particles at High Altitudes," The Physical Review 69: 377 (1946).

57. Leprince-Ringuet, L., et al., "Direct Measurement of the Mass of the Mesotron," The Physical Review 59: 461 (1941).

58. Bethe, H. A., "Multiple Scattering and the Mass of the Meson," The Physical Review 70:822 (1946).

59. Bethe, H. A., "Multiple Scattering and the Mass of the Meson," The Physical Review 70:827 (1946).

60. Leprince-Ringuet, L., et al., "Direkte Massenbestimmung Eines Mesotrons mit Hilfe des Elastischen Stosses," Zeitschrift für Physik 120:589-593 (1943).

61. Hughes, D. J., "Cloud-Chamber Photographs of Heavy Particles at High Altitudes," The Physical Review 69: 379 (1946).

62. Leprince-Ringuet, L., et al., "Direct Measurement of the Mass of the Mesotron," The Physical Review 59:460-461 (1941).

63. Leprince-Ringuet, L., and Crussard, J., "Etude des Particules de Grande Energie du Rayonnement Cosmique dans le Champ Magnetique de L'Electro-Aimant de Bellevue," Le Journal de Physique et le Radium 8: 207-213 (1937).

64. Leprince-Ringuet, L., and Lheritier, M., "Existence Probable d'une Particule de Masse 990 m_o dans le Rayonnement Cosmique," Comptes Rendus Hebdomadaires des Seances de l'Academie des Sciences 219:618-620 (1944).

65. Hughes, D. J., "Cloud-Chamber Photograph of Slow Mesotron Pair," The Physical Review 60:414 (1941).

66. Steinmaurer, R., "Zur Frage der Mesonenmassen," Die Naturwissenschaften 33:54-55 (1946).

67. Blau, M., Black, M. M., and Nafe, J. E., "Heavy Particles in Cosmic-Ray Stars," The Physical Review 76:860-861 (1949).

68. Hughes, D. J., "Cloud-Chamber Photographs of Heavy Particles at High Altitudes," The Physical Review 69:371-381 (1946).

69. Leprince-Ringuet, L., et al., "Direkte Massenbestimmung Eines Mesotrons mit Hilfe des Elastischen Stosses," Zeitschrift für Physik 120:588-597 (1943).

70. Neddermeyer, S. H., and Anderson, C. D., "Nature of Cosmic-Ray Particles," Reviews of Modern Physics 11:203 (1939).

71. Wilson, J. G., "Production of Secondary Electrons by Cosmic Ray Particles," Nature 142:73 (1938).

72. Das Gupta, N. N., and Ghosh, S. K., "A Report on the Wilson Cloud Chamber and Its Applications in Physics," Reviews of Modern Physics 18:264 (1946).

73. Livingston, M. S., and Bethe, H. A., "Nuclear Physics C. Nuclear Dynamics, Experimental," Reviews of Modern Physics 9:268-269 (1937).

74. Street, J. C., "Cloud Chamber Studies of Cosmic Ray Showers and Penetrating Particles," Journal of the Franklin Institute 227:783 (1939).

75. Brode, R. B., "An Apparatus for Mesotron Mass Measurements at High Altitudes," The Physical Review 73: 533 (1948).

76. Hughes, D. J., "Cloud-Chamber Photographs of Heavy Particles at High Altitudes," The Physical Review 69:375 (1946).

77. Hughes, D. J., "Cloud-Chamber Photographs of Heavy Particles at High Altitudes," The Physical Review 69:376 (1946).

78. Rüling, J., and Steinmaurer, R., "Zur Frage der Mesonenmassen," Experentia 2:108-109 (1946).

79. Brode, R. B., and Starr, M. A., "Nuclear Disintegrations Produced by Cosmic Rays," The Physical Review 53: 3-5 (1938).

80. Nishina, Y., Takeuchi, M., and Ichimiya, T.,"On the Nature of Cosmic Ray Particles," The Physical Review 52: 1198-1199 (1937).

81. Brode, R. B., MacPherson, H. G., and Starr, M. A., "The Heavy Particle Component of the Cosmic Radiation," The Physical Review 50:581-583 (1936).

82. Nishina, Y., Takeuchi, M., and Ichimiya, T., "On the Mass of the Mesotron," The Physical Review 55:585-586 (1939).

83. Retallack, G., and Brode, R. B., "The Mass of Cosmic-Ray Mesotrons," The Physical Review 73:532 (1948).

84. Johnson, T. H., and Shutt, R. P., "Cloud-Chamber Track of a Mesotron Stopped by a Gas," The Physical Review 61:380-381 (1942).

85. Williams, E. J., and Roberts, G. E., "Evidence for Transformation of Mesotrons into Electrons," Nature 145:102-103 (1940).

86. Pretter, W. B., and Brode, R. B., "Mass of Cosmic-Ray Mesotrons," The Physical Review 70:791 (1946).

87. Ruhlig, A. J., and Crane, H. R., "Evidence for a Particle of Intermediate Mass," The Physical Review 53:266 (1938).

88. Gardner, E., and Lattes, C. M. G., "Production of Mesons by the 184-Inch Berkeley Cyclotron," Science 107: 270-271 (1948).

89. Bishop, A. S., "Meson Mass Measurements. Part II. Experimental Results," The Physical Review 75:1468 (1949).

90. Burfening, J., Gardner, E., and Lattes, C. M. G., "Positive Mesons Produced by the 184-Inch Berkeley Cyclotron," U. S. Atomic Energy Comission Bulletin, AECD-2334 (1948).

91. Das Gupta, N. N., and Ghosh, S. K., "A Report on the Wilson Cloud Chamber and Its Applications in Physics," Reviews of Modern Physics 18:283 (1946).

92. Wheeler, J. A., and Ladenburg, R., "Mass of the Meson by the Method of Momentum Loss," The Physical Review 60:757 (1941).

93. Wheeler, J. A., and Ladenburg, R., "Mass of the Meson by the Method of Momentum Loss," The Physical Review 60:756 (1941).

94. Street, J. C., "Cloud Chamber Studies of Cosmic Ray Showers and Penetrating Particles," Journal of the Franklin Institute 227, 765-788 (1939).

95. Wheeler, J. A., and Ladenburg, R., "Mass of the Meson by the Method of Momentum Loss," The Physical Review 60:755 (1941).

96. Williams, E. J., "Primary Ionization in Helium and Hydrogen," Proceedings of the Cambridge Philosophical Society 33:180 (1937).

97. Livingston, M. S., and Bethe, H. A., "Nuclear Physics. C. Nuclear Dynamics, Experimental," Reviews of Modern Physics 9:267 (1937).

98. Bloch, F., "Bremsvermögen von Atomen mit Mehreren Elektronen," Zeitschrift für Physik 81:363 (1933).

99. Wilson, R. R., "Range and Ionization Measurements on High Speed Protons," The Physical Review 60:749-753 (1941).

100. Fretter, W. B., "The Mass of Cosmic-Ray Mesotrons," The Physical Review 70:625-627 (1946).

101. Fretter, W. B., "The Mass of Cosmic-Ray Mesotrons," The Physical Review 70:626 (1946).

102. Retallack, J. G., and Brode, R. B., "The Mass of Cosmic-Ray Mesotrons," The Physical Review 75:1716-1718 (1949).

103. Brode, R. B., "The Mass of the Mesotron," Reviews of Modern Physics 21:38 (1949).

104. Fretter, W. B., "The Mass of Cosmic-Ray Mesotrons," The Physical Review 70:628 (1946).

105. Fretter, W. B., "The Mass of Cosmic-Ray Mesotrons," The Physical Review 70:629 (1946).

106. Rossi, B., and Greisen, K., "Cosmic-Ray Theory," Reviews of Modern Physics 13:243-245 (1941).

107. Fretter, W. B., "The Mass of Cosmic-Ray Mesotrons," The Physical Review 70:629-630 (1946).

108. Wheeler, J. A., and Ladenburg, R., "Mass of the Meson by the Method of Momentum Loss," The Physical Review 60:756-757 (1941).

109. Brode, R. B., "The Mass of the Mesotron," Reviews of Modern Physics 21:39-40 (1949).

110. Johnson, T. H., and Shutt, R. P., "Cloud Chamber Track of a Mesotron Stopped by a Gas," The Physical Review 61:381 (1942).

111. Rossi, B., and Greisen, K., "Cosmic-Ray Theory," Reviews of Modern Physics 13:246 (1941).

112. Neddermeyer, S. H., and Anderson, C. D., "Cosmic-Ray Particles of Intermediate Mass," The Physical Review 54:88 (1938).

113. Retallack, J. G., and Brode, R. B., "The Mass of Cosmic-Ray Mesotrons," The Physical Review 75:1719 (1949).

114. Brode, R. B., "The Mass of the Cosmic-Ray Mesotrons," The Physical Review 75:904-905 (1949).

115. Nishina, Y., Takeuchi, M., and Ichimiya, T., "On the Mass of the Mesotron," The Physical Review 55:586 (1939).

116. Retallack, J. G., and Brode, R. B., "The Mass of Cosmic-Ray Mesotron," The Physical Review 75:1716-1721 (1949).

117. Neddermeyer, S. H., and Anderson, C. D., "Cosmic-Ray Particles of Intermediate Mass," The Physical Review 54:88-89 (1938).

118. Brode, R. B., "The Mass of the Mesotron," Reviews of Modern Physics 21:37-41 (1949).

119. Heitler, W., The Quantum Theory of Radiation. Oxford: Oxford University Press, 1949.

120. Williams, E. J., "Some Observations on Cosmic Rays Using a Large Randomly Operated Cloud Chamber," Proceedings of the Royal Society of London A 172:205-209 (1939

121. Williams, E. J., and Terroux, F. R., "Investigation of the Passage of 'Fast' β-Particles Through Gases," Proceedings of the Royal Society of London A 126: 289-310 (1930).

122. Hughes, D. J., "The Mass of the Mesotron as Determined by Cosmic-Ray Measurements," The Physical Review 71:390 (1947).

123. Williams, E. J., "Some Observations on Cosmic Rays Using a Large Randomly Operated Cloud Chamber," Proceedings of the Royal Society of London A 172:195-198 (1939).

124. Bearden, J. A., "Wilson Cloud Chambers with an Increased Time of Sensitivity," The Review of Scientific Instruments 6:256-259 (1935).

125. Frisch, O. R., "Eine Wilsonkammer mit Verlangerter Dauer des Ubersattigten Zustandes," Die Naturwissenschaften 23:166-167 (1935).

126. Williams, E. J., "Some Observations on Cosmic Rays Using a Large Randomly Operated Cloud Chamber," Proceedings of the Royal Society of London A 172:212 (1939).

127. Sen Gupta, R. L., "Application of a Randomly Operated Large Wilson Cloud Chamber for the Determination of the Mass of the Meson," Nature 154:705-707 (1944).

128. Corson, D. R., and Brode, R. B., "The Specific Ionization and Mass of Cosmic-Ray Particles," The Physical Review 53:774 (1938).

129. Oppenheimer, J. R., "Are the Formulae for the Absorption of High Energy Radiation Valid?" The Physical Review 47:45 (1935).

130. Williams, E. J., "The Passage of - and -Particles through Matter and Born's Theory of Collisions," Proceedings of the Royal Society of London A 135: 117-121 (1932).

131. Corson, D. R., and Brode, R. B., "The Specific Ionization and Mass of Cosmic-Ray Particles," The Physical Review 53:775 (1938).

132. Corson, D. R., and Brode, R. B., "The Specific Ionization and Mass of Cosmic-Ray Particles," The Physical Review 53:773 (1938).

133. Street, J. C., and Stevenson, E. C., "New Evidence for the Existence of a Particle of Mass Intermediate Between the Proton and Electron," The Physical Review 52:1003-1004 (1937).

134. Corson, D. R., and Brode, R. B., "The Specific Ionization and Mass of Cosmic-Ray Particles," The Physical Review 53:773-777 (1938).

135. Nielsen, C. E., and Powell, W. M., "Mesotron Mass and Heavy Tracks on Mt. Evans," The Physical Review 63: 384-385 (1943).

136. Williams, E. J., "Some Observations on Cosmic Rays Using a Large Randomly Operated Cloud Chamber," Proceedings of the Royal Society of London A 172: 194-212 (1939).

137. Williams, E. J., and Pickup, E., "Heavy Electrons in Cosmic Rays," Nature 141:684-685 (1938).

138. Ehrenfest, P., "Sur Deux Cliches de Rayons Cosmiques Penetrants Obtenus dans le Champ Magnetique de Bellevue, et l'Existence d'Une Particule Lourde," Comptes Rendus Hebdomadaires des Seances de l'Academie des Sciences 206:428-430 (1938).

139. Neddermeyer, S. H., and Anderson, C. D., "Nature of Cosmic-Ray Particles," Reviews of Modern Physics 11:199 (1939).

140. Neddermeyer, S. H., and Anderson, C. D., "Nature of Cosmic-Ray Particles," Reviews of Modern Physics 11:201 (1939).

141. Das Gupta, N. N., and Ghosh, S. K., "A Report on the Wilson Cloud Chamber and Its Applications in Physics," Reviews of Modern Physics 18:265 (1946).

142. Street, J. C., and Stevenson, E. C., "Design and Operation of Counter-Controlled Cloud Chambers," The Review of Scientific Instruments 7:347-353 (1936).

143. Reinganum, M., "Streuung und Photographische Wirkung der α-Strahlen," Physikalische Zeitschrift 12: 1076-1077 (1911).

144. Michl, W., "Über die Photographie der Bahnen Einzelner α-Teilchen," Akademie der Wissenschaften, Wien, (2a) 121:1431-1447 (1912).

145. Blau, M., "Die Photographische Wirkung von H-Strahlen aus Paraffin und Aluminium," Zeitschrift für Physik 34:285 (1925).

146. Blau, M., and Wambacher, H., "Zur Frage der Verteilung der α-Bahnen der Radiumzerfallsreihe," Akademie der Wissenschaften, Wien, (2a) 145:605-610 (1936).

147. Arley, N., and Heitler, W., "Neutral Particles in Cosmic Radiation," Nature 142:158-159 (1938).

148. Lovell, A. C. B., "Shower Production by Penetrating Cosmic Rays," Proceedings of the Royal Society of London A 172:568-582 (1939).

149. Møller, C., and Rosenfeld, L., "On the Field Theory of Nuclear Forces," Det Kgl. Danske Videnskabernes Selskab. 17:1-72 (1940).

150. Schwinger, J., "On a Field Theory of Nuclear Forces," The Physical Review 61:387 (1942).

151. Williams, E. J., "Concerning the Scattering of Fast Electrons and of Cosmic-Ray Particles," Proceedings of the Royal Society of London A 169:531-572 (1938-1939).

152. Bose, D. M., and Choudhuri, B., "A Photographic Method of Estimating the Mass of the Mesotron," Nature 148:259-260 (1941).

153. Wambacher, H., "Mehrfachzertrümmerung von Atomkernen durch Komische Strahlung; Ergebnisse aus 154 Zertrümmerungssternen in Photographischen Platten," Physikalische Zeitschrift 39:888 (1938).

154. Bose, D. M., and Choudhuri, B., "A Photographic Method of Estimating the Mass of the Mesotron," Nature 149:302 (1942).

155. Bose, D. M., and Choudhuri, B., "A Photographic Method of Estimating the Mass of the Mesotron," Nature 148:259 (1941).

156. Bose, D. M., and Choudhuri, B., "On the Variation in the Experimentally Determined Values of the Meson Mass," Indian Journal of Physics 18:289 (1944).

157. Lattimore, S., "The Mass of σ -Mesons," Nature 161: 518 (1948).

158. Goldschmidt-Clermont, Y., et al., "Determination of the Masses of Charged Particles Observed in the Photographic Plate," The Proceedings of the Physical Society 61:185-187 (1948).

159. Goldschmidt-Clermont, Y., et al., "Determination of the Masses of Charged Particles Observed in the Photographic Plate," The Proceedings of the Physical Society 61:186 (1948).

160. Goldschmidt-Clermont, Y., et al., "Determination of the Masses of Charged Particles Observed in the Photographic Plate," The Proceedings of the Physical Society 61:185 (1948).

161. Goldschmidt-Clermont, Y., et al., "Determination of the Masses of Charged Particles Observed in the Photographic Plate," The Proceedings of the Physical Society 61:187-190 (1948).

162. Brown, R., et al., "Observations with Electron-Sensitive Plates Exposed to Cosmic Radiation," Nature 163: 82-87 (1949).

163. Lattimore, S., "The Mass of σ-Mesons," Nature 161: 518-519 (1948).

164. Goldschmidt-Clermont, Y., et al., "Determination of the Masses of Charged Particles Observed in the Photographic Plate," The Proceedings of the Physical Society 61:183-194 (1948).

165. Wagner, N., and Cooper, D., "The τ-Meson," The Physical Review 76:449-450 (1949).

166. Bose, D. M., and Choudhuri, B., "On the Variation in the Experimentally Determined Values of the Meson Mass," Indian Journal of Physics 18:285-292 (1944).

167. Choudhuri, B., "Mass Determination of the Ionizing Particles Recorded in Photographic Plates Exposed to Cosmic Rays," Indian Journal of Physics 18:57-70 (1944).

168. Occhialini, G. P. S., and Powell, C. F., "Nuclear Disintegrations Produced by Slow Charged Particles of Small Mass," Nature 159:186-190 (1947).

169. Perkins, D. H., "Nuclear Disintegration by Meson Capture," Nature 159:126-127 (1947).

170. Lattes, C. M. G., Occhialini, G. P. S., and Powell, C. F., "A Determination of the Ratio of the Masses of π- and μ-Mesons by the Method of Grain Counting," The Proceedings of the Physical Society 61:174 (1948).

171. Lattes, C. M. G., Occhialini, G. P. S., and Powell, C. F., "A Determination of the Ratio of the Masses of π- and μ-Mesons by the Method of Grain Counting," The Proceedings of the Physical Society 61:176 (1948).

172. Brown, R., et al., "Observations with Electron-Sensitive Plates Exposed to Cosmic Radiation," Nature 163:83 (1949).

173. Lattes, C. M. G., et al., "Processes Involving Charged Mesons," Nature 159:695 (1947).

174. Barkas, W. H., Gardner, E., and Lattes, C. M. G., "Meson Mass Estimation by Grain Counting in Photographic Emulsions," The Physical Review 74:1558 (1948).

175. Occhialini, G. P. S., and Powell, C. F., "Nuclear Disintegrations Produced by Slow Charged Particles of Small Mass," Nature 159:186-191 (1947).

176. Lattes, C. M. G., et al., "Processes Involving Charged Mesons," Nature 159:694-697 (1947).

177. Occhialini, G. P. S., and Powell, C. F., "The Artificial Production of Mesons," Nature 161:551-552 (1948).

178. Franzinetti, C., "On the Mass of Charged Particles of Cosmic Radiation," The Philosophical Magazine 41: 91 (1950).

179. Franzinetti, C., "On the Mass of Charged Particles of Cosmic Radiation," The Philosophical Magazine 41: 95 (1950).

180. Barbour, I., "Magnetic Deflection of Cosmic-Ray Mesons Using Nuclear Plates," The Physical Review 76:320 (1949).

181. Powell, C. F., and Rosenblum, S., "A New Method for the Determination of the Mass of Mesons," Nature 161: 473-475 (1948).

182. Franzinetti, C., "On the Mass of Charged Particles of Cosmic Radiation," The Philosophical Magazine 41: 88 (1950).

183. Franzinetti, C., "On the Mass of Charged Particles of Cosmic Radiation," The Philosophical Magazine 41: 106 (1950).

184. Barbour, I., "Magnetic Deflection of Cosmic-Ray Mesons Using Nuclear Plates," The Physical Review 76:320-321 (1949).

185. Franzinetti, C., "On the Mass of Charged Particles of Cosmic Radiation," The Philosophical Magazine 41: 86-106 (1950).

186. Kar, K. C., and Roy, R. R., "A Self Consistent Method of Determining the Mass of Mesotrons," Indian Journal of Physics 17:316-320 (1943).

187. Kar, K. C., "Proton-Proton Interaction and Yukawa Particle," Indian Journal of Physics 16:187-196 (1942).

188. Smith, F. M., Gardner, E., and Bradner, H., "Mesons Produced by Neutrons from the Cyclotron," The Physical Review 77:562-564 (1950).

189. Lattes, C. M. G., et al., "Processes Involving Charged Mesons," Nature 159:697 (1947).

190. Brown, R., et al., "Observations with Electron-Sensitive Plates Exposed to Cosmic Radiation," Nature 163: 84-86 (1949).

191. Brode, R. B., "The Mass of the Mesotron," Reviews of Modern Physics 21:41 (1949).

192. Leprince-Ringuet, L., et al., "Photographic Evidence for the Existence of a Very Heavy Meson," Reviews of Modern Physics 21:42-43 (1949).

193. Lattes, C. M. G., Occhialini, G. P. S., and Powell, C. F., "A Determination of the Ratio of the Masses of π- and μ-Mesons by the Method of Grain Counting," The Proceedings of the Physical Society 61:180 (1948).

194. Rochester, G. D., and Butler, C. C., "Evidence for the Existence of New Unstable Elementary Particles," Nature 160:856 (1947).

195. Cowling, T. G., "Elementary Particles and the Geomagnetic Field," Nature 160:847 (1947).

196. Barnothy, J., "Mesons of Different Masses," Nature 161: 681 (1948).

197. Blackett, P. M. S., and Brode, R. B., "The Measurement of the Energy of Cosmic Rays. II. The Curvature Measurements and Energy Spectrum," Proceedings of the Royal Society of London A 154:575-579 (1936).

198. Williams, E. J., "Multiple Scattering of Fast Electrons and Alpha-Particles, and 'Curvature' of Cloud Tracks Due to Scattering," The Physical Review 58:298 (1940).

199. Bethe, H. A., "Multiple Scattering and the Mass of the Meson," The Physical Review 70:822 (1946).

200. Wilson, V. C., "Cosmic-Ray Intensities at Great Depths," The Physical Review 53:337-343 (1938).

201. Bethe, H. A., "Multiple Scattering and the Mass of the Meson," The Physical Review 70:821 (1946).

202. Bethe, H. A., "Multiple Scattering and the Mass of the Meson," The Physical Review 70:828 (1946).

203. Leprince-Ringuet, L., and Lheritier, M., "Existence Probable d'une Particule de Mass 990 m$_e$ dans le Rayonnement Cosmique," Comptes Rendus Hebdomadaires des Seances de l'Academie des Sciences 219:618 (1944).

204. Leprince-Ringuet, L., et al., "Direkte Massenbestimmung Eines Mesotrons mit Hilfe des Elastischen Stosses," Zeitschrift für Physik 120:596 (1942-1943).

205. Hughes, D. J., "Cloud-Chamber Photographs of Heavy Particles at High Altitudes," The Physical Review 69:373 (1946).

206. Hughes, D. J., "The Mass of the Mesotron as Determined by Cosmic-Ray Measurements," The Physical Review 71:388 (1947).

207. Retallack, J. G., and Brode, R. B., "The Mass of Cosmic-Ray Mesotrons," The Physical Review 73:532-533 (1948).

208. Bethe, H. A., "Multiple Scattering and the Mass of the Meson," The Physical Review 70:821-831 (1946).

209. Fretter, W. B., "The Mass of Cosmic-Ray Mesotrons," The Physical Review 70:630-631 (1946).

210. Retallack, J. G., and Brode, R. B., "The Mass of Cosmic-Ray Mesotrons," The Physical Review 75:1720 (1949).

211. Fretter, W. B., "The Mass of Cosmic-Ray Mesotrons," The Physical Review 70:631 (1946).

212. Street, J. C., "Cloud Chamber Studies of Cosmic Ray Showers and Penetrating Particles," Journal of the Franklin Institute 227:780-788 (1939).

213. Hughes, D. J., "The Mass of the Mesotron as Determined by Cosmic-Ray Measurements," The Physical Review 71:389 (1947).

214. Sheppard, S. E., et al., "The Temperature Coefficient of Photographic Sensitivity. Part II. Effect of Low Temperature on the Photographic Action of Alpha-Particles," Journal of the Franklin Institute 222: 417-460 (1936).

215. Goldschmidt-Clermont, Y., et al., "Determination of the Masses of Charged Particles Observed in the Photographic Plate," The Proceedings of the Physical Society 61:187 (1948).

216. Goldschmidt-Clermont, Y., et al., "Determination of the Masses of Charged Particles Observed in the Photographic Plate," The Proceedings of the Physical Society 61:193 (1948).

217. Choudhuri, B., "Mass Determination of the Ionizing Particles Recorded in Photographic Plates Exposed to Cosmic Rays," Indian Journal of Physics 17:68 (1944).

218. Dilworth, C. C., Occhialini, G. P. S., and Payne, R. M., "Processing Thick Emulsions for Nuclear Research," Nature 162:102-103 (1948).

219. Franzinetti, C., "Magnetic Deflection of Cosmic-Ray Mesons Using Nuclear Plates," The Philosophical Magazine 41:93 (1950).

220. Rossi, B., and Greisen, K., "Cosmic-Ray Theory," Reviews of Modern Physics 13:267 (1941).

221. Bethe, H. A., "Multiple Scattering and the Mass of the Meson," The Physical Review 70:825-831 (1946).

222. Hughes, D. J., "Cloud-Chamber Photographs of Heavy Particles at High Altitudes," The Physical Review 69: 375-376 (1946).

223. Ruhlig, A. J., and Crane, H. R., "Evidence for a Particle of Intermediate Mass," The Physical Review 53:266-267 (1938).

224. Leprince-Ringuet, L., and Lheritier, M., "Existence Probable d'une Particule de Masse (990±12 pour 100) m_o dans le Rayonnement Cosmique," Le Journal de Physique et le Radium 7:65-69 (1946).

225. Birge, R. T., "The Calculation of Errors by the Method of Least Squares," The Physical Review 40:213-223 (1932).

226. Retallack, J. G., and Brode, R. B., "The Mass of Cosmic-Ray Mesotrons," The Physical Review 75:1720-1721 (1949).

227. Wheeler, J. A., and Ladenburg, R., "Mass of the Meson by the Method of Momentum Loss," The Physical Review 60:761 (1941).

228. Williams, E. J., "Some Observations on Cosmic Rays Using a Large Randomly Operated Cloud Chamber," Proceedings of the Royal Society of London A 172:207 (1939).

229. Hogrebe, K., "Zur Existenz von Zwei Massenwerten für Mesonen," Zeitschrift für Naturforschung 3a:61 (1948).

230. Das Gupta, N. N., and Ghosh, S. K., "A Report on the Wilson Cloud Chamber and Its Applications in Physics," Reviews of Modern Physics 18:281 (1946).

231. Bloch, F., "Bremsvermögen von Atomen mit Mehreren Elektronen," Zeitschrift für Physik 81:363-376 (1933).

232. Wilson, R. R., "Range and Ionization Measurements on High Speed Protons," The Physical Review 60:753 (1941).

233. Bhabha, H. J., "On the Penetrating Component of Cosmic Radiation," Proceedings of the Royal Society of London A 164, 275 (1938).

234. Das Gupta, N. N., and Ghosh, S. K., "A Report on the Wilson Cloud Chamber and Its Applications in Physics," Reviews of Modern Physics 18:282 (1946).

235. Bethe, H. A., "Multiple Scattering and the Mass of the Meson," The Physical Review 70:830 (1946).

236. Bethe, H. A., "Multiple Scattering and the Mass of the Meson," The Physical Review 70:831 (1946).

237. Rossi, B., and Greisen, K., "Cosmic-Ray Theory," Reviews of Modern Physics 13:244 (1941).

Alichanian, A. I., and Alichanow, A. I., "Concerning New Elementary Particles in Cosmic Rays," Nature 163:761-762 (1949).

Anderson, C. D., et al., "On the Mass and the Disintegration Products of the Mesotron," The Physical Review 72:724-727 (1947).

Barbour, I., "On the Use of Nuclear Plates in a Magnetic Field," The Physical Review 74:507 (1948).

Barnothy, J., "Theoretical Values of Mass and Lifetime of Mesons," The Physical Review 75:1458 (1949).

Bethe, H. A., "On the Two-Meson Hypothesis," The Physical Review 72:506-507 (1947).

Blackett, P. M. S., "The Nature of the Penetrating Component of Cosmic Rays," Proceedings of the Royal Society of London A 165:11-31 (1938).

Born, M., "Application of 'Reciprocity' to Nuclei," Proceedings of the Royal Society of London A 166:552-557 (1938).

Callisen, F., "Über die Entwicklung und Anwendung Neuer Messmethoden in der Mesonenforschung," Zeitschrift für Naturforschung 2a:686-697 (1947).

Corson, D. R., and Brode, R. B., "Evidence for a Cosmic Ray Particle of Intermediate Mass," The Physical Review 53: 215 (1938).

Corson, D. R., and Wilson, R. R., "Particle and Quantum Counters The Review of Scientific Instruments 19:207-233 (1948).

Cullwick, E. G., "A Tentative Explanation of the Observed Mass of Mesons and Other Particles," The Physical Review 74: 707 (1948).

Forster, H. H., "Evidence for a Charged Heavy Meson," The Physical Review 77:733-734 (1950).

Furry, W. H., "Discussion of a Possible Method for Measuring Masses of Cosmic-Ray Mesotrons," The Physical Review 72: 171 (1947).

Gorodetzky, S., "La Determination xperimentale de la Masse des Mesotons par les Methodes d'Ionisation," Experentia 2:421-430 (1946).

Gorodetzky, S., "Sur la Determination de la Masse des Particules Chargees du Rayonnement Cosmique," Annales de Physique 19: 5-70 (1944).

Groetzinger, G., Kruger, P. G., and Smith, L., "Evidence for the Artificial Production of a New Neutral Radiation," The Physical Review 67:52 (1945).

Janossy, J., Cosmic Rays. Oxford: At the Clarendon Press, 1948.

Jauch, J. M., "Cosmic Rays - I," Nucleonics 4 (No. 4):39-51 (1949).

Lattes, C. M. G., and Gardner, E., "Production of Mesons by the 184-inch Berkeley Cyclotron. Part II. Mass Determination," The Physical Review 74:1236 (1948).

Lattes, C. M. G., "Meson Mass Measurements. Part III. Discussion of Results," The Physical Review 75:1468 (1949).

Lattes, C. M. G., Occhialini, G. P. S., and Powell, C. F., "Observations on the Tracks of Slow Mesons in Photographic Emulsions," Nature 160:453-456 (1947).

Leighton, R. B., Anderson, C. D., and Seriff, A. J., "The Energy Spectrum of the Decay Particles and the Mass and Spin of the Mesotron," The Physical Review 75:1432-1437 (1949).

Leprince-Ringuet, L., "Measurement of Meson Masses by the Method of Elastic Collision. Probable Existence of a Heavy Meson (1000 m_0) in the Cosmic Radiation," The Physical Review 70:791-792 (1946).

Lheritier, M., Peyrou, C., and Lagarrigue, A., "Sur la Masse des Particules de la Composante Penetrante du Rayonnement Cosmique," Comptes Rendus Hebdomadaires des Seances de l'Academie des Sciences, 225:1304-1306 (1947).

Lubanski, J. K., and DeJager, C., "The Scattering of Protons by Protons and the Meson Field of the Proton," Physica 14: 8-14 (1948-49).

Millikan, R. A., Electrons (+ and -), Protons, Photons, Neutrons, Mesotrons and Cosmic Rays. Chicago: University of Chicago Press, 1947.

Morrison, P., "Physics in 1946," Journal of Applied Physics 18:150 (1947).

Peyron, C., Lheritier, M., and Lagarrigue, A., "Sur la Masse des Particules de la Composante Penetrante du Rayonnement Cosmique," Comptes Rendus Hebdomadaires des Seances de l'Academie des Sciences 226:1271-1273 (1948).

Powell, W. M., "A Cloud-Chamber Analysis of Cosmic Rays at 14,120 Ft.," The Physical Review 69:385-405 (1946).

Retallack, J. G., "Further Measurements on the Mass of the Mesotron," The Physical Review 72:742-743 (1947).

Rochester, G. D., and Butler, C. C., "The Penetrating Particles in Cosmic-Ray Showers: I. Heavily-Ionizing Particles," The Proceedings of the Physical Society 61:307-312 (1948).

Snyder, C. W., "Current Ideas About Mesons," Nucleonics 5 (No. 1 42-52 (1949).

Yukawa, H., and Sokata, S., "Mass and Mean Lifetime of the Meson," Nature 143:761-762 (1939).

Witmer, E. E., "The Masses of the Mesons," The Physical Review 75:348 (1949).

APPENDIX I

BASIC EQUATIONS

From the theory of the motion of a charged particle in a magnetic field, a particle of rest mass M, charge Ze (esu), and momentum p moving at right angles to a magnetic field of H gauss describes a track with a radius of curvature ρ cm. where

$$pc = \frac{M\beta c^2}{(1 - \beta^2)^{1/2}} = Ze\ H\rho\ , \tag{24}$$

or, in more convenient units,

$$pc)_{ev} = 300\ Z\ H\rho\ ; \tag{25}$$

$pc)_{ev}$ is written for pc expressed in electron volts, and $H\rho$, the magnetic rigidity, is expressed in gauss cm. Hence, the momentum of a particle may be obtained directly, provided Z is known, by measuring $H\rho$.

If we assume Z = 1 in Eq. 24, we have

$$\frac{M}{m_e} = \frac{eH\rho}{m_e c^2} \frac{(1 - \beta^2)^{1/2}}{\beta}\ , \tag{26}$$

where M/m_e is the mass number k. Putting in the known values of m_e, c, and e in Eq. 26,

$$\frac{M}{m_e} = \frac{H\rho}{1704} \frac{(1 - \beta^2)^{1/2}}{\beta}\ . \tag{27}$$

Hence if $(1 - \beta^2)^{1/2}/\beta$ is determined from a measurement of

the energy loss per cm. due to collisions of the unknown particle, one can obtain directly M/m_e from $H\rho$ measurement.

From Eq. 25, the rate of change of momentum with respect to distance x may be found by differentiation to be

$$c\left(\frac{dp}{dx}\right) = 300\ Z\ H\ \left(\frac{d\rho}{dx}\right) = 300\ Z\ d\left(\frac{H\rho}{dx}\right) \qquad (28)$$

since H is assumed constant.

APPENDIX II

SPECIFIC IONIZATION AS A FUNCTION OF THE VELOCITY OF A PARTICLE

In considering the average rate of dissipation of energy through ionization and excitation by a fast primary particle of mass M, velocity $v = \beta c$, and charge Ze, Das Gupta and Ghosh (230) have given the energy loss as

$$\left(\frac{-dE}{dx}\right) = \frac{2\pi n e^4 Z^2}{m_e v^2} \times \left\{ \ln \frac{2m_e v^2 T_m}{I^2(1 - v^2/c^2)} - 2\frac{v^2}{c^2} \right\}, \qquad (29)$$

where n is the number of electrons per cubic centimeter of the stopping material, I is the mean excitation energy of these electrons, and Tm is the maximum kinetic energy to be transferred to an electron in elastic impact. The energy loss is independent of the mass of the primary particle except that the mass enters into Tm.

Elements of high atomic number are most effective in distinguishing mesons from electrons by the method of momentum loss discussed previously, but for these elements no direct determination of the mean excitation energy of the electrons is available. However, the stopping power is not too dependent on the value of I, and Bloch's theory (231) of excitation energies permits a satisfactory estimate of this quantity. According to Bloch, I for atoms of a material containing many electrons is proportional to the atomic number Z' of the substance. For the constant of proportionality he gives the

value

$$I/Z' = 0.96\ (m_e e^4/2\hbar^2) = 13.1\ \text{ev}$$

on the basis of experiments available in 1933, where $\hbar$ is written for $h/2\pi$, h being Planck's constant. Recently, Wilson (232) has given a more reliable estimate of Bloch's constant, namely,

$$I/Z' = 0.85\ (m_e e^4/2\hbar^2) = 11.5\ \text{ev}.$$

To obtain an expression for Tm, we consider the electron as having a kinetic energy T after a primary of total energy E has collided with it and that it is initially at rest. From the law of conservation of energy,

$$(E - T)^2 = E_r^2,$$

where E_r is the residual energy of the primary particle. Now,

$$E_r^2 = (p_r c)^2 + M^2c^4, \qquad (30)$$

where p_r is the residual momentum of the primary which, from the law of conservation of momentum, may be written

$$p_r^2c^2 = p_e^2c^2 + p^2c^2 - 2(pc)\ (p_e c)\cos\theta, \qquad (31)$$

p_e being the momentum of the electron after collision and θ the angle between the direction of emission of the electron and the path of the primary particle.

Eliminating p_r from Eqs. 30 and 31 and expressing p_e

in terms of the kinetic energy T of the electron, we get

$$T(E + m_e c^2) = pc \cos\theta \left[T(T + 2m_e c^2)\right]^{1/2}.$$

Solving for T,

$$T = 2m_e c^2 \frac{p^2 c^2 \cos^2\theta}{(E + m_e c^2)^2 - p^2 c^2 \cos^2\theta},$$

and Tm, the maximum transferable energy, is equal to, putting $\theta = 0$ (head-on collision),

$$Tm = 2m_e c^2 \frac{p^2 c^2}{m_e^2 c^4 + M^2 c^4 + 2Em_e c^2}.$$

If now $M >> m_e$, and $E << 1/2(M/m_e)Mc^2$,

$$Tm = 2m_e c^2 \frac{p^2}{M^2 c^2} = 2m_e c^2 \frac{\beta^2}{(1 - \beta^2)} . \qquad (32)$$

The critical energy E_c below which Eq. 32 holds is 10^{10} ev for mesons of mass 200 m_e.

Substituting the value of Tm from Eq. 32 in Eq. 29 we have

$$\frac{-dE}{dx} = \frac{4\pi n e^4 Z^2}{m_e \beta^2 c^2} \left\{ \ln \frac{2m_e \beta^2 c^2}{I(1 - \beta^2)} - \beta^2 \right\} . \qquad (33)$$

Taking $n = 3.9 \times 10^{20}$ and $I = 82.6$ ev for air, and assuming $Z = 1$, the energy loss becomes

$$\frac{-dE}{dx} = \frac{2 \times 10^2}{\beta^2} \left\{ 9.43 + 2 \ln \frac{\beta}{(1 - \beta^2)^{1/2}} - \beta^2 \right\} \qquad (34)$$

in ev per cm. of air. Table XI (91) gives calculated values of $-dE/dx$ for different values of $\beta/(1 - \beta^2)^{1/2}$. The calculated

TABLE XI

VALUES OF $-dE/dx$ AS FUNCTIONS OF $\beta/(1-\beta^2)^{1/2}$

$\frac{\beta}{(1-\beta^2)^{1/2}}$	$-dE/dx$ in 10^3 ev per cm. air
0.126	45.2
0.18	25.9
0.255	14.8
0.315	10.8
0.366	8.7
0.411	7.4
0.60	4.68
0.894	3.28
1.15	2.83
1.39	2.69
1.61	2.52
2.68	2.41
4.74	2.49

values hold for all particles for which the radiation loss is negligible. Curve 1 in Fig. 11 shows a plot of these values.

Fortunately, radiative losses can be neglected for mesons of much greater than electronic mass even for velocities such as $v = 0.9\ c$ and for substances of large atomic numbers ($Z = 82$). Bhabha (233) gives a formula for a particle's mean energy loss in the form of radiation. For a meson of mass 200 m_e and total energy $E = 150$ Mev traversing 1 cm. of lead, the mean energy loss computed by means of this formula is approximately 0.01 Mev, which is negligible in comparison with the meson's approximate 10 Mev loss by ionization.

APPENDIX III

RANGE AS A FUNCTION OF THE VELOCITY OF A PARTICLE

An approximate calculation of the range of a high energy meson as a function of its energy has been given by Euler and Heisenberg (234).

In Eq. 33, if the slow variation of dE/dx with $\ln \beta/(1-\beta^2)^{1/2}$ is neglected, and the approximation

$$\frac{-dE}{dx} = \frac{aZ^2}{\beta^2}$$

is used, where $a = 2.5 \times 10^3$ ev per cm. air, then the range is related to the energy by

$$R = \int \frac{dE}{-dE/dx} = \frac{1}{Z^2 a} \int \beta^2 dE.$$

Since $E^2 = p^2c^2 + M^2c^4$,

$$dE = \frac{pc^2}{E}\, dp = \beta c\, dp. \qquad (35)$$

Hence,

$$R = \frac{c}{Z^2 a} \int_o^p \beta^3 dp = \frac{c}{Z^2 a} \int_o^p \frac{p^3 dp}{(p^2 + M^2c^2)^{3/2}},$$

$$R = \frac{c}{Z^2 a} \left[\frac{2M^2c^2 + p^2}{(p^2 + M^2c^2)^{1/2}} \right]_o^p,$$

$$R = \frac{c}{Z^2 a} \left[\frac{2Mc + p^2/Mc}{\left(1 + \frac{p^2}{M^2c^2}\right)^{1/2}} \right]_o^p,$$

$$R = \frac{Mc^2}{Z^2 a}\left[\frac{2 + (p/Mc)^2}{[1 + (p/Mc)2]^{1/2}}\right]_o^p ,$$

$$\text{and } R = \frac{Mc^2}{Z^2 a}\left[\frac{2 + (p/Mc)^2}{[1 + (p/Mc)^2]^{1/2}} - 2\right].$$

Values of $RZ^2/(M/m_e)$ are plotted in Fig. 11 against $\beta/(1 - \beta^2)^{1/2}$

APPENDIX IV

GEOMETRICAL DETERMINATION OF THE AVERAGE COULOMB SCATTERING ANGLE OF A MESON IN PASSING THROUGH AN EMULSION

Let ABC in Fig. 40 be the projection of a section of a meson track in the plane of an emulsion, and the lengths AB and BC, measured along the track, be each equal to X. Draw the tangent NBN' to the track at B, and join AB and BC as shown. The angle (ψ) between the chords is equal to ($\phi_1 \pm \phi_2$). Therefore,

$$(\psi^2)_{av} = (\phi_1^2)_{av} + (\phi_2^2)_{av}.$$

If the perpendicular AN and CN' of lengths y_1 and y_2, respectively, are drawn to NBN', we may write

$$\phi_1 = y_1/X \text{ and } \phi_2 = y_2/X.$$

Hence,

$$(\phi_1^2)_{av} = \frac{(y_1^2)_{av}}{X^2} \text{ and } (\phi_2^2)_{av} = \frac{(y_2^2)_{av}}{X^2}.$$

If the angle between the tangents drawn to the path at A and B is designated by θ, and that between the tangents at B and C as θ_2, Lattimore (157) gives

$$(y_1^2)_{av} = 1/3\ X^2\ (\theta_1^2)_{av}, \text{ and}$$

$$(y_2^2)_{av} = 1/3\ X^2\ (\theta_2^2)_{av}.$$

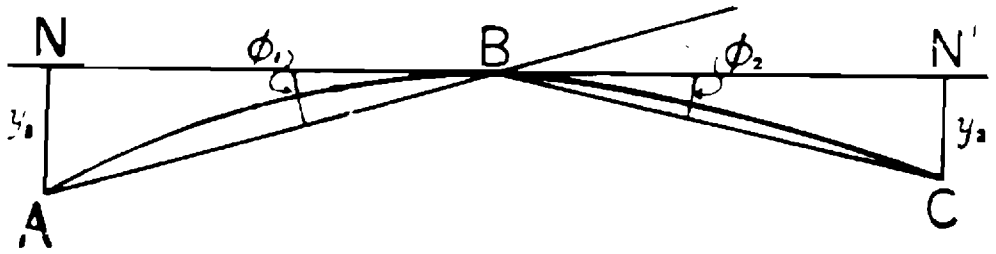

Figure 40. Diagram to determine the average Coulomb scattering angle of a meson in a photographic emulsion.

Therefore,

$$(\psi^2)_{av} = 1/3[(\theta_1^2)_{av} + (\theta_2^2)_{av}].$$

The formula for $(\theta^2)_{av}$ as given by Lattimore is

$$(\theta^2)_{av} = \frac{4\pi e^4 Z^2 nX}{p^2 v^2} \ln(\frac{\theta_{max}}{\theta_{min}}),$$

where

$$\theta_{min} = (\frac{m_e c}{p}) (\frac{Z^{1/3}}{181}),$$

and θ_{max} is the smallest angle that is recognizable as a single deflection.

APPENDIX V

MEASUREMENT OF RECOIL ELECTRON TRACKS OF CONSIDERABLE CURVATURE

It is assumed that a circle is fitted as best as possible to a section of the electron track such as AB in Fig. 10b. This amounts essentially to measuring the distance AB = 2a and the length of the sagitta s of the curve AB. If AB were a circle its radius would be

$$\rho = a^2/2s + s/2. \qquad (36)$$

This equation will be used as the definition of the measured radius of the curve.

Assuming that the magnetic field alone would deflect the electron by an angle 2α over the distance B to A, and that the radius of curvature in the magnetic field alone is r_o, the track length from the point P to either A or B will be nearly $r_o \alpha$. The actual deflection from P to A will be $\alpha + \theta_1$, where the probable value of θ_1 is calculated from Eq. 22 with $X = r_o \alpha$. The lateral displacement of the track with respect to the circle of radius r_o and the point A is given by Bethe (199) as follows:

$$(y_1^2)_{av} = (y_2^2)_{av} = (1/3)\, r_o^2\, \alpha^2\, [\theta^2_{av}]_{pl}, \qquad (37)$$

where $[\theta^2_{av}]_{pl}$ is given by Eq. 22 and y_1 and y_2 are the distances of the end points of a track from the tangent to the track at its midpoint.

Letting BPA in Fig. 41 (235) represent the circle in the magnetic field alone and y_1 and y_2 be the lateral displacements at A and B respectively, the track length is increased by z_1 and z_2, respectively, at its two end points (giving the new end points A' and B' for the actual track) in order to have the same ordinates for the end points. The vertical displacement of A' with respect to A is

$$V_1 = y_1 \cos \alpha + z_1 \sin \alpha ,$$

and that of B' with respect to B is

$$V_2 = y_2 \cos \alpha + z_2 \sin \alpha .$$

The sagitta s of the observed track B'PA' is

$$s = \rho_o(1 - \cos \alpha) + Y \cos \alpha + Z \sin \alpha ,$$

where

$$Y = 1/2 \ (y_1 + y_2), \quad Z = 1/2 \ (z_1 + z_2).$$

The cord A'B' is

$$2a = 2r_o \sin \alpha - 2 Y \sin \alpha + 2 Z \cos \alpha .$$

By using Eq. 36, it may be shown that the radius is

$$\rho = r_o - \frac{y_1 + y_2}{2(1 - \cos \ )} . \qquad (38)$$

Considering a circle of the ideal radius r_o which starts

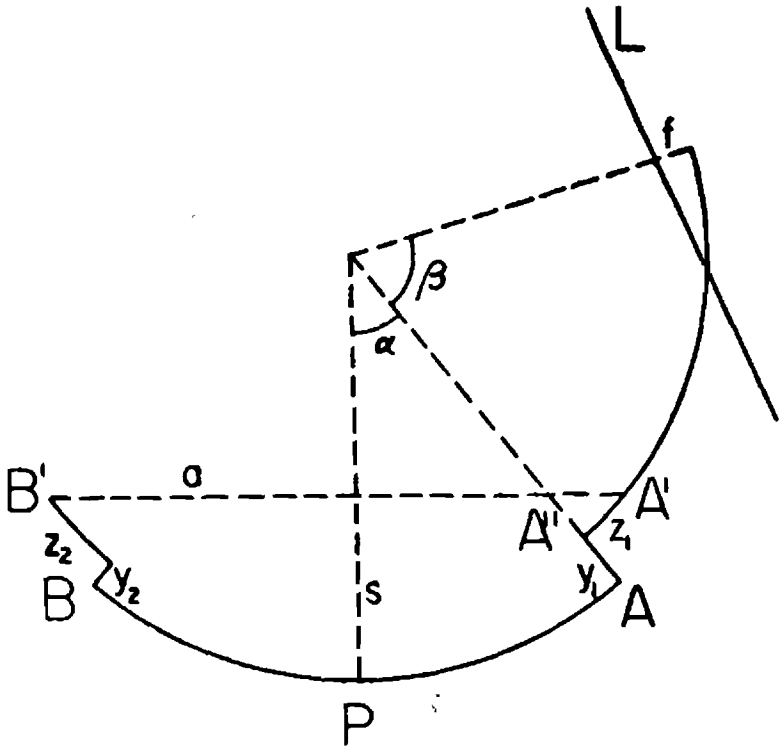

Figure 41. Mass determination by the method of elastic collision. BPA is a section of the circle which a recoil particle would describe in a magnetic field alone, the actual path being from B' to A' via P. Its continuation beyond A' is shown up to a point where the path is parallel to the straight line L which represents the path of the primary particle.

from A' in the actual direction of the path, and considering the actual path to be a circle and to be displaced with respect to this ideal circle by a lateral displacement y_3 which can be calculated from Eqs. 22 and 37 with the value α^2 replaced by a value β^2, the distance between the two circles at the angle β from their common starting point A' as given by Bethe (236) is

$$\rho\sigma\sin\beta + (r_o - \rho)(1 - \cos\beta), \qquad (39)$$

where the radius of the ideal circle is r_o, that of the assumed circle is ρ, and σ is the angle between the two circles given by

$$\sigma = \theta_1 - \frac{y_2 + y_1 (1 + 2\cos\alpha)}{2 r_o \sin\alpha} .$$

Inserting Eq. 38 for $(\rho - r_o)$ and the above value for σ into Eq. 39 and adding y_3, we obtain for the change in the sagitta f (measured f minus true f)

$$\Delta f = r_o\theta_1 \sin\beta - y_1\left(\frac{1 + 2\cos\alpha}{2\sin\alpha}\sin\beta + \frac{1 - \cos\beta}{2(1 - \cos\alpha)}\right)$$

$$-y_2\left(\frac{\sin\beta}{2\sin\alpha} + \frac{1 - \cos\beta}{2(1 - \cos\alpha)}\right) + y_3.$$

Although y_1, y_2, and y_3 are statistically independent of one another, the correlation between y_1 and θ_1 as given by Bethe (236) is

$$(y_1\theta_1)_{av} = 1/2\ X'\ (\theta_1^2)_{av},$$

where X' is the distance from the midpoint of a track to either end point (assumed to be large compared with y_1 and y_2). Using Eq. 37, the mean square error for the sagitta f may be determined.

Bethe gives the error in the measured curvature as

$$\Delta\left(\frac{1}{\rho}\right) = \frac{y_1 + y_2}{2r_o^2(1 - \cos \alpha)} ,$$

which reduces to

$$\Delta\left(\frac{1}{\rho}\right) = \frac{y_1 + y_2}{r_o^2 \alpha^2}$$

in the limit of small α.

APPENDIX VI

THE DIFFERENTIAL COLLISION PROBABILITY

Defining a function N(E,T) as the differential collision probability, where E is the energy of a particle of mass M, charge ± 1, traversing a thickness dx, and transferring an amount of energy between T and T + dT to a free electron, the Rutherford formula* gives the relation for small values of E

$$N(E,T)dT = (2Cm_e/\beta^2)dT/(T)^2. \qquad (40)$$

The value of the constant C is

$$C = 0.150\ (Z'/A),$$

where Z' and A are the atomic number and the atomic weight of the material traversed by the particle M. If Eq. 40 is multiplied by dx (measured in gm./cm.^{2}), the probability for the energy transfer is obtained. This equation is arrived at no matter if the problem is treated by classical methods or by quantum-mechanical methods as long as small values of T are considered. The general expression for N, however, depends in an essential way on the spin of the primary particle and on whether or not it is distinguishable from the secondary electron.

---

*Formula taken from Rossi, B., and Greisen, K.,"Cosmic-Ray Theory," Reviews of Modern Physics 13:243 (1941).

Since the spin of mesons is not yet known, the following expressions (237) for the collision probabilities are for values of the spin 0, 1/2, and 1. Quantities of the order of m_e/M are neglected in comparison with unity.

Spin 0: $$N(E,T)dT = \frac{2Cm_e}{\beta^2}\frac{dT}{(T)^2}(1 - \beta^2\, T/Tm) \qquad (41$$

Spin 1/2: $$N(E,T)dT = \frac{2Cm_e}{\beta^2}\frac{dT}{(T)^2}\left[1 - \beta^2\, T/Tm + 1/2\left(\frac{T}{E+M}\right)^2\right] \qquad (42$$

Spin 1: $$N(E,T)dT = \frac{2Cm_e}{\beta^2}\frac{dT}{(T)^2}\left[(1 - \beta^2\, T/Tm)\left(1 + \frac{1}{3}\frac{T}{E_c}\right) + \frac{1}{3}\left(\frac{T}{E+M}\right)^2\left(1 + \frac{1}{2}\frac{T}{E_c}\right)\right] \qquad (43$$

where Tm is the maximum transferable energy as given in Appendix II, and $E_c = M^2/m_e \sim 2 \times 10^{10}$ ev.

If T is small compared with both E and E_c, Eqs. 42 and 43 reduce to 41, which means that the collision probability is independent of the spin. When $T \ll Tm$, Eq. 41 reduces to Eq. 40.

The influence of the spin on the collision probability of mesons manifests itself only for very close collisions. Theoretical predictions depend essentially on the hypothesis that the electromagnetic field of the meson can be described in the ordinary way even at distances smaller than 10^{-13} cm. from the so-called center of the meson itself. So far, this hypothesis lacks any experimental support.